Anatomical and Functional Organization of Domain-General Brain Regions

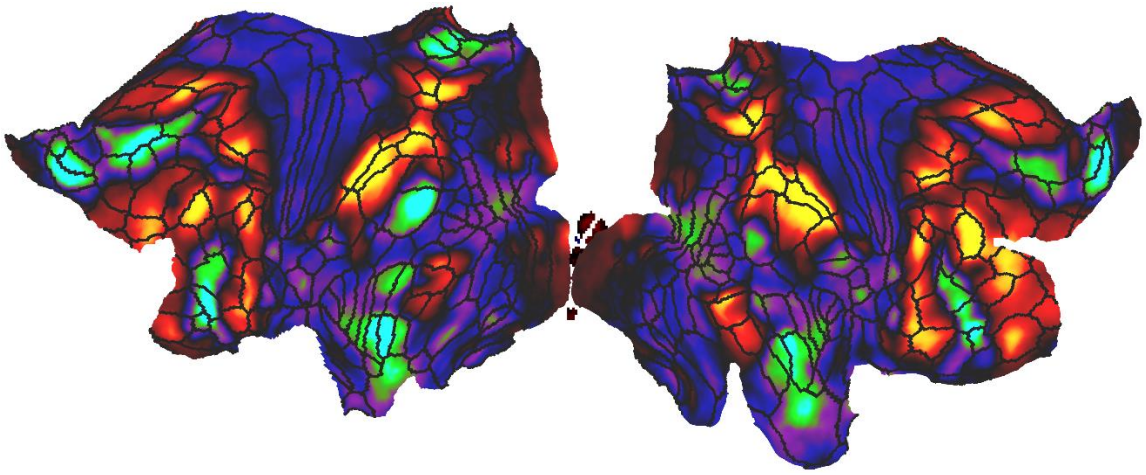

Moataz Ibrahim Mohamed Assem

Hughes Hall

MRC Cognition and Brain Sciences Unit
School of Clinical Medicine
University of Cambridge

This dissertation is submitted for the degree of Doctor of Philosophy

September 2020

PREFACE

This thesis is the result of my own work and includes nothing which is the outcome of work done in collaboration except as declared in the preface and specified in the text. It is not substantially the same as any work that has already been submitted before for any degree or other qualification except as declared in the preface and specified in the text. This thesis does not exceed the prescribed limit of 60,000 words as specified by the degree committee of the Faculties of Clinical Medicine and Clinical Veterinary Medicine.

The study in chapter 2, preliminary results from chapter 4, and some parts of chapters 1 and 5 have been published in the following references:

Assem M, Glasser MF, Van Essen DC, Duncan J. (2020) A Domain-General Cognitive Core Defined in a Multimodally Parcellated Human Cortex. Cerebral Cortex, 30(8):4361-4380. doi.org/10.1093/cercor/bhaa023

Duncan J, Assem M, Shashidhara S. (2020) Integrated Intelligence from Distributed Brain Activity. Trends in Cognitive Sciences. 24(10):838-852. https://doi.org/10.1016/j.tics.2020.06.012

Assem M, Hart MG, Coelho P, Romero-Garcia R, Ingham J., McDonald A, Villa L, Sinha R, Suckling J, Duncan J, Santarius T, Erez Y. (2019) Intraoperative Mapping of Cognitive Control Regions in the Frontal Cortex Using Electrocorticography. IBRO Reports 6, S446. https://doi.org/10.1016/j.ibror.2019.07.1412

Erez Y, Assem M, Coelho P et al. Intraoperative mapping of executive function using electrocorticography for patients with low-grade gliomas. Acta Neurochir (2020). https://doi.org/10.1007/s00701-020-04646-6

The study in chapter 2 was done in collaboration with Matt Glasser and David Van Essen who provided the preprocessed data. The study in chapter 3 was done in collaboration with Sneha Shashidhara who helped in the study design, data collection and preliminary analysis. The study in chapter 4 was done in collaboration with Yara Erez who helped in study design, data collection and preliminary analysis.

SUMMARY

ANATOMICAL AND FUNCTIONAL ORGANIZATION OF DOMAIN-GENERAL BRAIN REGIONS

MOATAZ IBRAHIM MOHAMED ASSEM

How does complex brain activity organize thought and behaviour? Theoretical proposals have long emphasized that intelligent behaviour must be supported by a flexible control system. Numerous brain imaging studies identified a domain-general or "multiple-demand" (MD) brain system co-activated accompanying many tasks and is hypothesised to play a central role in cognitive control. However, the limited spatial localization provided by traditional imaging methods precluded a consensus regarding its anatomy and physiology. To address these limitations, the experiments in chapters 2 and 3 capitalize on novel multi-modal magnetic resonance imaging (MRI) methods developed by the Human Connectome Project. Chapter 2 delineated nine cortical MD patches per hemisphere and subdivided them into 10 regions forming a core of most strongly activated and functionally interconnected regions, surrounded by a penumbra of 17 additional regions. MD activations were also identified in specific subcortical and cerebellar regions. Chapter 3 investigated the relation between the newly defined MD regions and previously identified sensory-biased cortical regions. Contrasting auditory and visual low working memory demands revealed the strongest sensory-biases are localized just outside of MD regions. And additional working memory demands revealed MD activations showed no sensory biases. Chapter 4 used human electrophysiological recordings from the lateral frontal cortex to functionally map cognitive control regions during awake neurosurgeries. By contrasting a hard vs easy cognitive demand, spectral analysis revealed localized power increases in the gamma range (>30 Hz) that overlap with a canonical mask of the fronto-parietal control network. These findings contrast with spatially non-specific power decreases in the beta range (12-30 Hz). Thus, using similar task difficulty manipulations, electrophysiology and MRI functional signals converged on localizing lateral frontal regions related to cognitive control and support their clinical potential for intraoperative mapping of cognitive control. All together, the distributed anatomical organization, mosaic functional preferences, and strong functional interconnectivity of MD regions, suggest a skeleton for integrating and organizing the diverse components of cognitive operations. The precise anatomical delineation of MD regions provides the groundwork for refined analyses of their functions.

ACKNOWLEDGMENTS

To everyone who enriched my experience during the PhD training, thank you.

To my supervisor, John Duncan, I am forever in debt for everything: from inspiring a naïve undergraduate student with your book, to making the PhD experience smooth and fun, and to being there not just as a supervisor but as a friend.

To my co-supervisor Yaara Erez, thank you for your continuous guidance throughout the PhD. I truly enjoyed your company during the countless hours we spent in the surgeries and localizing electrodes.

To the CBU, it is truly a privilege to belong to such a supportive and friendly community. I would like to thank the methods and IT teams for their help with setting up the HCP MRI sequences and analysis pipelines. Specifically, I would like to that Marta, Marius, Karen, Steve, Jeff, Russel and Howard. I would also like to thank Sneha, Verity, Shraddha and Julia, Tanya, Courtney and HP for the board games and friendship. To Kirsty for being the perfect office buddy. To Victoria, for your positive energy. To the countless friends and colleagues at CBU, you make this place special.

To my friends in Cambridge, Steven, Samuel, Noura, Youmna, Nadi, Shadi and Fiona, thank you for the warmth of your friendship. To my friends beyond Cambridge, Hafez, Ghoneem, Serag and Salma, till we meet again.

To my parents, Ibrahim and Maha, and sister, Mariam, I am forever grateful for your unconditional support and love. I never felt like you were away.

To my wife Melek, you are simply the best.

I am grateful for the financial support provided by the Cambridge Trust-Yousef Jameel Scholarship.

To fellow wanderers,
may you find in the next pages,
a cure for your curiosity

TABLE OF CONTENT

CHAPTER 1

INTRODUCTION: A BRAIN SYSTEM FOR ASSEMBLING COGNITIVE STRUCTURES

What is the brain basis of human intelligence? A working definition of human intelligence is the ability to solve novel and complex problems like solving algebra, building a house, playing football, cooking and writing stories. What is common among these examples is how each complex activity consists of fragments of thought and behaviour, carefully organized or structured according to the organism's needs. How then does the human central nervous system support such complex behaviour? Scientific evidence has divided the human brain into multiple biological systems serving, for example, vision, movement, language and homeostasis (Kandel et al. 2013). If all of these different systems worked independently, we would not be able to conceive of any form of organized thought or behaviour. Over the past century, neuroscience research has made several long strides in understanding how each system works. And we are just beginning to understand how they work together and the consequences of a breakdown in their communication.

This thesis investigates a brain system that has previously been proposed to play a critical role in coordinating complex brain activity. Over the past 20 years it has been referred to as the task-positive, cognitive control, domain-general, fronto-parietal, attention, executive control or Multiple-demand (MD) system (Cole and Schneider 2007; Duncan 2010; Petersen and Posner 2012; Fedorenko et al. 2013; Di and Biswal 2014; Hugdahl et al. 2015; Marek and

Dosenbach 2018). During my medical training a surgeon once taught us that if there are numerous surgery names to solve one problem it probably means that none of these approaches are fully addressing the problem. Each of the previous labels for this brain system stem from different theoretical frameworks about how brain operations are organized. And each theoretical account drags behind it a set of incomplete experimental evidence due to limitations in the technologies used in human neuroscience research. My PhD training coincided with major advancements in non-invasive brain imaging based on Magnetic Resonance Imaging (MRI) methods developed by the international team of the Human Connectome Project (HCP) (Glasser, Smith, et al. 2016). In this thesis I capitalize on these MRI advancements to reveal novel findings about the anatomical and functional organization of this brain system. Further, using unique electrophysiological data from invasive neurosurgeries in human patients, the thesis also reveals novel electrophysiological properties that should constrain the potential neural mechanisms operating in this brain system. These findings, I argue, offer a common ground for reconciling the different theoretical frameworks and experimental findings and pave a path forward for accumulating experimental knowledge about the system's fundamental operations.

Critically, I hope this thesis emphasises the fact that to understand any single brain function one needs a map of its components, how they are connected and their functional properties. Even in simple neural circuits consisting of a handful of neurons, it is impossible to infer the circuit's anatomical structure from just measuring changes in the circuit's output to a varying input. This is due to the potential existence of parallel pathways that can give rise to identical observations (Marder 2015). Yet, discovering the anatomical connectome is only the first step because different combinations of the physiological properties of its neurons can give rise to several mechanisms that can identically account for the observed data (Marder 2015). This thesis manages to uncover bits of both the anatomical and functional organization of a complex system in the adult human brain. While much remains unknown, it opens an important door for a new phase of understanding how complex brain activity is organized.

In the first part of this chapter, I review a recent theoretical proposal (Duncan 2013; Duncan et al. 2020) about how human behaviour during complex tasks can be reconceptualised around a core process of building computational or

cognitive structures that guide intelligent behaviour. Then I review existing experimental evidence for a brain system supporting such a process, surveying brain lesions, non-invasive brain imaging and invasive electrophysiological studies. I then discuss how traditional brain imaging methodologies have held back progress in understanding the system's operations and introduce the novel HCP brain imaging techniques and their potential to transform our understanding of brain macroscale organization. I finally describe the remaining structure of this thesis.

Before starting, the ubiquity of the complex term "cognition" in this thesis necessitates giving it an operational definition. In non-biological studies, cognition is used to refer to the mind, mental operations, thoughts or knowledge. Planning your day is cognition. Remembering yesterday's events is cognition. In biological studies, cognitive signals are defined as physiological signals that are difficult to interpret or directly relate to experimental variables such as a stimulus or an action. Neural spikes during a temporary period of remembering recent information are cognitive signals. In my use of the word cognition throughout this thesis, I lean towards defining it using Alan Newell's analogy (Newell 1973):

> *"The problem of determining what control system is used by the human is analogous to determining what machine language is used by a computer, given that you can never see any written code, but only the outputs of running programs."*

So the terms "cognition" or "cognitive" in this thesis can be thought of as referring to the unreadable scripts guiding human behaviour.

1.1 The theory: assembling cognitive structures

Complex systems like the brain force us to divide any explanation of its functions into multiple levels. On its own, the substantial complexity of neurobiology makes it considerably difficult to comprehend the functions of biological systems from the bottom up. Theoretical frameworks, or top-down views, are thus essential guides through the biological jungle (Marr and Poggio

1977). Much of our theoretical frameworks about brain function were developed based on studying animal and human behaviour. And as empirical neurobiological findings are discovered, theories are pruned, edited or replaced by better ones.

Students of animal and human behaviour have long documented that, despite its seemingly complex nature, behaviour can be fragmented into simpler pieces. For example, some of fish or bird behaviour has been described through fixed action patterns, also known as the innate-release mechanisms (IRMs), which are hard wired programs, or sequence of behaviours, triggered by internal or external stimuli (Tinbergen 1951; Lorenz 1970). On the contrary, human thoughts and behaviours are hardly fixed, yet still breakable into fragments (Miller et al. 1960; Luria 1966). Writing a novel is one example of how infinite creativity results from different combinations of specific finger and hand movements, vocabulary, grammatical rules and memories. These same behavioural fragments can be used to guide cooking a meal. And one can flip back and forth between writing and cooking. Thus, this conception of behavioural fragments demands from them to be organized through some form of a plan or a program (Miller et al. 1960; Luria 1966; Newell 1990).

Importantly, any complex system capable of flexible behaviour must be equipped with an equally flexible set of heuristic programs, or meta-plans, capable of assembling new programs to support its flexibility (Miller et al. 1960; Luria 1966; Newell 1990). For example, our ability to solve the following arithmetic problem (985 + 632 x 3) is highly unlikely to be based on selecting the correct answer from an infinitely large storage of all possible answers of all possible arithmetic combinations. This would be a very inefficient way to learn and solve problems. Instead specific addition and multiplication rules are applied to solve the problem. This reasoning can be extended to almost all aspects of human behaviour, sparing the automated reflexes. For example, speech is the product of putting together words in an appropriate structure based on syntactic and grammatical rules (and social rules when the situation is more complex). Thus, rules, heuristic programs or meta-plans are fundamental components of flexible behaviour.

1.1.1 A heuristic program: segment and integrate

What heuristic programs, then, support human flexibility in solving complex problems? When it comes to finding patterns in human behaviour, a fundamental finding is that performance on almost all kinds of cognitive abilities tend to positively correlate with each other (Spearman 1927). Put in other words, good performance on any task tends to predict similarly good performance on almost any other task. This finding has been termed the positive manifold (Spearman 1904). The simplest, and still the most powerful, model to explain these correlations suggests that all cognitive abilities share a common general factor (g) (Spearman 1904, 1927). More interestingly, novel and complex problems were found to be the best predictors of performance on a diverse range of other tasks. Performance on such problems has been labelled fluid intelligence and Raven's Progressive Matrices are one example of these tasks (Raven 1982). Could it be that matrix tests are measuring a fundamental component of human behaviour, a heuristic program, which is equally important for all other tasks?

In classical symbolic artificial intelligence (AI) systems, numerous heuristic programs were developed for problem solving. But those most ubiquitous and powerful converged on a common strategy: decomposing a problem into simpler solvable fragments. For example, Newell, Simon and Shaw designed a heuristic program that was capable of solving problems in logic, chess and trigonometry. The heuristic was called the "means-ends analysis", which solves a problem in a sequence of sub-problems (Newell 1990). It went something like this: (1) Search if this problem can be solved using a currently existing program (2) If not, search if this problem can be transformed in a way that reduces the difference between the current state and the desired state and apply it (3) Repeat step 1. With each loop, the problem is gradually decomposed and becomes easier to solve. This general strategy of decomposing a problem – in a sense creating a goal-subgoal hierarchy - has been successfully employed to solve numerous complex problems from navigating mazes (Sacerdoti 1974) to planning everyday errands (Hayesroth and Hayesroth 1979). It has also been recently highlighted as a major potential missing architecture to allow modern deep learning AI systems to generalize their successes to new tasks (Russin et al. 2020).

Could a similar heuristic – segmenting a problem into a sequence of sub-problems – support human problem solving abilities as well? A recent experiment investigated this using two versions of the matrix problems (Duncan et al. 2017). In the first version, the matrix problem was simplified to zone in on the ability to segment (**Figure 1.1a**). To minimize any confounds related to working memory (the temporary capacity to store and manipulate information) participants drew their answers in the response box as they solved each step of the matrix. Despite the simplicity of this format, participants with low fluid intelligence scores (measured using an independent test) performed poorly (**Figure 1.1c, blue dots)**. In the second version, the same matrix problems were pre-segmented i.e. participants were now required to solve just one sub-problem at a time (**Figure 1.1b**). This time, all participants performed well (**Figure 1.1c, red dots)**. Thus segmentation must be a core strategy for human complex problem solving.

But this story is incomplete without recognizing the other face of the segmentation coin: integration. Think about Newell's means-end analysis program solving one step in a chess game, for example, deciding on the best move to protect the king. This goal must be linked with the rules of the game, the current arrangement of the pieces on the board, the values of each piece, all embedded within an overall structure of goals (in this case it was a five goal program with king safety as the first goal). Thus the *step exists as* rules, pieces, values all linked through an algorithm or a computational structure. In other words, the step existed as "arrays of memory that can be manipulated by computations *that do not depend on the specific content stored there*" (Russin et al. 2020). Similarly, consider what it would take to solve just one step in the matrix problem (**Figure 1.1a**): there is the feature (e.g. an arrow), comparing it with other features, in other boxes, and the overall concept of solving a matrix problem, all integrated in a cognitive structure (Duncan 2013, 2020).

Thus, this process of assembling a computational or cognitive structure – through segmentation and integration, henceforth referred to as attentional integration [after (Duncan et al. 2020)] - underscores a fundamental operation in problem solving. Beyond solving matrix problems, attentional integration plausibly plays a core role in all aspects of human behaviour. For example, think about someone wanting to travel to Japan. This high-level goal cannot directly

control what the person would do with their right hand. Instead, the goal is broken into a series of hierarchical sub-goals of flying, buying a plane ticket, accessing a website, moving a mouse. The problem space now is much constrained and the latter sub-goal is capable of controlling the hand movement (**Figure 1.2**). In the following section, the different theoretical frameworks on cognitive control are assessed from the point of view of the attentional integration process.

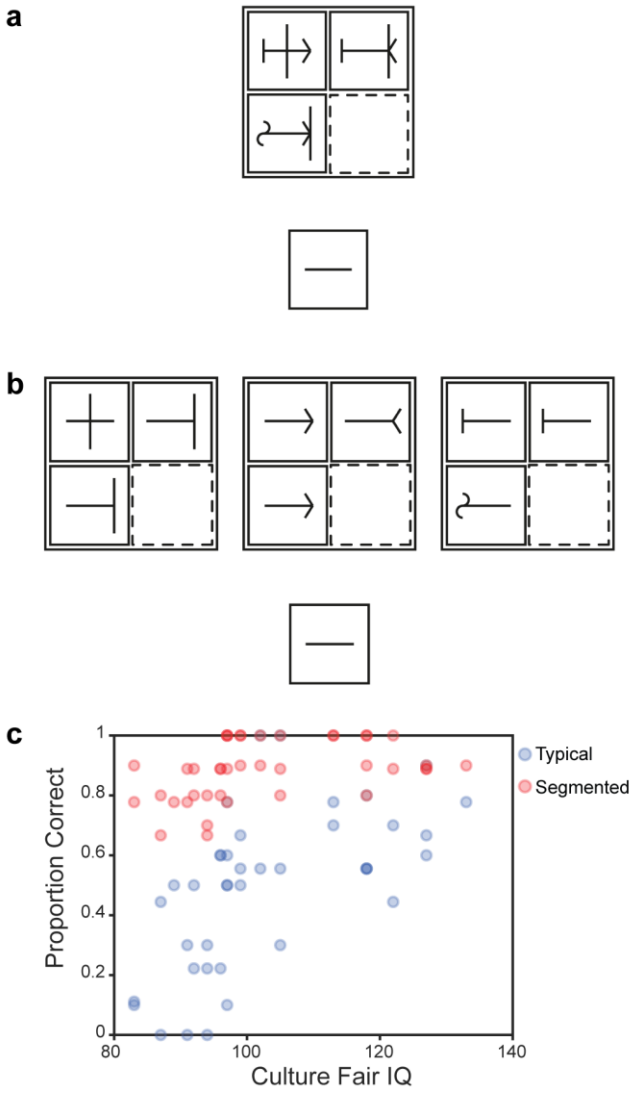

Figure 1.1 (a) Example of a typical simplified matrix problem. Participants were asked to complete the empty box by "making it look right". One strategy, for example, would be to identify the features that changed between both columns in the top row, and use this knowledge to fill in the missing box in the bottom row. Answers were to be drawn in the allocated response box, where a horizontal line was drawn as a common core to simplify solving the problem (b) The same matrix problem now segmented into the three separate steps required to solve the problem (c) Scatter plot of each subject's fluid intelligence score vs their performance on the typical (blue) and segmented (red) matrix problems. Note how performance improved markedly on the segmented problems.

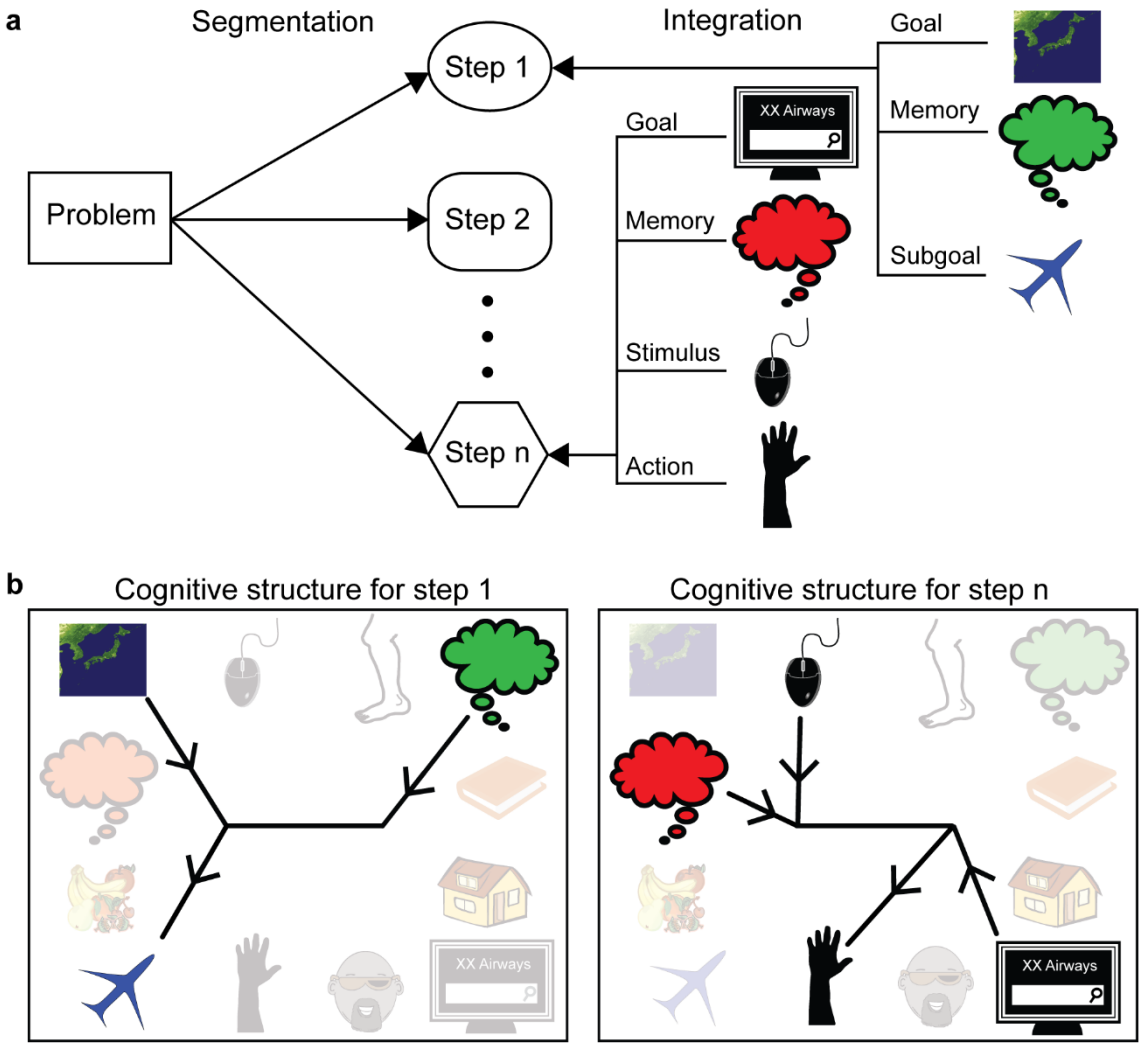

Figure 1.2 The attentional integration heuristic illustrated through an example task of booking a flight ticket to travel to Japan. (a) In this task, the complex problem is segmented it into a series of steps (step 1: set goal to travel to japan; step n: use a computer to book the ticket online). With each step solved, the task becomes progressively simpler to solve. Attention to each step means integrating its relevant components into a computational or a cognitive structure (b) A detailed illustration of each step's cognitive structure: Here only the relevant components are bound together into a computational sequence. Arrows towards horizontal line suggest inputs to the structure, arrows away suggest outputs of the computational sequence.

1.1.2 Theoretical accounts of cognitive control

Numerous models were proposed to account for how cognition is organized and controlled. The different frameworks, while on their own addressing important aspects of cognition, are often hard to reconcile into a unified account. In this section, some of the relevant cognitive control models are assessed through the eyes of assembling cognitive structures. The intention is not to provide a detailed unified theory of cognitive control but to offer a broad lens through which the different models can be viewed.

One of the most common accounts of cognitive control emphasises its hierarchical nature (Lashley K.S. 1951; Miller et al. 1960; Newell 1990; Cooper and Shallice 2006; Badre 2008). In the previously mentioned example of travelling to Japan, the complex problem was divided into a hierarchy of goals and sub-goals. In classical hierarchical models, routine actions like finger tapping are conceptualized as lower-level units at the bottom of the hierarchy (Cooper and Shallice 2000). This is because finger tapping can be used flexibly in different behaviours such as clicking on a mouse, typing on a keyboard etc… However, some investigators argued that purely hierarchical representations were not capable of dealing with quasi-hierarchical structures (Botvinick and Plaut 2004). To borrow from the previous example on finger tapping, how should a hierarchical model represent the finger tapping routine if it is to be used multiple times at different steps if it is only represented at the lowest levels? Botvinick and Plaut (2004) demonstrated that a recurrent neural network with one layer was capable of solving this problem, not using hierarchical modelling, but through distributed representation of the task sequences in the network units. An obvious limitation to their account is that such a connectionist model would lack the flexibility needed for novel planning or problem solving. Specific hierarchical solutions were proposed to solve such a problem (Cooper and Shallice 2006). However, the concept of a cognitive structure offers a simpler and a more flexible solution. As shown in **Figure 1.2,** a cognitive structure is created for each level (step). And each cognitive structure is capable of recruiting the relevant components (finger tapping) flexibly without relegating certain components to lower levels. From this point of view, any routine or cognitive operation can be utilized flexibly for any step of solving the problem.

Another influential cognitive control model that is tightly linked to fluid intelligence is working memory (WM) (Baddeley and Hitch 1974; Baddeley 2012). The WM model first proposed by Baddley and Hitch offered an account of two memory systems for the temporary storage of information, namely phonological and visual memory (Baddeley and Hitch 1974), overseen by a central executive. Some proposals promoted the capacity of these storage systems (WM capacity) as a core component in cognitive control (Engle 2002). However, as shown in the previous section, such accounts would fail to explain the poor performance on the simplified matrix problems (**Figure 1.1**) (Duncan et al. 2017). Similar accounts of WM maintenance and resistance to distraction (Kane and Engle 2002), can be considered as useful properties of a cognitive structure but not a heuristic program capable of assembling one.

Several proposals were put forward to understand the central executive or cognitive control in terms of focused, divided or selective attention (Norman and Shallice 1986; Duncan et al. 1997; Baddeley 2012). For example, Norman and Shallice (1986) viewed human behaviour to be guided by competing automatic processes and when they conflict, a set of controllers would use attention to favour or bias some automatic processes over others. Not surprisingly, distraction to attention leads to significant drops in problem solving performance (Robbins et al. 1996). But is attention itself a program? There is a subtle difference between conceiving of attention as a method to select vs the process that decides what information to select. If attention is to be viewed as a program, then current models of attentional control have fallen short on explaining the control part. More appropriately, accounts of attentional (or top-down) bias fit as a property of a heuristic program. From the point of view of attentional integration, *attention is* the cognitive structure with its different elements linked.

A different kind of model fractionates cognitive control into processes such as set shifting, updating and inhibition (Miyake et al. 2000; Friedman and Miyake 2017). It seems reasonable to consider such processes as fundamental programs required for controlling behaviour. For example, any flexible system would require a method to update its content or inhibit an unwanted automated action initiated by an environmental trigger. However, on their own, how far can such simple programs be used to explain the diversity of human behaviour? These proposals are broadly similar in spirit to factorial fractionations of the g

factor (Thomson 1939). In Thomson's model, correlations in performance between diverse tasks are conceived as fractionated specialized programs that are shared between tasks. These fractionations raise a critical question about the processes organizing them. A common explanation put forward is that complex behaviour is an "emergent property" of these interacting factors (Courtney 2004; Postle 2006). According to this view, in complex systems, when internal biases are coupled with external inputs, complex behaviour "emerges". A property that is larger than the smaller pieces of the system. However, "emergence" does little to explain or predict useful properties in a complex system. Upon closer scrutiny it is possible to conceive of all these fractionated processes as different programs utilized by a heuristic program assembling the different steps of a behaviour. This would provide another way to interpret why these fractionations still highly correlate with each other. In fact, such a conception predicts that more fractionations could be found as long as the tests that heavily load on the relevant program are used for behavioural assessment.

Before moving to the next section on neurobiology, a common criticism to the presented "assembly of cognitive structures" framework is that behaviour is too complex to be accounted for by one process. An interesting analogy put forward compares the quest to find a core process behind *g* factor to the quest of finding a single explanation for physical fitness (Kievit et al. 2012). Loosely defined, physical fitness obviously depends on the efficient performance of several biological systems (cardiovascular, musculo-skeletal, respiratory, metabolic etc…). Thus it seems unlikely that it could be accounted for by a single process. This analogy is important because it certainly highlights that the success of a heuristic program in assembling a cognitive structure will also depend on the integrity of its components such as long-term memory systems, the systems processing online inputs or motor output etc…. A deficit in any one of these will affect the overall cognitive structure. However, the analogy with physical fitness is subtly misplaced because the program for a physical activity is fixed: a muscle contracts, needs more blood oxygen, the heart pumps more blood, oxygen is exchanged through the lungs etc… From this point of view a "physical fitness *g*" is the fixed sequence of events just described. A calf muscle will not pump blood or exchange oxygen with the environment. However, the thoughts and behaviours produced by the brain are essentially infinite and a

fixed program cannot account for such flexibility. Thus, some programs must have an inherent flexibility and be heuristic in nature. It remains an open question whether more heuristic programs could account for other aspects of human behaviour.

In summary, heuristic programs are essential building blocks for flexible behaviour of complex systems like the brain. A process of attentional integration accounting for solving complex problems in a series of cognitive structures was reviewed and compared to existing models of cognitive control. The next section explores the experiments that are starting to reveal the neurobiological mechanisms that could account for such a process.

1.2 The neurobiology: a Multiple-demand brain system

Where and how could cognitive structures be assembled by the brain? The limitations of any single neuroscience methodology force a complementary approach combining insights from different methodologies. This section explores findings from patients with brain damage, non-invasive brain imaging of healthy adult humans and invasive electrophysiology studies in human patients and non-human primates (NHPs).

1.2.1 Insights from patients with brain damage

Candidate regions for the assembly of cognitive structures are ones which if damaged would be associated with widespread disorganization in behaviour. Early studies highlighted that damage to the frontal lobes rendered patients incapable of performing simple tasks which consisted of a sequence of actions (Luria 1966; Duncan 1986; Shallice and Burgess 1991). For example, when a frontal lobe patient was asked to prepare a meal, the steps necessary for its preparation were preserved (e.g. slicing, pouring etc…) but their order was disturbed, suggesting a deficit in making a plan for the separate actions (Schwartz et al. 1991). Modern brain imaging methods have allowed

neuropsychology studies, the enterprise of detailed examination of patients with brain damage, to provide a crisper picture of brain regions associated with disorganized behaviour. First, not all frontal lobe regions cause the same behavioural deficits (Glascher et al. 2012; Warren et al. 2014; Woolgar et al. 2018). Second, quantitative assessments of behaviour link poor executive functions and fluid intelligence scores to a distributed set of localized frontal and parietal regions: around premotor cortex, middle frontal gyrus, dorso-medial prefrontal cortex (PFC), the intra-parietal sulcus and its surroundings and the insular cortex (Glascher et al. 2010, 2012, Woolgar et al. 2010, 2018; Warren et al. 2014).

Studies assessing the effect of subcortical or cerebellar damage on executive functions are less common. A recent study associated lesions in the medio-dorsal thalamus with deficits in executive functions (Hwang et al. 2020). Cerebellar lesions were also associated with executive functions disturbances; however, a quantitative assessment of anatomical locations of such lesions is currently lacking (Gottwald 2004; Schweizer et al. 2008).

Thus evidence points to a distributed set of fronto-parietal, subcortical and cerebellar regions as likely candidates for a brain system for assembling cognitive structures. However, a critical neuroanatomist might object to these conclusions. Their main concern would be that the typical patients involved in the previous studies suffer from extensive, rather than localized, damage and this raises several confounds. First, cortical damage is likely to extend beyond the cortical mantle into the underlying white matter tracts which do not necessarily carry local information. In other words, the location of the damage might disrupt the transfer of information between distant areas which might be the ones related to the cognitive operation of interest. Unfortunately lesion studies rarely take into account the contribution of white matter damage on the observed behavioural deficits, partly because a clear characterization of white matter tracts is lacking in MRI scans and is not routinely incorporated into the neuropsychology analysis pipelines. One recent study assessed the contribution of every brain voxel on *g* deficits and the voxels with the largest effects where localized in the white matter the authors characterized to belong to the superior longitudinal, arcuate and uncinate fasciculi (Glascher et al. 2010). These tracts connect major frontal, parietal and temporal regions, significantly blurring the

resolution needed to make meaningful conclusions. That said, this study confirms that *g* depends on communication between widely distributed brain regions. The second concern relates to the finer grained resolution of damage to the cortical mantle. Cyto-architectural, electrophysiological and functional MRI (fMRI) studies of the cortex divide frontal and parietal association areas into numerous neighbouring areas, with sharp functional boundaries (Van Essen and Glasser 2018). Lesions, especially due to vascular incidents like stroke, are especially large and might engulf multiple functionally distinct regions. Thus typical lesion studies might only be able to broadly point to large territories of interest. But a finer-grained spatial resolution is needed for a tighter grasp on the possible brain regions related to the assembly of cognitive structures. The following section digs deeper to reveal a crisper picture of the relevant functional territories.

1.2.2 Insights from functional MRI

1.2.2.1 A primer on functional MRI

Since its introduction as a tool to the fields of psychology and neuroscience around 25 years ago, functional MRI (fMRI) has played a major role in advancing our understanding about the diverse properties of different brain regions. FMRI is presently the only method available for non-invasively measuring whole brain activity with an inherent spatial resolution of around 3-5 mm (Turner 2002). Before delving into the insights it has provided us, it is worth clarifying the type of brain signals it measures and how it relates to neural activity. Its premise is built on indirectly measuring neurophysiological properties through their effect on blood flow. Blood oxygen level dependent (BOLD) is the most common signal measured with fMRI. An over simplified account of BOLD is that an increase in local physiological activity (excitatory, inhibitory or non-neural in origin) will lead to vasodilation of local arterioles followed by a rush of oxygenated blood to meet the metabolic demands. This rush of oxygenated blood sweeps away deoxygenated blood which leads to an increase in the strength of the signal measured (Buxton et al. 1998). Critically, the relation between neural activity and vascular effects, neuro-vascular

coupling, is complex and not completely understood (Logothetis 2008; Drew et al. 2020). That said, several studies converge on a decent overlap between simultaneous measures of neural activity, recorded invasively in animals or humans, and the BOLD signal. Local increases in neural spiking rate in primary sensory or motor regions were correlated with increases in BOLD signal. But there is also evidence that BOLD signal correlates better with local field potentials (LFPs), the voltage changes due to all ionic movements within a local area (Logothetis et al. 2001; Nir et al. 2007; Logothetis 2008; Engell et al. 2012; Hermes et al. 2012). Further, BOLD fMRI is capable of identifying the somato-topic organization of the somato-sensory cortex and retinotopic organization of the visual cortex (Glasser, Coalson, et al. 2016). In a further demonstration of its neuroanatomical precision, an epileptic patient with implanted invasive electrodes, first underwent a fMRI scan to identify brain regions that selectively increase their BOLD activity in response to faces in the fusiform cortex. After the patient was implanted with electrodes along the fusiform cortex, sending electrical stimuli through the contacts that overlapped with fMRI activated regions, but not the contacts nearby, disrupted the patient's perception of faces (Parvizi et al. 2012). These results thus demonstrate that fMRI is capable of providing insights into the functional organization of the brain. An important limitation to keep in mind, besides that BOLD fMRI is an indirect measure of neural activity, is its slow temporal resolution. Vascular changes occur in the order of seconds (peaking at around 5-7 seconds after an impulse response) while neurophysiological activities rapidly change within a few milliseconds (Logothetis 2008; Drew et al. 2020).

1.2.2.2 Co-activations to multiple task demands

How might fMRI help to find the brain regions related to the assembly of cognitive structures? One obvious approach is to scan participants while they perform a novel and complex problem, like the Raven matrices. Such experiments revealed localized regions in bilateral lateral PFC, parietal and occipito-temporal regions (**Figure 1.3a)** (Prabhakaran et al. 1997; Duncan 2000).

If indeed activations during fluid intelligence tasks reflect a core mechanism common in all behaviour, another obvious litmus test is to investigate the spatial distribution of activations common to many other cognitive tasks. An early meta-analysis highlighted activation foci from diverse tasks (perceptual difficulty, working memory, response conflict, task novelty, verbal episodic memory retrieval) clustered in specific regions along the lateral and medial PFC (Duncan and Owen 2000). In the 20 years that followed, thousands of fMRI studies have identified a similar pattern of co-activated regions along similar frontal and also parietal regions. These tasks included working memory (Gray et al. 2003; Owen et al. 2005; Chein et al. 2011; Fedorenko et al. 2013; Engelhardt et al. 2019), task switching (Yeung 2006; Vallesi et al. 2015; Engelhardt et al. 2019), response inhibition (Wager et al. 2005; Hampshire et al. 2010; Dodds et al. 2011), selective attention (Corbetta et al. 1998; Gitelman et al. 1999; LaBar et al. 1999), episodic memory retrieval (Nyberg et al. 2003; Wagner et al. 2005), verb generation (Dosenbach et al. 2006; Tremblay and Gracco 2006), language control (Hervais-Adelman et al. 2015; Jackson 2020), math (Amalric and Dehaene 2016, 2017), theory of mind (Koster-Hale and Saxe 2011), learning a new task (Niv et al. 2015) and many more (Hugdahl et al. 2015). A reasonable summary from this overwhelming number and diversity of tasks is that contrasting almost any type of complex cognitive demand with a simpler demand was bound to illuminate some sort of fronto-parietal activations.

To investigate whether these activations were really overlapping and not just nearby activations that are blurred together, a conjunction of activations from 7 different hard vs easy cognitive demands found overlapping fronto-parietal regions at the single voxel level (Fedorenko et al. 2013). This study helped sharpen the spatial locations of these co-activations: along anterior and middle frontal gyrus, premotor cortex, anterior insula, anterior cingulate, intraparietal sulcus and occipito-temporal regions (**Figure 1.3b**). This set of regions, henceforth, will be referred to as the Multiple-demand (MD) system [after (Duncan 2010, 2013)] reflecting their co-activation by multiple cognitive demands. MD activity is not limited to the cortex only. Subcortical and cerebellar MD activity have long been recognized but less frequently investigated. For example, the Fedorenko et al study noted caudate, thalamic and

cerebellar hotspots (Fedorenko et al. 2013). Invasive animal studies have long implicated subcortical regions in cognitive control [e.g. (Halassa and Kastner 2017)]. However, the lack of a careful characterization of MD subcortical activations has held back progress in this field.

Taken together, thousands of fMRI studies converge on a specific set of cortico-subcortical MD regions that co-activate across a diverse set of cognitive demands.

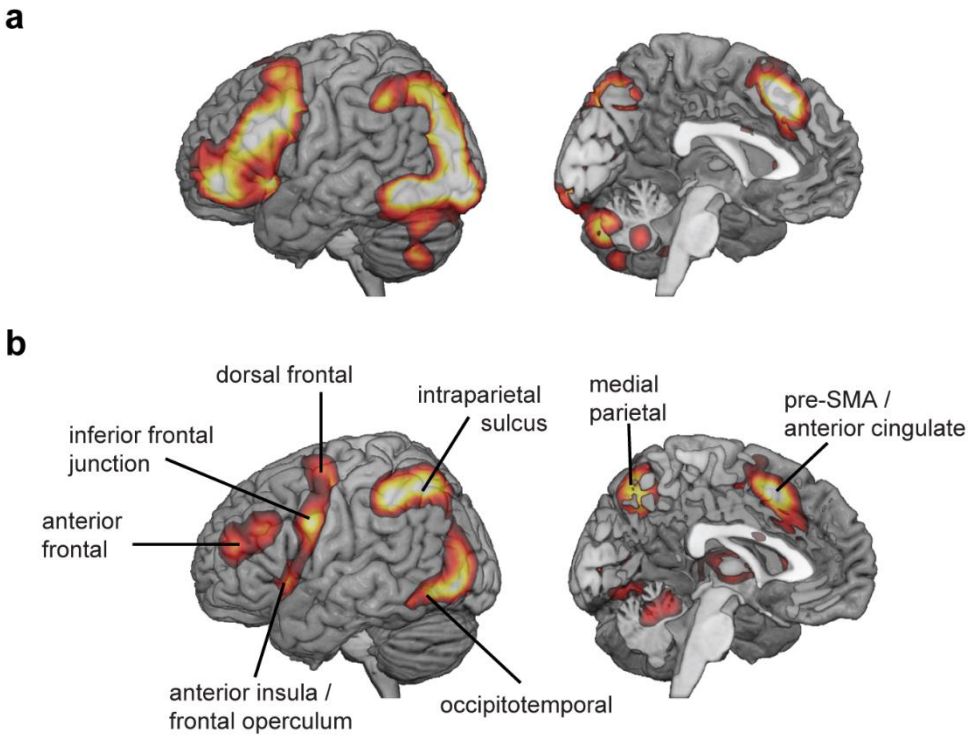

Figure 1.3 (a) Left hemisphere activation t-map associated with a standard test of fluid intelligence (similar to Duncan et al 2000). Similar activity is also seen on the right. Unpublished data, N = 252, threshold t > 11. (b) MD pattern (beta activations) obtained by averaging activations across 7 hard vs easy contrasts. Bilateral activity was similar hence here activations have been averaged across hemispheres and projected onto the left. Adapted from Fedorenko (2013).

1.2.2.1 Functional and structural connectivity

An important question is whether, despite strong and replicable co-activations, MD regions should be conceived of as a functional network? To investigate this, the field turned to analysing resting-state fMRI (rfMRI) data. This involves measuring time-series correlations between different brain regions during a "resting" period (i.e. lying silently in the scanner performing no active task). Such studies converged on a similar set of fronto-parietal regions characterized by stronger time-series correlations with each other more than with other cortical regions (Cole and Schneider 2007; Dosenbach et al. 2007; Power et al. 2011; Yeo et al. 2011a). This set is commonly known as the fronto-parietal network (FPN) and includes subcortical and cerebellar components (Buckner et al. 2011; Ji et al. 2019). However, careful comparison of the spatial overlap between rfMRI FPN and task fMRI MD activations is currently lacking (see chapter 2).

A limitation of rfMRI findings is that they neither provide direct evidence of connectivity between MD regions nor do they provide information on the directionality of the connections. Yet understanding the structural connectome is vital for a clearer understanding of the MD system's architecture. Invasive tracer injections in NHPs remain the "gold standard" for structural connectome studies. A recent tour-de-force series of studies mapping areal connections in monkeys revealed that cortical connections are much more dense (~70% of all possible connections do exist) than previous estimates (~45%) (Markov et al. 2013). This high-density architecture is inconsistent with current graph theoretical small-world conceptions which emphasise path lengths as a critical feature of the connectome. However, in high density connectomes, path lengths are already pre-determined by the connection density. Instead, the critical feature of the network is related to connection weight strengths, with a special emphasis on weak connections (Markov et al. 2013). Further probing feedforward vs feedback connections, the studies revealed a dual cortical counter-stream architecture across cortical layers (Markov et al. 2013). Put simply, two pairs of feedforward and feedback streams were discovered, one pair running in superficial cortical layers and the other pair in deeper layers. These findings were synthesised to propose a new hierarchical "bow-tie" cortical architecture which predicts the existence of a highly densely connected cortical core (~92%)

through which both feedforward and feedback connections pass (Markov et al. 2013) (**Figure 1.4**).

These findings are broadly consistent with proposals of a "global workspace" for information transformation and exchange (Dehaene et al. 1998). Further, in line with the proposal in this chapter, a cortical core is considered an essential ingredient for a complex system to be able to assemble flexible cognitive structures. Critically, the predicted cortical core consists of distributed cortical areas across frontal, parietal and temporal cortices. That said, cross-species comparisons are a work in progress (Mars et al. 2018) as well as non-invasive tractography using diffusion MRI in humans which remains limited (Van Essen et al. 2014). The structural connectome of MD regions remains one of the most important challenges for a proper understanding of the system's architecture and function.

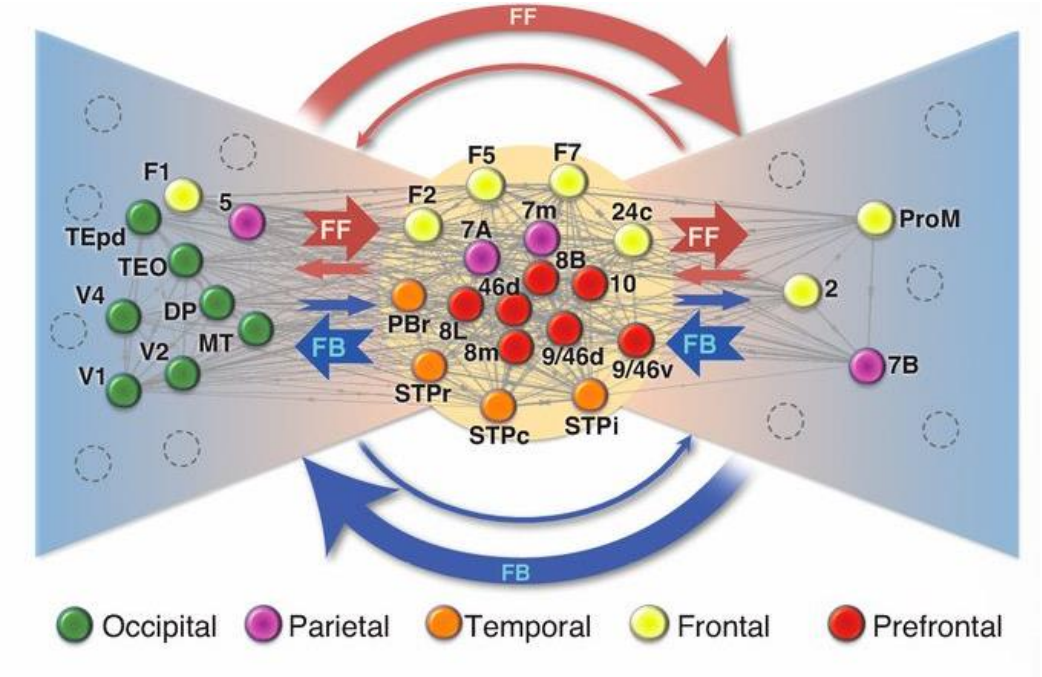

Figure 1.4 A bow-tie representation of the graph of 29x29 cortical areas. The dense core is shown in the middle. The left wing mostly sends feedforward signals, while the right wing sends feedback signals. From Markov et al 2013.

1.2.2.2 Control signals and functional preferences

A complementary approach when searching for regions related to cognitive structures is to look for specific control-related signals. The findings from this approach have ranged from finding uniform signals across MD regions or differential signals fractionating MD regions into subsystems. However, such functional dissociations are often interpreted in modular conceptions, leaving open questions regarding the accuracy of their spatial distribution and co-localization with other signals. This section explores some of these control signals and their relation to the MD activation pattern.

An important control signal is related to the assembly of cognitive structures. This could be triggered, for example, by starting a new task. This is also referred to as configuring a task set. Experiments have commonly probed this by isolating signals related to presenting a task cue. Traditionally, cue activations were found to especially activate dorsal portions of frontal and parietal MD regions, which were separately grouped into a dorsal attention network (DAN) (Corbetta and Shulman 2002). However, better powered fMRI studies showed that cue activations extend beyond DAN and overlap with all major MD regions including the insula and anterior frontal regions (Dosenbach et al. 2006). DAN was also proposed as the source of top-down attentional signals (Corbetta and Shulman 2002). Again, this formulation is inconsistent with studies showing that top-down attention engages all MD regions (Corbetta et al. 1998; Barch et al. 2013). Another control signal is related to updating the task set or cognitive structure. In one study, new task rules were introduced every 10 seconds, which corresponded with phasic responses of MD regions (Dumontheil et al. 2011), suggesting a role for MD regions in updating the ongoing cognitive structure.

Task completion is another important event that should be associated with disassembly of a cognitive structure or the assembly of a new one (the theory predicts that a cognitive structure should always be in operation) (Miller et al. 1960). This has traditionally been investigated through tasks that involve target detection. Indeed, the moment of target detection elicits strong activity across MD regions (Hampshire et al. 2008) which could be linked to strong attentional demands of target detection (Duncan 1980). Studies have also explicitly probed

signals related to event boundaries, such as finishing subtasks or whole tasks (Farooqui et al. 2012; Wen et al. 2020). For example, a recent study scanned participants while they completed a series of steps towards a final goal (e.g. cooking). As participants progressed through the task, MD activity ramped up, and the completion of every step (like chopping or boiling) elicited strong MD phasic responses (Wen et al. 2020).

An influential cognitive control model proposed the existence of at least two systems: a lateral fronto-parietal system (FPN) related to moment-to-moment processing of task requirements and a cingulo-opercular system (CON) related to task set maintenance (Dosenbach et al. 2006, 2008). The spatial overlap between these proposed systems and the MD system until recently has not been directly investigated (see chapter 2). However, it is clear that this conception refuses to recognize grouping insular or medial PFC components together with lateral fronto-parietal components into one system. Critically, this division was based on failing to find sustained activity in fronto-parietal regions during task execution. Instead, the most prominent fronto-parietal signals were transient ones related to task cues and error trials. However, these results conflict with overwhelming evidence that lateral fronto-parietal regions, as well as medial PFC and insular regions, sustain their activity during various cognitive demands (Dumontheil et al. 2011; Soreq et al. 2019; Wen et al. 2020). More recent finer-grained studies based on rfMRI suggest that separate regions within insular and medial PFC belong to FPN and CON networks, as will be discussed in more detail in chapter 2 (Yeo et al. 2011a; Ji et al. 2019; Assem et al. 2020). These findings leave the question open regarding the functional role of the CON.

In summary, MD regions show a diversity of control signals related to the assembly of cognitive structures. That said, the blurry spatial resolution of most fMRI studies (see below Neuroimaging 2.0) has held back consensus on whether functional dissociations (Hampshire et al. 2012; Lorenz et al. 2018) overlap with MD regions or reflect nearby non-MD regions.

1.2.2.3 Adaptive activation patterns

Another expected property from cognitive structures is flexibility: as behavioural needs change, the ongoing control structure adapts by binding contents that are

relevant to current purposes. Delving deeper into fine-grained activation patterns indeed revealed that MD patterns dynamically change to reflect current behaviourally-relevant content such as stimulus features, rules, goals, actions etc… (Woolgar et al. 2011; Erez and Duncan 2015; Shashidhara et al. 2020; Wen et al. 2020). For example, a recent experiment asked participants to solve a hierarchical task such as making a stew. During the task, participants had to choose a pre-learned order of steps (e.g. making a stew: take food from fridge, wash vegetables etc…). The study revealed that MD activation patterns reliably represented the step information, thus reflecting MD involvement in representing online-task information (Wen et al. 2020). And a recent review of multi-variate pattern analysis studies across the whole brain over the past 20 years highlighted that MD activation patterns represent the most diverse types of task features (Woolgar et al. 2016).

A common finding with MD activation patterns is that as task difficulty increases, the behavioural context is more easily decodable from MD activation patterns (Woolgar et al. 2011, 2015; Etzel et al. 2020). One explanation suggests this reflects a sharpening of the representation of task information, which facilitates its readout by downstream neurons. However, most previous experiments probed MD patterns on a block-by-block basis (i.e. averaging activity over several trials). In an interesting task switching experiment tracking trial-by-trial activation patterns, it was found that MD context representation was *weaker* on the initial switch trials (Qiao et al. 2017) then later recovered to reflect the new task rules. Further, the weakness of MD context representations correlated with longer switch reaction-times. While this might seem counter-intuitive, the moment of a switch trial requires re-assembling a different cognitive structure for the new context. This aligns well with univariate evidence of weaker MD activity at the moment of target detection in participants with low fluid intelligence (Tschentscher et al. 2017).

These findings collectively suggest that the strength of MD activations and the sharpness of their representations reflects the fidelity of the formed cognitive structure.

1.2.3 Insights from electrophysiology

Electrophysiological data are vital to understand the rapid temporal dynamics hidden behind the slow fMRI signal as well as to bring insight into neural mechanisms underlying the assembly of cognitive structures. As discussed in the previous section, an important property of cognitive structures is to be able to flexibly represent changing task content. The fine-grained fMRI activation patterns in MD regions showed such a property. Similar observations were made from recording neural spikes from MD regions in humans. For example, a recent study showed that firing rates in dorso-medial PFC represent information about which task a person was performing (a memory recall vs categorization) (Minxha et al. 2020). Interestingly, on a trial-by-trial basis, the moment of switching from one task to another was associated with inability to decode task information. This finding aligns well with the fMRI study tracking trial-by-trial MD patterns discussed in the previous section (Qiao et al. 2017). These two findings provide converging evidence of a process reflecting a reconfiguration of the on-going cognitive structure.

Not only do MD firing patterns change across tasks but within task phases. Numerous recordings from potentially homologous MD regions in NHPs show that correlations between neural firing patterns between task steps can reflect the hierarchical structure of the task (Sigala et al. 2008). Importantly, such correlations are generally weak and often orthogonal. For example, a recent study has shown that neural firing patterns in lateral frontal and parietal putative MD regions during choice and feedback phases of a complex task were orthogonal (**Figure 1.5a)** (Kadohisa et al. 2020).

But what neural ingredient might support these observations? Studies characterize neurons in these putative MD regions with non-linear conjunctions of task events (Mante et al. 2013; Rigotti et al. 2013; Stokes et al. 2013; Naya et al. 2017). This property was termed “mixed selectivity” and while neurons with such properties have been observed across several brain regions such as hippocampus and amygdala (McKenzie et al. 2014; Saez et al. 2015), they are especially abundant in higher association areas. For example, **Figure 1.5b** shows the responses of a neuron in ventro-lateral PFC of a NHP to the same stimulus during different contexts (cue 1 and 2). Clearly the neuron is responding to a specific stimulus but only during cue 1 (top).

How might mixed selectivity and adaptive dynamics play a role in binding the relevant behavioural content? One proposed mechanism from a computational perspective states that mixed-selectivity neurons increase the "dimensionality" of the possible conjunctions between the task events. In other words, randomly connected neurons will allow a greater potential for different signals to mix (Fusi et al. 2016). These "high dimensional" representations can then be easily read out if downstream neurons are conceived as linear classifiers. Another proposed mechanism is that the initial activity state of putative MD neurons will route an incoming input through a context-dependent trajectory towards a decision activity state (**Figure 1.5c**) (Stokes et al. 2013). This suggests that the initial activity state reflected a structure binding the target input with the behavioural decision. Importantly, in this study there was no anatomical differentiation between the neurons coding for the context, input stimulus or decision. These findings suggest potential mechanisms through which mixed-selectivity neural properties can build flexible cognitive structures.

Collectively, electrophysiological studies are beginning to find structure in the complex and adaptive dynamics that characterize responses in putative MD regions. It is important to note again that without information about the underlying structural connectome of the recorded circuits, countless mechanisms could account for the observed recordings (Marder 2015). Like fMRI studies, invasive electrophysiology studies usually report findings in the form of broad anatomical terms such as "the vicinity of the arcuate sulcus". As numerous studies in both humans and NHPs have shown, the cytoarchitectural, functional and connectivity features of these regions are anything but homogenous (Van Essen and Glasser 2018). One of the rare studies that recorded neural firing rates across much of the monkey cortex simultaneously, during a simple delayed-matching task, confirmed widely different neural dynamics in nearby patches of the cortex (Dotson et al. 2018). These details become increasingly important with the growing trend of analysing signals from populations of neurons or "population dynamics" (Vyas et al. 2020). What a group of electrodes is reading out from a cortical patch could reflect artifactual dynamics if the downstream neural connections are not reading out information in the same way. For example, the frontal eye field (FEF), a popular region to record from, was found to consist of overlapping yet functionally distinct populations of neurons, one

active during saccades and the other involved in covert shifts of attention (Thompson et al. 2005; Schafer and Moore 2007). An experiment blind to these distinct populations, yet grouping their responses in a "population code" might lead to false conclusions. Thus, it is imperative to improve our understanding of the anatomical and functional properties and consider accurate cross-species mapping techniques.

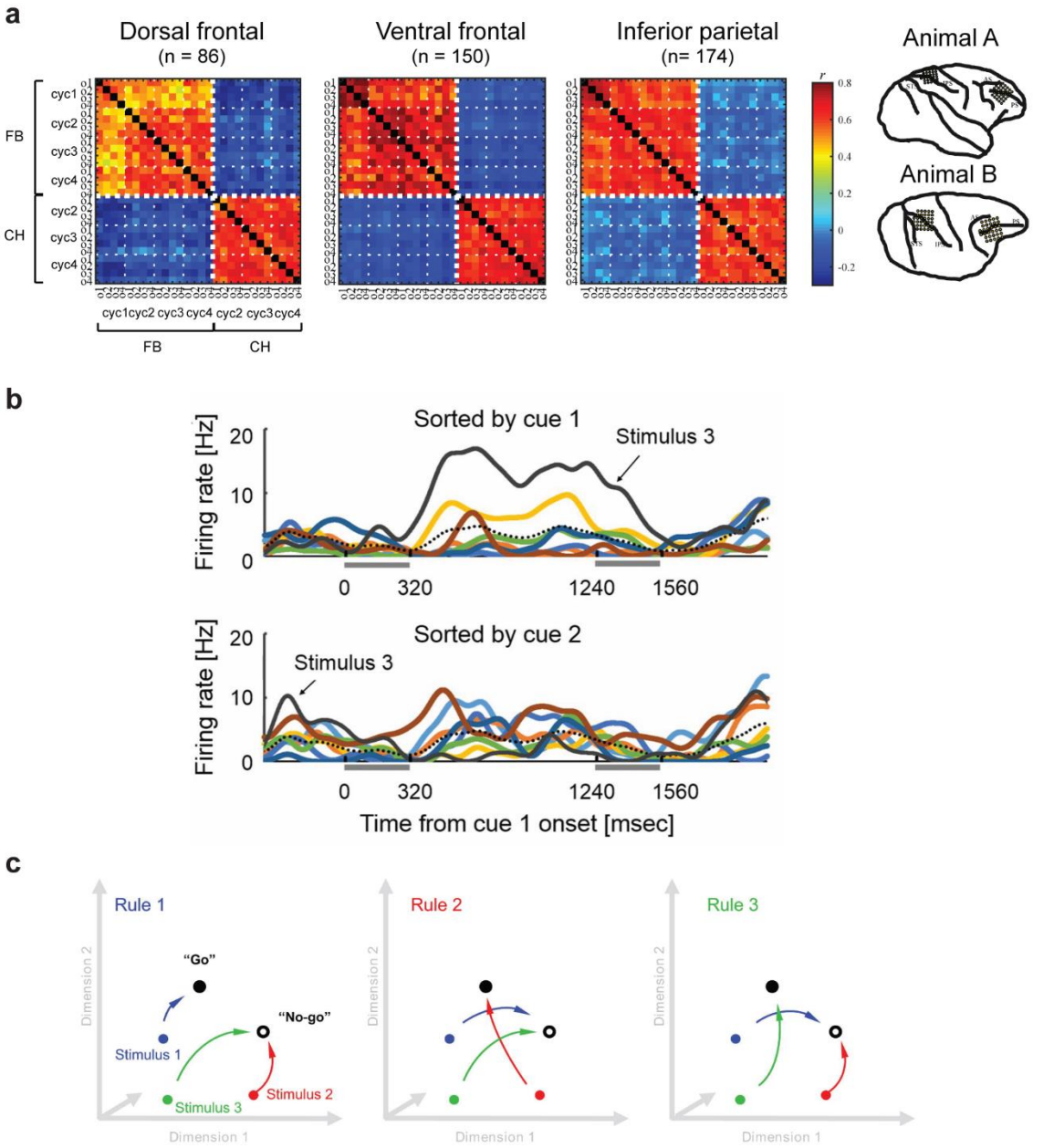

Figure 1.5 (a) Pearson correlation of population firing rates during feedback (FB) and choice (CH) periods. Recording areas in each monkey are shown on the right. Adapted from Kadohisa et al 2020. (b) Responses of an example ventro-lateral PFC neuron to the

same stimulus (stimulus 3) preceded by cue 1 (top) and cue 2 (bottom). Note that the neuron responds to a conjunction of the stimulus and the cue. Adapted from Naya et al 2017 (c) A schematic of the observed trajectories. Each rule is matched to a target stimulus (e.g. rule 1 for stimulus 1) and each rule will guide its corresponding stimulus to the relevant behavioural decision (Go or no-go). From Stokes et al 2013.

1.3 Neuroimaging 2.0

Thousands of brain imaging studies over the past two decades have helped identify major functional territories of the brain such as the MD pattern. Most of these studies, however, have followed a traditional pipeline that has significantly held back progress in finer spatial localization in brain function by as much as 65% from what could be achieved using state-of-the-art approaches (Coalson et al. 2018) **Figure 1.6a**. Such traditional pipelines use low-quality scans and volumetric based processing which do not conform to brain geometry. For brain alignment, the go to approach is to match a subject's brain to a template scan [such as the Montreal Neurological Institute (MNI)]. This matching or normalization process is heavily based on using cortical folds as guiding features. However, empirical evidence shows that cortical folds are highly variable across individuals, even across twins, and especially in higher association areas (Glasser, Smith, et al. 2016). This is compounded by the fact that the MNI template is approximately 37% larger than the average human brain leading to biologically unrealistic distortions and blurring of signal (Glasser, Smith, et al. 2016). Prior to statistical analysis, functional images are further blurred using unconstrained volumetric smoothing which leads to mixing signals between regions close in 3D Euclidean space but far in 2D geodesic space (e.g. at opposing sides of a sulcus). In cases of excessive smoothing (e.g. 8 mm FWHM, a common smoothing value in studies), brain anatomy is completely distorted (**Figure 1.6b**). And statistical thresholds for functional images are based on arbitrary cut-offs that do not necessarily align with known underlying neurobiological features. Region of interest (ROI) analysis often defines cortical areas as homogenous spheres of arbitrary sizes. These limitations and others are extremely important to recognize as they make it

exceedingly difficult to localize brain functions and relate it to the underlying neurobiology.

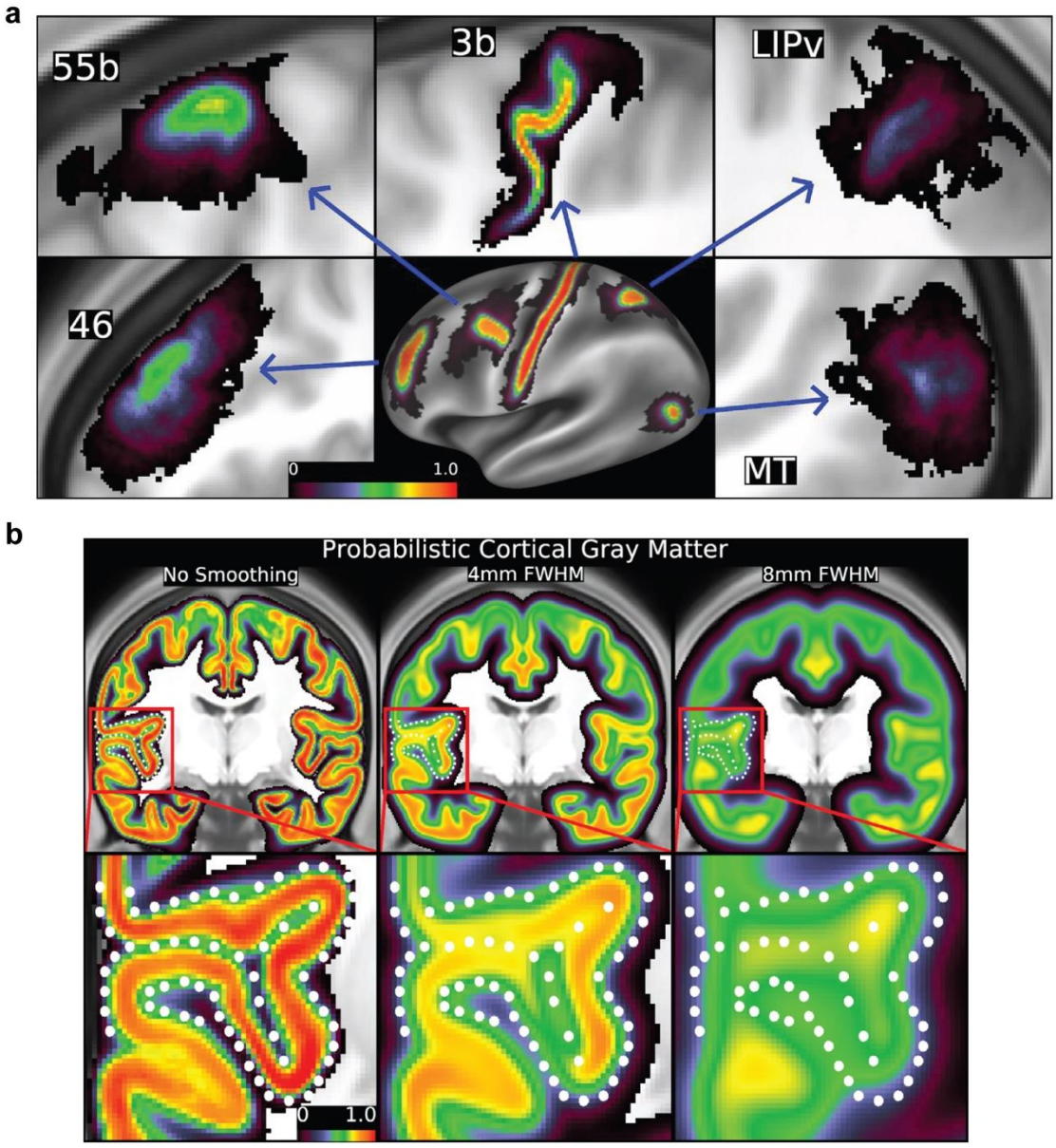

Figure 1.6 (a) A comparison of alignment of a representative sample of cortical areas across subjects between the novel HCP approach (cortical surface) and traditional volumetric approach (surrounding insets). The cortical areas were defined for each individual on the surface using HCP pipelines based on neurobiologically grounded multi-modal MRI criteria (Glasser et al 2016). Areas were then transformed back to each individual's volumetric space and re-aligned using a traditional volumetric pipeline. Note how the probability cortical areas overlaps across subjects after volumetric alignment is much worse than after HCP areal feature based alignment (b) A demonstration of how unconstrained volumetric smoothing distorts cortical anatomy, mixes signals across sulci and from white matter. Both figures from Coalson et al 2018.

To address these limitations, the Human Connectome Project (HCP) has developed a neuroimaging approach based on seven core tenets: *"(i) collect multimodal imaging data from many subjects; (ii) acquire data at high spatial and temporal resolution; (iii) preprocess data to minimize distortions, blurring and temporal artifacts; (iv) represent data using the natural geometry of cortical and subcortical structures; (v) accurately align corresponding brain areas across subjects and studies; (vi) analyze data using neurobiologically accurate brain parcellations; and (vii) share published data via user-friendly databases."* (Glasser, Smith, et al. 2016). These advances are detailed extensively elsewhere (Glasser et al. 2013; Uğurbil et al. 2013; Glasser, Smith, et al. 2016; Van Essen and Glasser 2018) and will be expanded upon throughout the thesis wherever relevant.

Here I would like to highlight one important advancement related to the surface-based alignment of cortical regions based on cortical areal features. Since cortical folds proved to be unreliable landmarks for brain alignment, the HCP turned to more reliable cortical features such as myelin maps and areal patches defined based on resting state functional connectivity. This approach was dubbed multi-modal surface matching (MSM) (Robinson et al. 2014, 2018). **Figure 1.7a** demonstrates an earlier version of MSM (Robinson et al. 2014) on task fMRI activation clusters using each modality separately for alignment (cortical folds, myelin, resting-state). Importantly, a frontal hotspot that was not apparent using MSMsulc (folding-based) alignment is now maximally highlighted using MSM resting-state alignment. **Figure 1.7b,c** demonstrates the results from a newer version of MSM that was capable of using multiple modalities for alignment (MSMAll). Again the results demonstrate superiority over traditional folding based approaches.

Collectively, the new HCP approach opens the door for a new phase in the field of neuroimaging that is bound to reveal novel findings for neuroanatomical localization of brain functions.

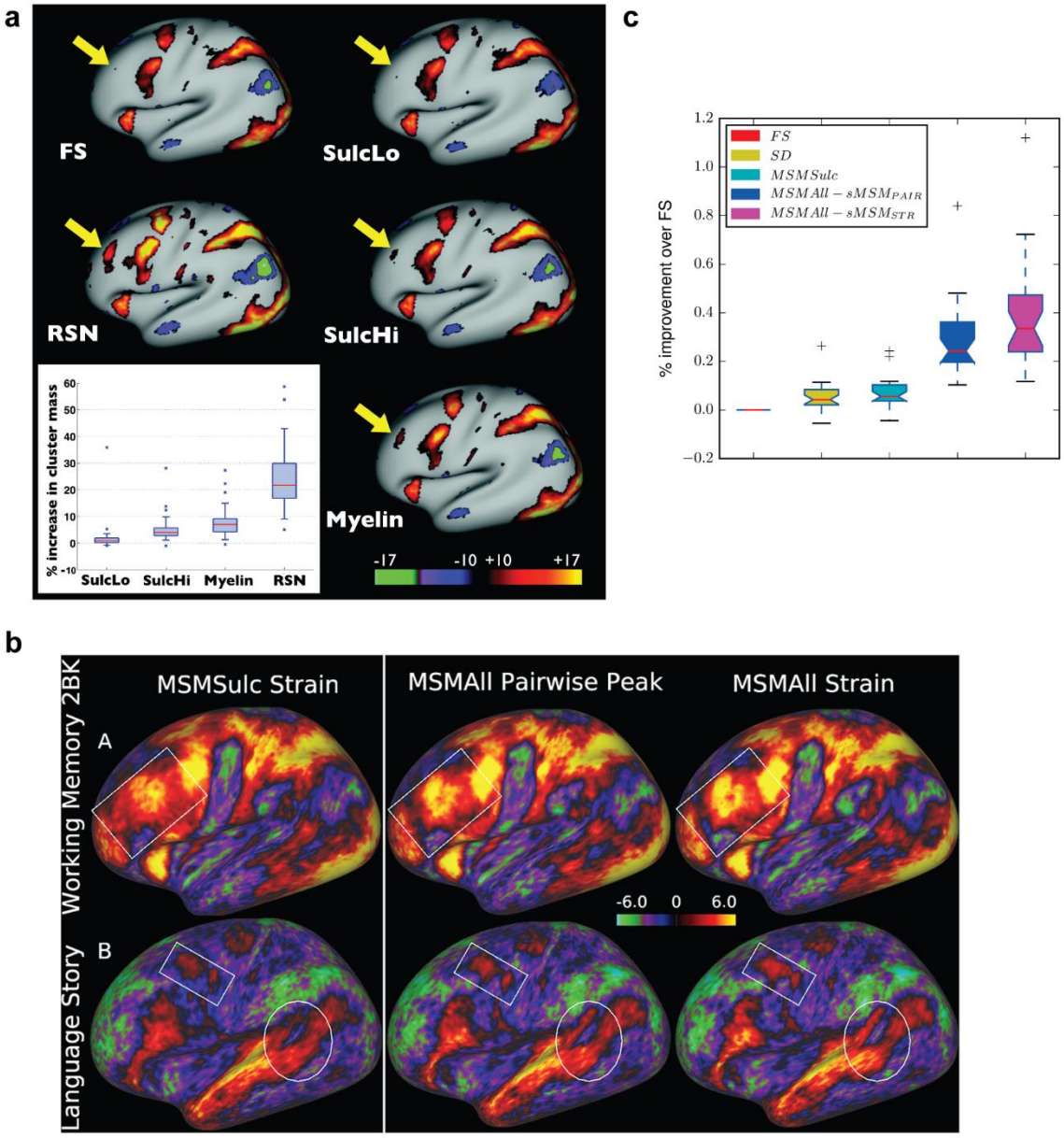

Figure 1.7 (a) Comparison of different MSM surface alignment methods on task fMRI cluster size (z-statistic maps) (FS: free surfer, SulcLo: sulcal features with low constraints, SulcHi: sulcal features with high constraints, Myelin: using myelin maps calculated as the T2w/T1w ratio, RSN: resting-state networks). Note the frontal hotspot (yellow arrow) which becomes more visible as more reliable and granular areal features are used for alignment. Adapted from Robinson et al 2014. (b) Comparing results (z-statistic maps) of a newer version of the MSM algorithm between MSMSulc and two algorithms for MSMAll. Note crisper and stronger activations in MSMAll over MSMSulc (boxes and circles). (c) Bar chart quantifying % improvement task fMRI cluster sizes across HCP task categories using different alignment algorithms over and above the standard freesurfer algorithm. (b) and (c) adapted from Robinson et al 2018.

1.4 Thesis structure

Armed with the state-of-the-art HCP neuroimaging methods, chapter 2 looks at the conjunction of activations related to three cognitive demands across a cohort of hundreds of HCP subjects. The aim of the project was to improve the anatomical and functional description of MD regions based on the HCP methods and in relation to a ground breaking recent multi-modal parcellation of the human cerebral cortex (Glasser, Coalson, et al. 2016). Chapter 3 investigates one example of putative MD functional dissociations highlighted in the literature. Specifically, this chapter investigates sensory-modality preferences of the MD system using matched auditory and visual versions of a working memory task. Chapter 4 attempts to map MD regions using electrophysiological data acquired by electrocorticography from human patients undergoing awake neurosurgeries. This aim of this experiment is to find links between findings from fMRI and electrophysiology as well as identify a potentially useful signal for expanding clinical intraoperative mapping into the domain of cognitive control. Chapter 5 discusses how the results from the three experiments cast the MD system in a new light. Future directions with HCP-style experiments will also be discuss.

CHAPTER 2

A DOMAIN-GENERAL COGNITIVE CORE DEFINED IN A MULTIMODALLY PARCELLATED HUMAN CORTEX

2.1 Introduction

Thought and behaviour can be conceptualized as complex cognitive structures within which simpler steps are combined to achieve an overall goal (Miller et al. 1960; Luria 1966; Newell 1990). Each step or cognitive episode involves a rich combination of relevant external and internal inputs, computations, and outputs, assembled into the appropriate relations as dictated by current needs. Theoretical proposals have long emphasized that any system capable of such behaviour must be equipped with a flexible control structure that can appropriately select, modify and assemble each cognitive step on demand (Norman and Shallice 1986; Duncan et al. 1997; Dehaene et al. 1998; Baddeley 2000; Duncan 2001, 2013; Miller and Cohen 2001; Rigotti 2010).

In line with a system's role in organizing complex cognition, selective damage to specific regions in the frontal and parietal cortex is associated with disorganized behaviour (Milner 1963; Luria 1966; Norman and Shallice 1986), including significant losses in fluid intelligence (Duncan et al. 1995; Glascher et

al. 2010; Roca et al. 2010; Woolgar et al. 2010, 2018; Warren et al. 2014). Numerous functional neuroimaging studies converge on a similar set of frontal and parietal regions that are co-activated when performing a diverse range of cognitively demanding tasks, including selective attention, working memory, task switching, response inhibition, conflict monitoring, novel problem solving and many more (Duncan and Owen 2000; Dosenbach et al. 2006; Cole and Schneider 2007; Fedorenko et al. 2013; Hugdahl et al. 2015). We refer to this network as the multiple-demand (MD) system, reflecting their co-recruitment by multiple task demands (Duncan 2010, 2013; Fedorenko et al. 2013). MD activation is commonly reported in lateral and dorsomedial prefrontal cortex, in the anterior insula, and within and surrounding the intraparietal sulcus, with an accompanying activation often reported near the occipito-temporal junction.

Fine-grained activation patterns in MD regions encode many kinds of task-relevant information, including stimulus features, goals, actions, rules and rewards, suggestive of flexible representations shaped by current cognitive requirements (for a recent comprehensive review see (Woolgar et al. 2016)). Consistent with these data from human studies, single-cell studies of putative MD regions in the alert macaque monkey show dynamic, flexible, densely-distributed encoding of information relevant to a current task (Duncan 2001; Miller and Cohen 2001) in which single neurons often show “mixed selectivity”, or nonlinear response to conjunctions of multiple task features (Miller and Cohen 2001; Sigala et al. 2008; Rigotti et al. 2013; Stokes et al. 2013; Fusi et al. 2016; Naya et al. 2017). We and others have proposed that MD regions lie at the heart of cognitive integration, selecting diverse components of cognitive operations across multiple brain systems and binding them together into appropriate roles and relations (Cole and Schneider, 2007; Duncan 2010, 2013**;** Miller and Cohen 2001; Fusi et al. 2016). Indeed, the MD activation pattern is frequently revealed by studies either employing a task with integrative demands (Prabhakaran et al. 2000) or studies employing a theory-blind search for brain regions with integrative properties, most commonly through indices of connectivity with other brain regions (Power et al. 2013; Shine et al. 2016; Gordon et al. 2018).

While MD activation has been reported since the early days of human brain imaging (Duncan and Owen 2000), a consensus is lacking over five core

questions. (i) What is the precise extent and topography of MD regions in human cortex and their relation to other immediately adjacent regions that have very different functional properties (e.g. see Fedorenko et al. 2012)? (ii) What is the degree of functional differentiation within the MD network? There are many rival proposals and little agreement across studies (Champod and Petrides, 2010; Dosenbach et al., 2007; Hampshire et al., 2012; Lorenz et al., 2018; Yeo et al., 2015). (iii) What is the precise relationship to "canonical" resting-state fMRI (rfMRI) brain networks revealed by various ways of grouping regions based on the strength of their time-series correlations? A "fronto-parietal network" (FPN) shows strong anatomical similarity with MD activations (Power et al. 2011; Yeo et al. 2011a; Blank et al. 2014; Laumann et al. 2015; Ji et al. 2019), but a finer examination of its overlap with MD activations and relations with other networks is currently lacking. (iv) What are the links – long suspected but rarely examined in detail – with accompanying MD activation in regions of the basal ganglia, thalamus and cerebellum (Buckner et al. 2011; Choi et al. 2016; Halassa and Kastner 2017)? (v) What are the correspondences with putative cortical MD regions identified in other primates (Ford et al. 2009; Mitchell et al. 2016; Premereur et al. 2018)?

Our understanding of these and other aspects of MD function will surely benefit from improved anatomical localization. MD activation has often been described in terms of large, loosely-defined regions such as "dorsolateral prefrontal cortex" that also include regions having very different functional responses and sharp transition boundaries (Glasser, Coalson, et al. 2016). Traditional fMRI analysis methods typically use non-optimal inter-subject registration and apply substantial smoothing, both of which blur across functional boundaries. While problems of this sort may be offset by individual-subject region of interest (ROI) methods, for many questions consensus ROIs are lacking, limiting comparison and integration of results across studies.

To address these issues, we turned to the large-scale data and novel analysis approach of the Human Connectome Project (HCP). To improve delineation of functional regions, HCP analyses used high quality multimodal MRI features (cortical thickness, myelin content, rfMRI connectivity, task fMRI activation), along with surface-based analysis methods (Glasser et al. 2013; Glasser, Smith, et al. 2016; Coalson et al. 2018) and new areal-feature-based

registration algorithms (Robinson et al. 2014, 2018). Here we relate MD activation to the state-of-the-art multi-modal HCP parcellation of human cortex into 360 regions (180 per hemisphere), in which areal delineations were derived using overlapping multi-modal criteria, and areas were named to reflect correspondences with the neuroanatomical literature.

We analysed data from 449 HCP subjects, each having a defined individual-specific cortical parcellation. Our analysis was based on three suitable fMRI task contrasts available in the HCP data: working memory 2-back versus 0-back (WM 2bk>0bk), hard versus easy relational reasoning (Relational H>E), and math versus story (Math>Story). The first two are standard hard>easy contrasts as commonly used to define MD activation (Duncan and Owen, 2000; Fedorenko et al., 2013; e.g. for n-back MD activation: Gray et al., 2003; Owen et al., 2005; e.g. for reasoning MD activation: Duncan, 2000; Watson and Chatterjee, 2012). Math>Story was added because previous results show a strong MD-like activation pattern associated with arithmetic processing (Amalric and Dehaene 2016, 2017). For working memory and relational reasoning, stimuli were visual, whereas for Math>Story, stimuli were auditory. The other four HCP tasks lacked typical MD contrasts and were not used. Combining data from the 3 task contrasts, we determined which areas show MD properties and examined their functional profiles, patterns of resting state connectivity, and relations to subcortical structures.

Our results reveal an extended, largely symmetrical MD network of 27 cortical areas, distributed across frontal, parietal and temporal lobes. We divide this extended MD system into a core of 10 regions most strongly activated and strongly interconnected, plus a surrounding penumbra, and we relate this functional division to canonical resting state networks also derived from HCP data (Ji et al. 2019). Across the extended MD system, activation profiles for our 3 task contrasts suggest a picture of substantial commonality, modulated by modest but highly significant functional differentiations. MD activation, and strong functional connectivity with the cortical MD core, are also identified in several subcortical regions. Our results define a highly specific, widely distributed and functionally interconnected MD system, which we propose forms an integrating core for complex thought and behaviour.

2.2 Materials and Methods

2.2.1 Subjects

The analysed dataset consisted of 449 healthy volunteers from the Human Connectome Project (HCP) S500 release. Subjects were recruited from the Missouri Twin Registry (186 males, 263 females), with age ranges 22-25 (n=69), 26-30 (n=208), 31-35 (n= 169), and 36+ (n=3). Informed consent was obtained from each subject as approved by the institutional Review Board at Washington University at St. Louis.

2.2.2 Image Acquisition

MRI acquisition protocols have been previously described (Glasser et al. 2013; Smith et al. 2013; Uğurbil et al. 2013). All 449 subjects underwent the following scans: structural (at least one T1w MPRAGE and one 3D T2w SPACE scan at 0.7 mm isotropic resolution), rfMRI (4 runs X 15 minutes), and task fMRI (7 tasks, 46.6 minutes total). Images were acquired using a customized 3T Siemens 'Connectom' scanner having a 100mT/m SC72 gradient insert and using a standard Siemens 32-channel RF receive head coil. Whole brain rfMRI and task fMRI data were acquired using identical multi-band EPI sequence parameters of 2 mm isotropic resolution with a TR=720 ms. Spin echo phase reversed images were acquired during the fMRI scanning sessions to enable accurate cross-modal registrations of the T2w and fMRI images to the T1w image in each subject (standard dual gradient echo fieldmaps were acquired to correct T1w and T2w images for readout distortion). Additionally, the spin echo field maps acquired during the fMRI session (with matched geometry and echo spacing to the gradient echo fMRI data) were used to compute a more accurate fMRI bias field correction and to segment regions of gradient echo signal loss.

2.2.3 Task Paradigms

Each subject performed 7 tasks in the scanner over two sessions. In the current study we analyzed data from 3 tasks: working memory (performed in session 1),

math/language and relational reasoning (performed in session 2). Subjects performed 2 runs of each task. The following task details are adapted from Barch et al. (2013) on HCP fMRI tasks.

Working Memory: Each run consisted of 8 task blocks (10 trials of 2.5 s each, for 25 s) and 4 fixation blocks (15 s each). Within each run, 4 blocks used a 2-back working memory task (respond 'target' whenever the current stimulus was the same as the one two back) and the other 4 used a 0-back working memory task (a target cue was presented at the start of each block, and a 'target' response was required to any presentation of that stimulus during the block). A 2.5 s cue indicated the task type (and target for 0-back) at the start of the block. On each trial, the stimulus was presented for 2 s, followed by a 500 ms ITI. In each block there were 2 targets, and (in the case of the 2-back task) 2–3 non-target lures (repeated items in the wrong n-back position, either 1-back or 3-back). Stimuli consisted of pictures of faces, places, tools and body parts; within each run, the 4 different stimulus types were presented in separate blocks. Subjects had to respond to non-targets using a middle finger press and to targets using an index finger press.

Math/language: Each run consisted of 4 blocks of a math task interleaved with 4 blocks of a story task. The lengths of the blocks varied (average of approximately 30 s), but the task was designed so that the math task blocks matched the length of the story task blocks, with some additional math trials at the end of the task to complete the 3.8 min run as needed. The math task required subjects to complete addition and subtraction problems, auditorily presented. Each trial had a problem of the form "X + Y =" or "X – Y =", followed by two choices. The subjects pushed a button to select either the first or the second answer. Problems were adapted to maintain a similar level of difficulty across subjects. The story blocks presented subjects with brief auditory stories (5–9 sentences) adapted from Aesop's fables, followed by a 2-alternative forced choice question that asked the subjects about the topic of the story. The example provided in the original Binder paper (p. 1466) is "For example, after a story about an eagle that saves a man who had done him a favor, subjects were asked, 'That was about revenge or reciprocity?'". For more details on the task, see (Binder et al. 2011).

Relational Reasoning: Stimuli were drawn from a set of 6 different shapes filled with 1 of 6 different textures. In the hard condition, subjects were presented with 2 pairs of objects, with one pair at the top of the screen and the other pair at the bottom of the screen. They were told that they should first decide what dimension(s) differed across the top pair of objects (shape or texture) and then they should decide whether the bottom pair of objects also differed along the same dimension(s) (e.g., if the top pair differs only in shape, does the bottom pair also differ only in shape?). In the easy condition, subjects were shown two objects at the top of the screen and one object at the bottom of the screen, and a word in the middle of the screen (either "shape" or "texture"). They were told to decide whether the bottom object matched either of the top two objects on that dimension (e.g., if the word is "shape", is the bottom object the same shape as either of the top two objects?). Subjects responded with their right hand, pressing one of two buttons on a handheld button box, to indicate their response ("yes" or "no"). For the hard condition, stimuli were presented for 3500 ms, with a 500 ms ITI, with four trials per block. In the easy condition, stimuli were presented for 2800 ms, with a 400 ms ITI, with 5 trials per block. Each type of block (hard or easy) lasted a total of 18 s. In each of the two runs of this task, there were 3 hard blocks, 3 easy blocks and 3 16 s fixation blocks.

2.2.4 Data preprocessing

Data were preprocessed using the HCP's minimal preprocessing pipelines (Glasser et al. 2013). Briefly, for each subject, structural images (T1w and T2w) were corrected for spatial distortions. FreeSurfer v5.3 was used for accurate extraction of cortical surfaces and segmentation of subcortical structures. To align subcortical structures across subjects, structural images were registered using non-linear volume registration to Montreal Neurological Institute (MNI) space.

Functional images (rest and task) were corrected for spatial distortions, motion corrected, and mapped from volume to surface space using ribbon-constrained volume to surface mapping. Subcortical data were also projected to the set of extracted subcortical structure voxels and combined with the surface data to form the standard CIFTI grayordinates space. Data were smoothed by a

2mm FWHM kernel in the grayordinate space that avoids mixing data across gyral banks for surface data and avoids mixing areal borders for subcortical data. Rest and task fMRI data were additionally identically cleaned up for spatially specific noise using spatial ICA+FIX (Salimi-Khorshidi et al. 2014) and global structured noise using temporal ICA (Glasser et al. 2018).

For accurate cross-subject registration of cortical surfaces, a multi-modal surface matching (MSM) algorithm (Robinson et al. 2014) was used to optimize the alignment of cortical areas based on features from different modalities. MSMSulc ('sulc': cortical folds average convexity) was used to initialize MSMAll, which then utilized myelin, resting state network (RSN) and rfMRI visuotopic maps. Myelin maps were computed using the ratio of T1w/T2w images (Glasser and Van Essen 2011; Glasser et al. 2014). Individual subject RSN maps were calculated using a weighted regression method (Glasser, Coalson, et al. 2016).

2.2.5 HCP multi-modal parcellation and areal classifier

The HCP multi-modal parcellation map (MMP) 1.0 (Glasser, Coalson, et al. 2016) was first created using a semi-automated approach utilizing the group average maps of multiple modalities (cortical thickness, myelin, resting state functional connectivity, and task activations). For each modality, the gradient was computed as the 1st spatial derivative along the cortical surface; ridges were local regions with the highest value and thus the most sudden change in a feature. Overlapping gradient ridges across modalities were used to draw putative areal borders with manual initialization and algorithmic refinement. Defined areas were reviewed by neuroanatomists, compared whenever possible to previously identified areas in the literature, and labelled. This resulted in defining 180 areas per hemisphere. A multi-modal areal classifier was then used for automated definition of areas in each subject using the multi-modal feature maps. The classifier was trained, tested and validated on independent groups of subjects from the same 449 cohort used in this study (Glasser, Coalson, et al. 2016).

2.2.6 Task fMRI analysis

Task fMRI analysis steps are detailed in Barch et al. (2013). Briefly, autocorrelation was estimated using FSL's FILM on the surface. Activation estimates were computed for the preprocessed functional time series from each run using a general linear model (GLM) implemented in FSL's FILM (Woolrich et al. 2001). For the *working memory* task, 8 regressors were used - one for each type of stimulus in each of the N-back conditions. Each predictor covered the period from the onset of the cue to the offset of the final trial (27.5 s). For the *math* task, 2 regressors were used. The math regressor covered the duration of a set of math questions designed to roughly match the duration of the story blocks. The story regressor covered the variable duration of a short story, question, and response period (~30 s). For the *relational reasoning* task, two regressors were used, each covering the duration of 18 s composed of four trials for the hard condition and five trials for the easy condition. In each case, linear contrasts of these predictors were computed to estimate effects of interest: WM 2bk>0bk, Relational H>E, and Math>Story.

All regressors were convolved with a canonical hemodynamic response function and its temporal derivative. The time series and the GLM design were temporally filtered with a Gaussian-weighted linear highpass filter with a cutoff of 200 seconds. Finally, the time series was prewhitened within FILM to correct for autocorrelations in the fMRI data. Surface-based autocorrelation estimate smoothing was incorporated into FSL's FILM at a sigma of 5mm. Fixed-effects analyses were conducted using FSL's FEAT to estimate the average effects across runs within each subject.

For further analysis of effect sizes, beta 'cope' maps were generated using custom built MATLAB scripts after moving the data from the CIFTI file format to the MATLAB workspace and after correction of the intensity bias field with an improved method (Glasser et al 2016a). Activation estimates on cortical surface vertices were averaged across vertices that shared the same areal label in a given subject. Unless mentioned otherwise, parametric statistical tests (one-sample and paired sample t-tests) were used.

2.2.7 rfMRI Functional connectivity analysis

For each subject, a 'parcellated' functional connectivity (FC) map was computed by averaging the time series across cortical vertices that shared the same areal label and correlating the average time series, giving a 360x360 cortical FC matrix for each subject.

For comparison of connection types (Figure 3b, Figure 4b), connectivities for each subject were simply averaged across each group of areas following r-to-z transformation. 1-r was used as the distance measure for the multi-dimensional scaling analysis (MATLAB function cmdscale).

Subcortical analysis was based on the group average dense FC maps for a split-half division of the subjects (210P and 210V; the parcellation and validation groups used in Glasser, Coalson, et al. 2016). For each subcortical voxel, an average connectivity to the cortical MD core was obtained by first calculating FC with each core area (after averaging across each area's vertices), and then averaging these connectivities following r-to-z transformation. A permutation testing approach (100,000 permutations) was used to identify significant voxels by building a null distribution for each voxel based on its FC estimate to sets of 10 randomly selected cortical areas across both hemispheres. A voxel was determined as significantly connected to the MD system when its FC estimate was in the top 97.5^{th} percentile.

Data availability. Data used for generating each of the imaging-based figures are available on the BALSA database (https://balsa.wustl.edu/study/B4nkg). Selecting the URL at the end of each figure will link to a BALSA page that allows downloading of a scene file plus associated data files; opening the scene file in Connectome Workbench will recapitulate the exact configuration of data and annotations as displayed in the figure.

2.3 Results

2.3.1 Cortical organization of the MD system at the group level

For an initial overview of the MD activation pattern, we calculated a group average MD map by averaging the group average beta maps of the 3 task contrasts and overlaying the resulting combined map on the HCP MMP 1.0 parcellation areal borders **(see Figure 2.1 for each contrast separately).** Group average maps were generated by aligning each subject's multi-modal maps using areal-feature-based surface registration **(**MSMAll, Robinson et al 2014; 2018**).** MSMAll registration is initialized by cortical folding patterns and then uses myelin and connectivity features to significantly improve the alignment of areas across subjects (Coalson et al. 2018**),** thus allowing us to identify cortical areas most strongly overlapping with MD activations.

The resulting overview is shown on left and right inflated cortical surfaces in **Figure 2.2a,** and on a cortical flat map of the left hemisphere in **Figure 2.2b**. The results highlight 9 patches of activation distributed across the cortical sheet. On the lateral frontal surface are four clearly distinct patches that show strong bilateral symmetry, with surrounding inactive regions: a dorsal region (patch 1), a premotor region (patch 2), a mid-frontal region (patch 3) and a frontal pole region (patch 4). Patch 5 is delineated in and surrounding the anterior insula. Tight bands of MD activation are also identifiable in dorsomedial frontal cortex (patch 6), along the depths of the intraparietal sulcus spreading up to the gyral surface (patch 7), and in dorsomedial parietal cortex (patch 8). The MD region often reported near the occipito-temporal border is also evident in posterior temporal cortex (patch 9). The right hemisphere view in **Figure 2.2a** identifies cortical areas showing the strongest MD activations.

For comparison, Figure 1c shows a previous MD group-average volumetric map generated from the conjunction of 7 hard>easy task contrasts (Fedorenko et al. 2013). Though the two maps are broadly similar, this comparison highlights the improved definition obtained with the HCP data and surface-based and areal-feature-based registration methods. Even based on these

average data, the improved co-registration of the HCP data allows clearer delineation of functional regions, as predicted by Coalson et al., 2018. Rather than broad, fuzzy swaths of MD activation, these data provide evidence for a more tightly localized, though anatomically distributed network of MD regions.

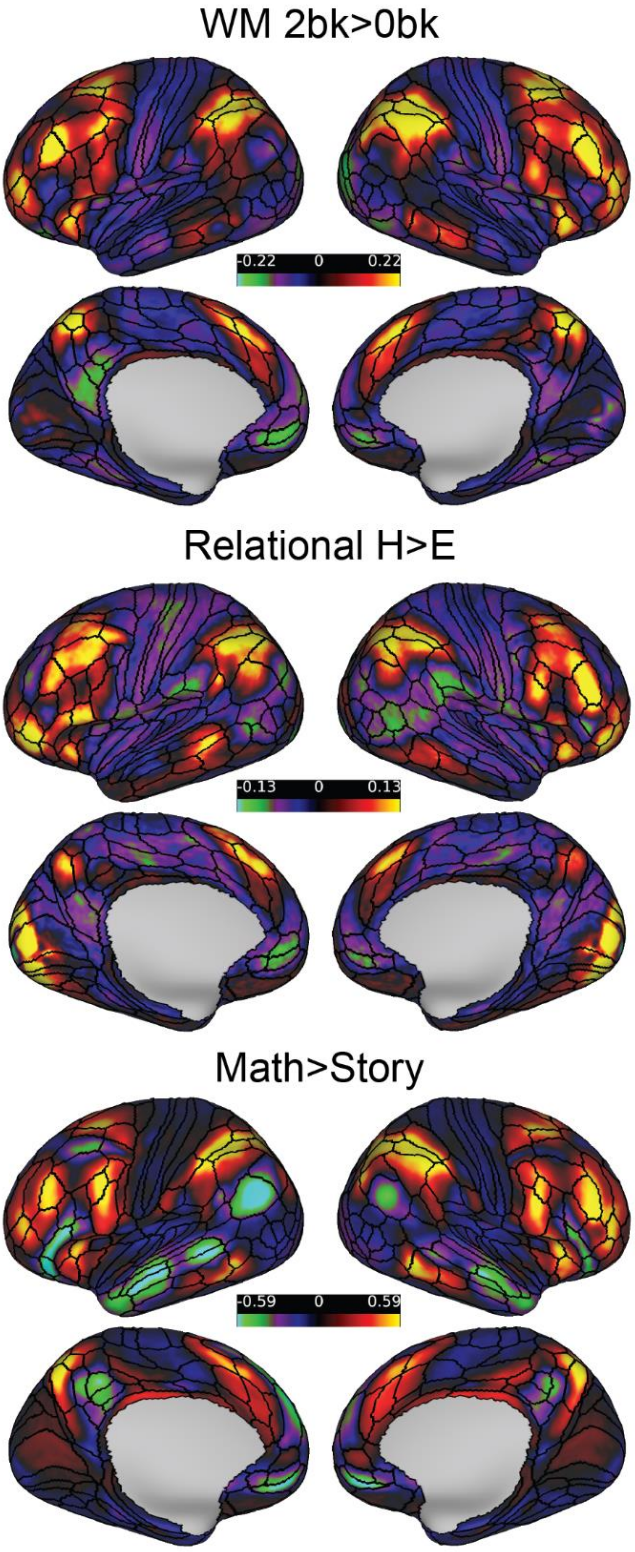

Figure 2.1 Contrast maps for each task. Activation values are beta estimates. Data available at https://balsa.wustl.edu/zp9XZ

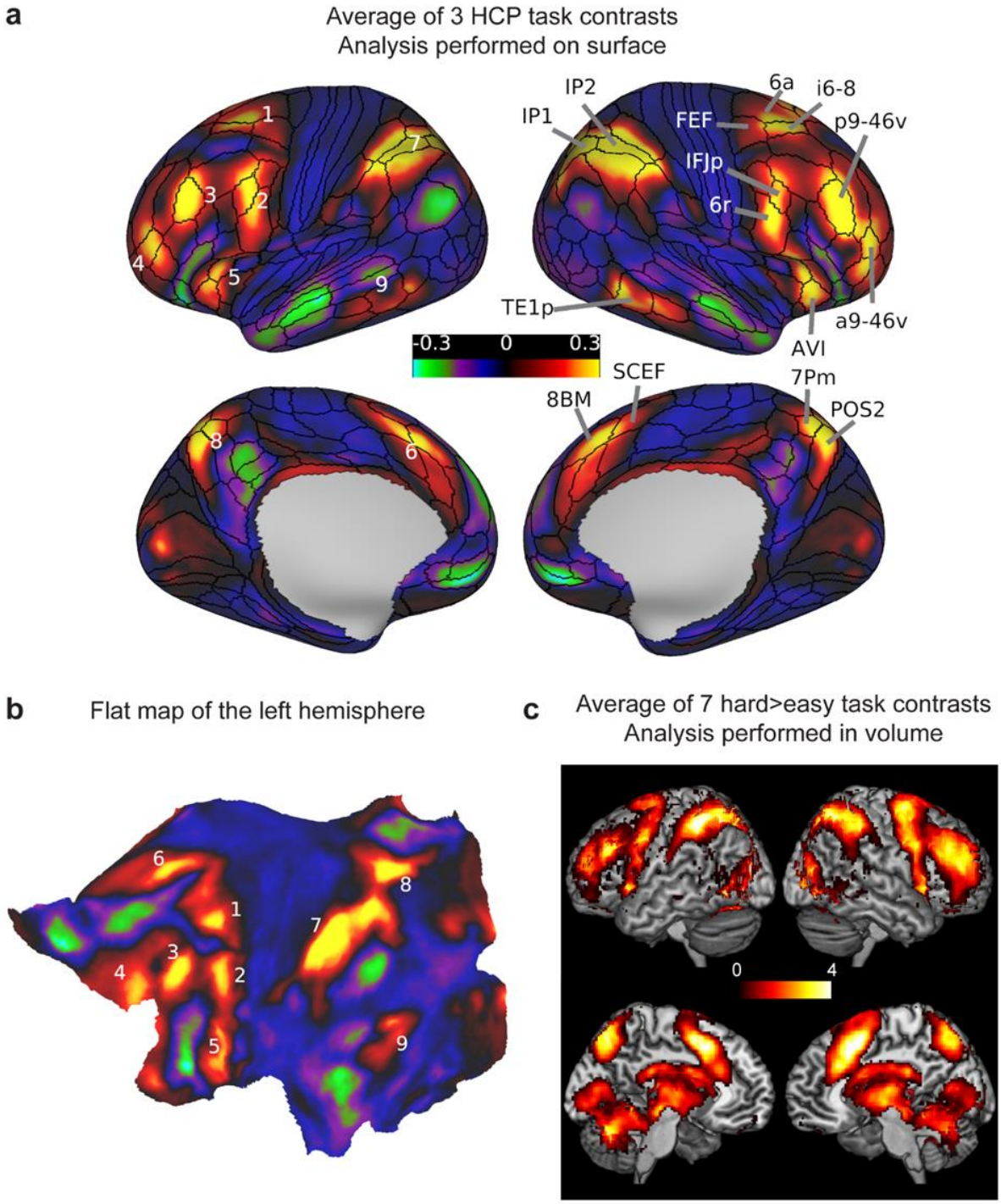

Figure 2.2 (a) Average of the 3 HCP group average task contrasts (WM 2bk>0bk, Relational H>E, Math>Story). Values are beta estimates. Black contours correspond to the HCP multi-modal parcellation MMP_1.0 (210V) areal borders. Numbers on the left hemisphere correspond to visually separable patches of activity distributed across the cortex. (b) The same activity of the left hemisphere projected on a flattened cortical sheet. Numbers correspond to the same patches labelled in (a). (c) Volumetric MD map from Fedorenko et al. (2013) computed by averaging 7 hard>easy task contrasts (2mm smoothed) displayed on a volume rendering of lateral surface (above) and medial slice (below) of the MNI template. Values are t-statistics. Data available at http://balsa.wustl.edu/lL9nj

2.3.2 Definition of extended and core MD regions using subject-specific cortical parcellation

For our primary analysis, each subject's cerebral cortex was parcellated into 360 regions (180 per hemisphere) corresponding to the HCP Multi-Modal Parcellation (MMP) 1.0. Parcellation used an automated classifier to define the borders of each area based on learned features from multiple MRI modalities, including cortical thickness, myelin content, rfMRI connectivity and task fMRI activations **(see section 2.2.5)**. Subject-specific parcellation ensured that task and rest fMRI signals extracted from the defined areas would respect individual differences in their sizes, shapes and locations even in the case of subjects having atypical topologic arrangements. We averaged beta values across vertices within each area, yielding one value per area per subject. For each of our 3 behavioral contrasts, we identified areas with a significant positive difference across the group of 449 subjects ($p<0.05$, Bonferroni corrected for 180 areas)**.** Given largely bilateral activation **(Figure 2.2),** to improve signal-to-noise ratio (SNR) and statistical power we averaged areal activations across hemispheres.

The conjunction of significant areas across the 3 contrasts revealed a set of twenty-seven areas, which we refer to as the extended MD system **(Figure 2.3a;** note that average activations from the two hemispheres are projected onto the left**)**. The distribution of the areas closely matches the activations observed in **Figure 2.2a** and has broad similarity to previous characterizations of MD activation but with substantially improved anatomical precision and several novel findings.

On the dorsal lateral frontal surface, we identify area i6-8 which is immediately anterior to area FEF (a common assignment for activations in this region). i6-8 is a newly defined area in the HCP MMP1.0, in the transitional region between classical BA6 and BA8. Localization of MD activation in i6-8, rather than FEF, suggests distinctness from activations driven simply by eye movements in complex tasks. In the HCP MMP1.0, FEF is clearly defined as a distinct area from i6-8 based on several criteria including its location as a moderately myelinated patch just anterior to the eye-related portion of the motor

cortex and its strong functional connectivity with the LIP/VIP visual complex and the premotor eye field area (PEF) (Glasser et al., 2016).

Near the frontal pole, we identify area a9-46v as a strongly active MD region, separated from the posterior region p9-46v. This separation confirms prior indications of a distinct anterior MD frontal region **(see Figure 2.2c).** Both a9-46v and p9-46v areas overlap with area 9-46v as delineated cyto-architectonically by Petrides and Pandya (1999) but here are separated into anterior and posterior portions by intervening areas 46 and IFSa that differ in their myelin and functional connectivity profiles (Glasser et al., 2016). Posterior to p9-46v is a further focus of activation in IFJp, with weaker activation in the surrounding regions 8C and 6r.

In the anterior insula, we identify AVI and an adjacent region of the frontal operculum, FOP5. AVI overlaps with superior portions of the architectonic area Iai of Öngür et al., 2003 (see Glasser et al., 2016). Previous work has attempted to distinguish activation in the anterior insula from the adjacent frontal operculum, with the peak often near the junction of the two (Amiez et al. 2016). In our data, AVI is the more strongly activated.

While previous characterizations of parietal MD activation have focused on the intraparietal sulcus broadly, our results reveal a more detailed picture, with strongest MD activation in intraparietal sulcus areas IP1 and IP2, bordered by relatively weaker MD areas dorsally (AIP, LIPd, MIP) and ventrally (PFm, PGs). In dorso-medial parietal cortex, there have been previous indications of an additional MD region (see **Figure 2.2c**). Here we robustly assign this mainly to area POS2, a newly defined MMP1.0 area that differs from its neighbors in all major multi-modal criteria.

On the lateral surface of the temporal lobe we identify two further MD areas, TE1m and TE1p. In many previous studies, fronto-parietal MD activation has been accompanied by a roughly similar region of activity in temporo-occipital cortex (e.g. Fedorenko et al., 2013). In many cases, a reasonable interpretation would be higher visual activation, reflecting the visual materials of most imaging studies. In the current study, however, the arithmetic task was acoustically presented, whereas the other two contrasts were visual, suggesting a genuine MD region.

In **Figure 2.2a,** the dorso-medial frontal activation spans the border between 8BM/SCEF. In the individual-subject analysis, however, SCEF was not significantly activated across all 3 contrasts. We thus investigated whether the activation indeed spans the border between the two areas. For each subject-specific areal definition, we divided each of the two areas into 10 equal segments along their anterior to posterior extent. **Figure 2.3a** shows that activation in this region starts to build up midway along SCEF, peaks at the border and is sustained throughout 8BM. We then tested whether each segment would survive as an extended MD region on its own. Indeed, all 8BM segments (except for the one most anterior segment on the left hemisphere) survived, whereas only the anterior 2 segments of SCEF were statistically significant (**Figure 2.3a**; see **Figure 2.4** for further independent evidence of heterogeneity around the 8BM/SCEF border). Based on these results, for subsequent analyses we combined the statistically significant segments of 8BM and SCEF into a single 'area' labelled 8BM/SCEF.

To evaluate the reliability of our results, we identified extended MD regions after splitting our subjects into two independent groups constructed to avoid shared family membership (210P and 210V, the parcellation and validation groups, respectively, used to create the HCP MMP1.0 in Glasser et al., 2016). Using similar criteria as for **Figure 2.3a** (i.e., conjunction of 3 positive contrasts across the group of 210 subjects, each contrast $p<0.05$ Bonferroni corrected for 180 areas), we identified 24 out of 27 regions in the 210P group (missing regions: 6r, AIP, FOP5) and 25 regions in the 210V group (missing regions: a47r, AIP). No additional regions were identified in either group. Thus for the remainder of the analysis, we retained the full set of 27 regions based on the complete data set.

To delineate more precisely the most active areas within the extended MD system, for each contrast we identified areas with activation stronger than the mean across the full set of 27 regions (one sample t-test, $p<0.05$, Bonferroni correction for the 27 extended MD areas). Seven areas were significant in all three contrasts: i6-8, p9-46v, a9-46v, combined 8BM/SCEF area, AVI, IP2 and IP1. Three more areas were significant in two of the three contrasts (**Figure 2.3b**): IFJp (relational reasoning and math), 8C and PFm (working memory and

relational reasoning). We refer to this group of 10 areas as the core MD system, with remaining areas of the extended MD system termed the MD penumbra.

Though our main analysis used individual-specific cortical parcellations, we wondered how well results would replicate using just the group-average parcellation. For most areas, previous work shows that the areal-fraction of individually defined parcels captured by group-defined borders reaches 60%-70% (Coalson et al. 2018). To investigate this question, we repeated our analysis using the HCP_MMP1.0 group average parcellation. As expected, using group-defined regions, we identified the same set of 27 MD regions, plus 4 more (areas 44, IFJa, 9-46d, 7Pm). While individual-specific parcellations likely provide the best available areal delineation, for many purposes the group-defined cortical parcellation may be sufficient.

Overall, these results identify an extended set of domain-general MD regions. Using HCP data and analysis allowed the identification of several novel MD areas and improved localization of previously reported ones. In the following sections, we further explore the functional properties of the 27 core and penumbra regions.

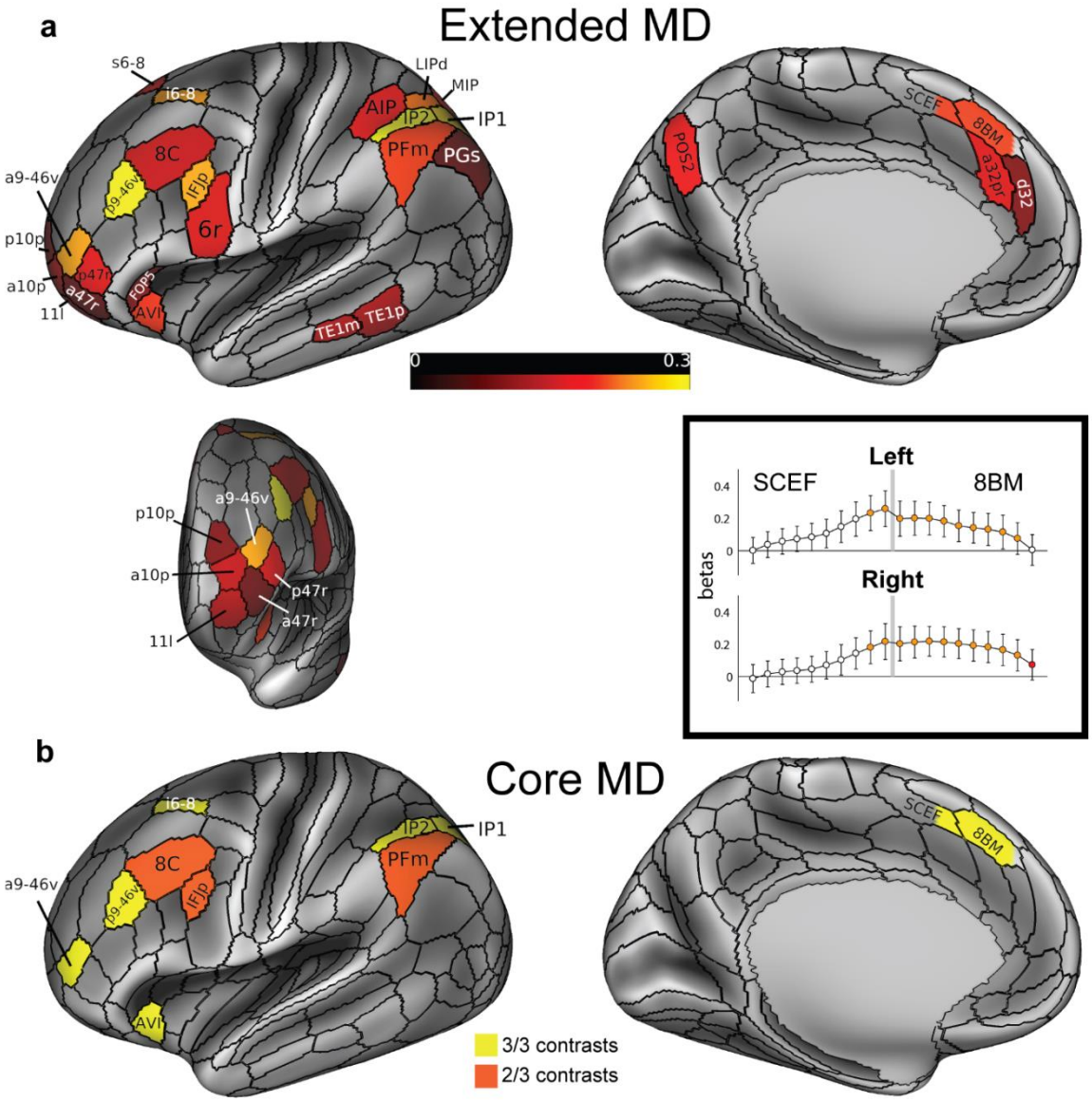

Figure 2.3 (a) The extended MD system: conjunction of significant areas across 3 functional contrasts. Areal colours reflect average beta values across the 3 contrasts analysed in relation to subject-specific parcellations. Data are averaged across hemispheres, and for illustration projected here onto the left lateral and medial surfaces (*top*) and an anterior view of frontal pole parcels (*bottom left*)**.** Box (*bottom* right) displays pattern of activity in regions SCEF (posterior) and 8BM (anterior), divided into posterior to anterior segments in relation to subject-specific parcellations. Grey bar indicates 8BM/SCEF border. Orange indicates segments that are part of the extended MD system when activity from both hemispheres is combined (i.e. segments with activity significantly above zero in all 3 behavioural contrasts). Red indicates one additional segment that survives as part of the extended MD system when activity from each hemisphere is tested separately. **(b)** The core MD system: areas with activity estimates that were significantly higher than the mean activity of all extended MD areas in all 3 contrasts (yellow) and 2 out of 3 contrasts (orange). Data available at http://balsa.wustl.edu/qNLq8

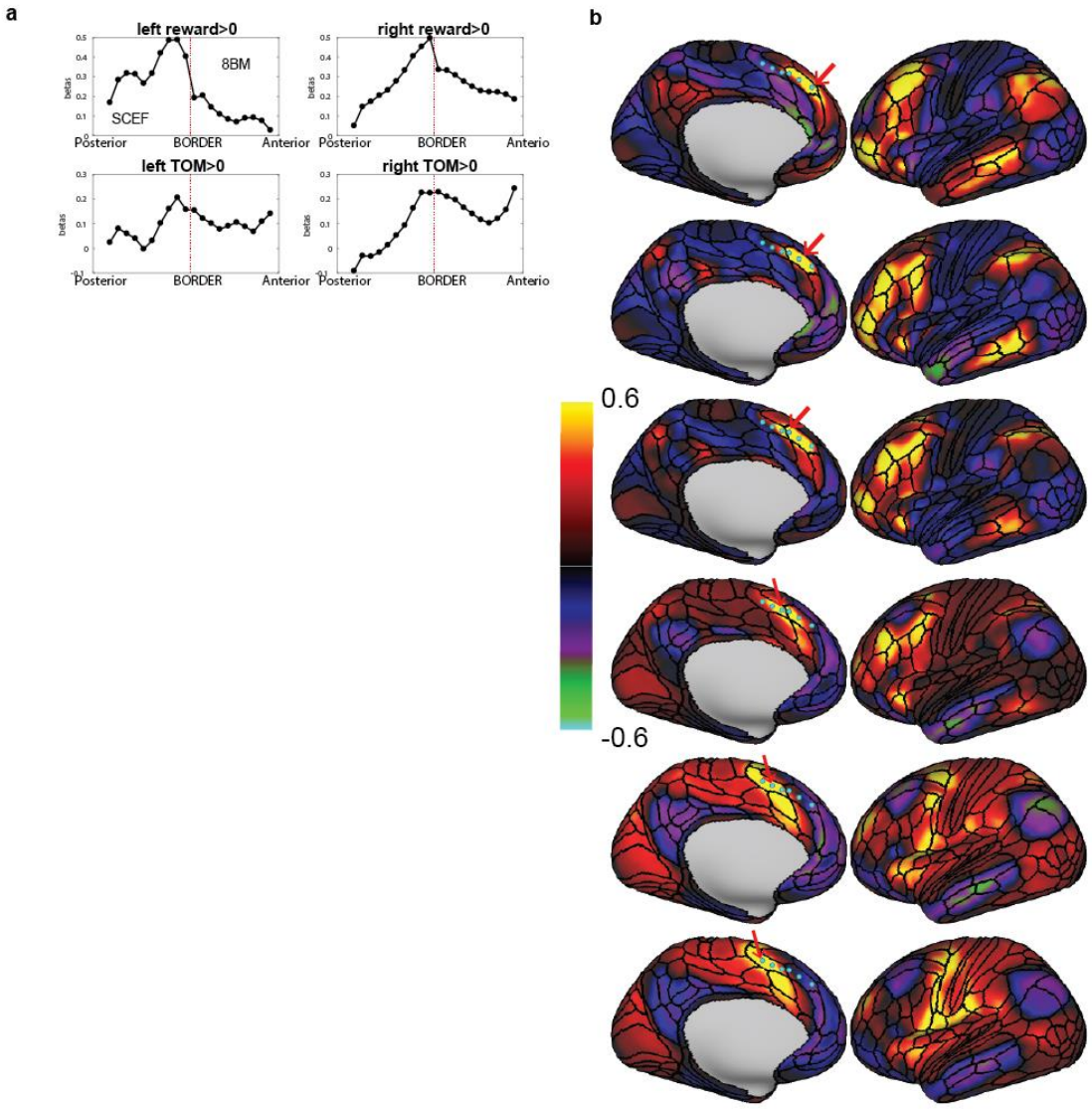

Figure 2.4 8BM/SCEF border. (a) Group average responses (beta values) for two HCP contrasts across the 8BM/SCEF border, Reward>fix and Theory of Mind (TOM)>fix, showing a similar pattern of build up within SCEF reaching a peak near the 8BM/SCEF border. (b) Functional connectivity maps for seeds (210V map, left hemisphere) along an antero-posterior gradient for the left 8BM/SCEF areas. Arrows mark the seed related to each column's maps. Note how the seed in row 4 is in SCEF near the 8BM/SCEF border and still shows an MD like connectivity pattern, especially the strong connectivity to i6-8. More posterior seeds in SCEF show a markedly different pattern with strong connectivity to FEF. Colour scale is Pearson correlation (r). Data available at https://balsa.wustl.edu/X5q36

2.3.3 Functional connectivity of the multiple-demand cortex and its relation to resting-state networks

To investigate functional connectivity (FC) patterns within the MD network and in relation to the rest of the brain, a FC matrix for each subject was calculated (180x180 areas per hemisphere; full correlation of spatial ICA+FIX and temporal ICA-cleaned time series; **see section 2.2.7**). In this analysis, we retained the original 8BM and SCEF parcellation, considering 8BM as core and SCEF as penumbra.

Figure 2.5a shows the group average connectivity matrix for the extended MD system, separated into core and penumbra. Despite their wide spatial separation, core MD areas show stronger functional connectivity with each other than with the penumbra. To test the robustness of these patterns, for each subject we calculated mean FC values for 6 different groups of cortical connections and compared them using multiple paired sample t-tests **(Figure 2.5b; see section 2.2.7)**. In both hemispheres, FC between core MD regions was significantly stronger than both their connectivity with the penumbra (left $t(448)= 93.1$, right $t(448)= 79.4$), and the internal penumbra connectivity (left $t(448)= 79.4$, right $t(448)= 66.3$). For both core and penumbra MD areas, mean FC with non-MD cortical areas was near zero.

We next investigated the spatial similarity between the MD network defined from our conjunction of 3 task contrasts and canonical fMRI resting state networks. For this purpose, we utilized the recent Cole-Anticevic Brain Network Parcellation (CAB-NP), which analysed resting state data from 337 HCP subjects and identified network communities across HCP MMP1.0 areas (Ji et al. 2019). A comparison of the extended MD and the CAB-NP (**Figure 2.6a)** indicates points of both convergence and divergence. Most strikingly, all 10 core MD areas are within the fronto-parietal network (FPN), (**Figure 2.6a**, **top left**). In contrast, penumbra MD areas are scattered among four networks: several in the FPN (yellow, 8 on the left and 10 on the right), 4 in the cingulo-opercular network (CON, purple), 3 in the dorsal attention network (DAN, green) and several in the default mode network (DMN, red; 3 on the left and 1 on the right) **(Figure 2.6a, top right).** Importantly, examination of the whole CAB-NP FPN

network (total 28 areas right, 22 left) shows most but not all areas within the MD core or penumbra (right FPN: 10 core, 10 penumbra, 8 non-MD; left FPN: 10 core, 8 penumbra, 4 non-MD) **(Figure 2.6a, bottom)**.

To emphasize the central role of core MD, we again compared different connectivity subgroups (**Figure 2.6b;** paired sample t-tests, $p<0.05$, Bonferroni corrected). Within the FPN, we found that core MD regions have significantly stronger FC with other FPN regions (core-core vs core-penumbra: left $t(448)=53.3$, right $t(448)=46.8$; and core-core vs core-non-MD FPN regions: left $t(448)=75.1$, right $t(448)=84.2$). Also within the FPN, core-penumbra FC is stronger than core-non-MD FC (left $t(448)=47.1$, right $t(448)=73.0$). We also found higher FC between core MD regions, all within FPN, and penumbra vs non-MD regions within each of DAN, CON and DMN (DAN (left $t(448)=47.6$, right $t(448)=41.0$), CON (left $t(448)=41.1$, right $t(448)=40.5$) and DMN (left $t(448)=70.1$, right $t(448)=80.4$) **(Figure 2.6b)**.

Many previous studies have separated cognitive control regions into two distinct networks: fronto-parietal (dorso-lateral frontal and intra-parietal sulcus regions) and cingulo-opercular (insular, dorsomedial frontal and anterior lateral frontal regions) (Crittenden et al., 2016; Dosenbach et al., 2008, 2006; Dosenbach et al., 2007; Yeo et al., 2011). We wondered whether our extended MD network would show a similar separation. Multi-dimensional scaling of connectivities between extended MD regions showed core MD regions centrally clustered together (**Figure 2.7; see section 2.2.7)** with no strong trend for a distinct CON among these core regions. Instead, matching their network assignments in CAB-NP, the results suggest a relatively distinct CON cluster including dorsomedial frontal region SCEF and insular region FOP5, These results suggest that the main cingulo-opercular network is distinct from core MD regions, with the two networks in close anatomical proximity.

In summary, while these results show substantial overlap between MD and FPN – especially for the MD core – there are additional organizational aspects revealed by the FC analysis. Connectivity is especially strong between regions within the extended MD system, and strongest between core regions within the canonical FPN. Strong functional connectivity, especially for the core, suggests a suitable architecture for widespread integration of distributed brain states.

Connectivity delineating the MD network can also be revealed by recent work using temporal ICA (tICA), which generates components that are temporally independent (Glasser et al., 2019, 2018; see also Van Essen and Glasser, 2018). By correlating our group average MD map (**Figure 2.2a)** with the tICA components from (Glasser et al. 2018), we identified at least one rest and one task tICA component having strong spatial similarity to the group average MD map (whole brain absolute Pearson correlation r= 0.74 and 0.76 respectively; **Figure 2.8)**.

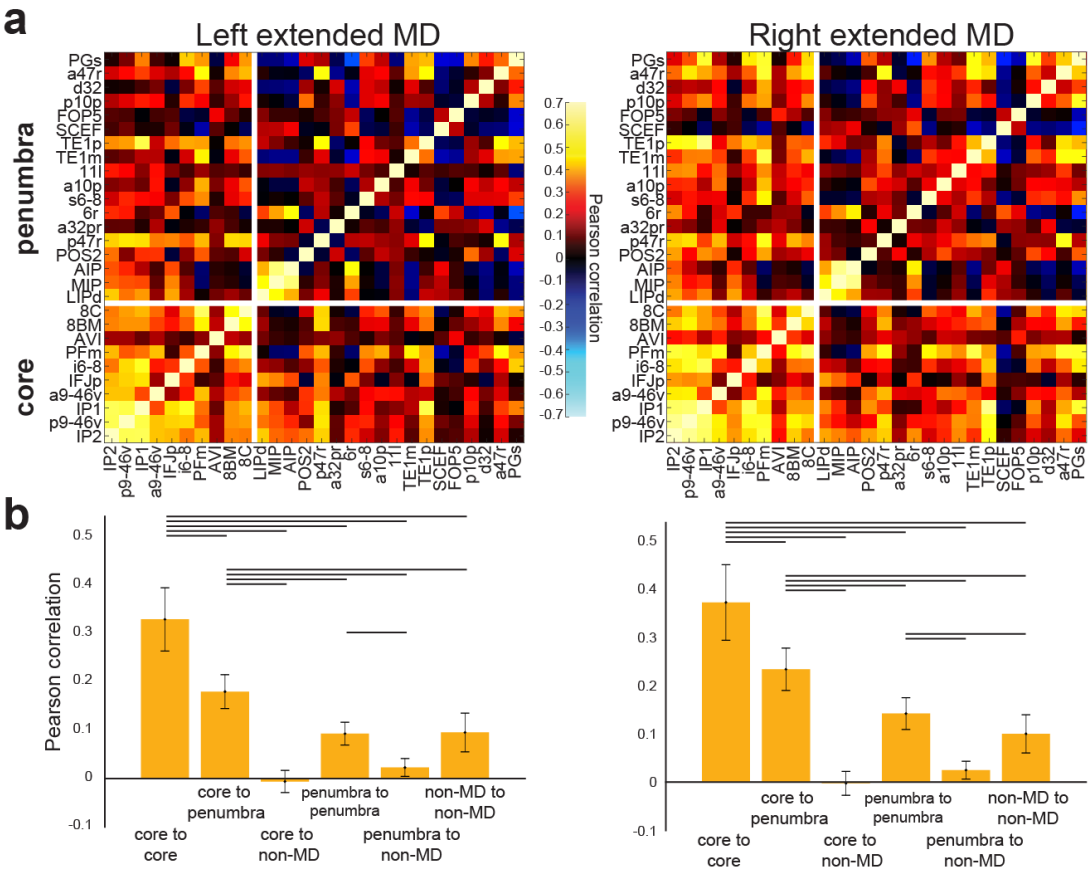

Figure 2.5 Functional connectivity (FC) of the MD system. (a) FC (Pearson correlation) across the MD system. Regions of the extended MD system are separated into core and penumbra, with regions within each set ordered by mean activation (beta) across our 3 functional contrasts. Note the strength of core MD connectivity (lower left box) vs penumbra connectivity (upper right box). (b) Statistical comparison (paired sample t-test) between different groups of cortical connections. Lines highlight a statistically significant difference ($p<0.05$, Bonferroni corrected for 30 comparisons). Data available at http://balsa.wustl.edu/jjL1x

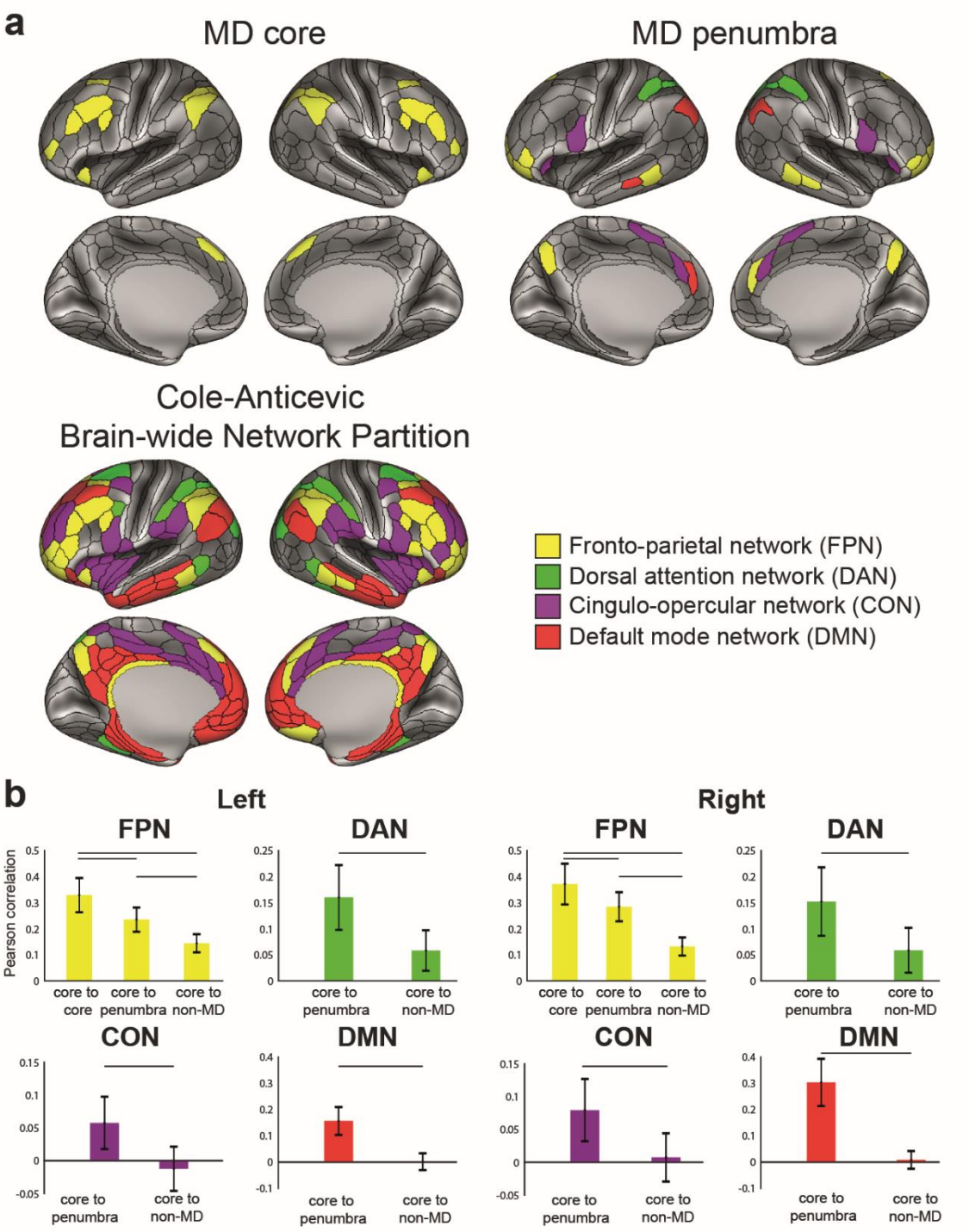

Figure 2.6 MD system and resting state networks (a) Resting state network assignments from the Cole-Anticevic Brain-wide Network Parcellation (CAB-NP; Ji et al., 2019) for the core (top left) and penumbra (top right) MD areas, compared to the whole CAB-NP fronto-parietal network (bottom left). (b) Statistical comparison (paired sample t-test) of cortical connection types for each CAB-NP network. Data available at http://balsa.wustl.edu/wNGV6

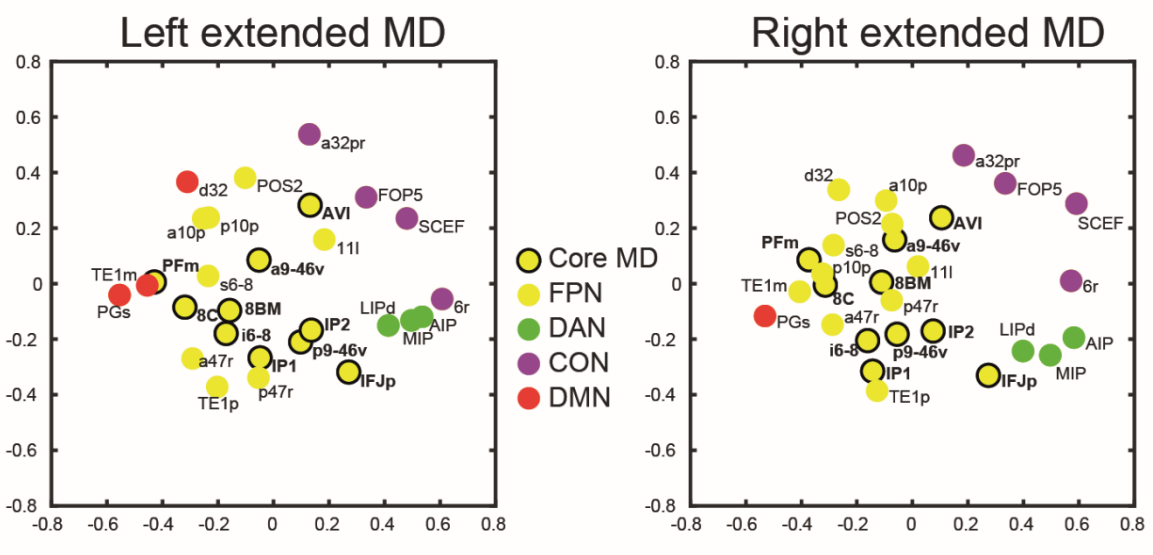

Figure 2.7 Multi-dimensional scaling plot of the connectivities between extended MD regions. Axis units are arbitrary. Data available at http://balsa.wustl.edu/jjL1x

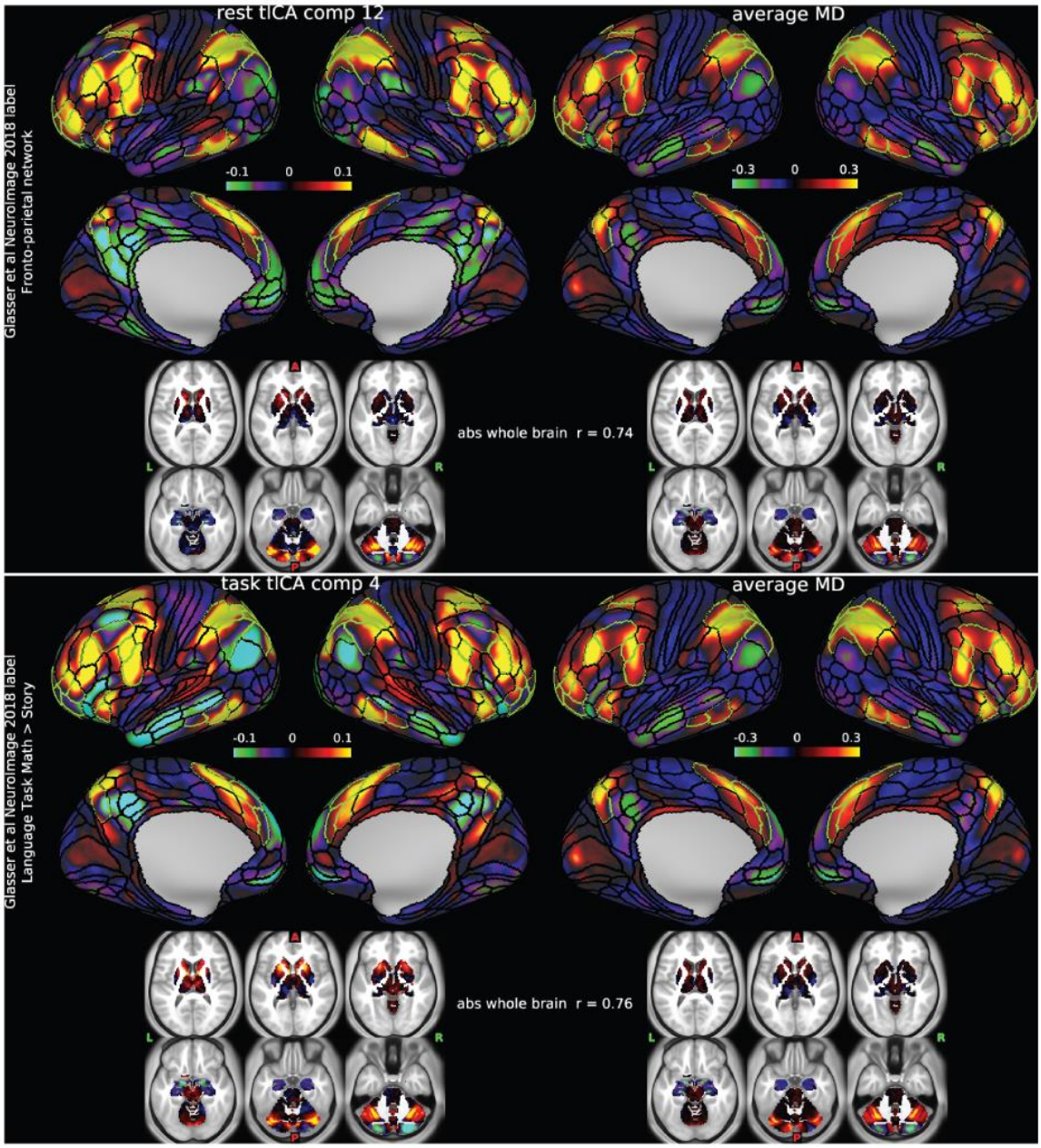

Figure 2.8 MD and temporal ICA. Most correlated temporal ICA components (arbitrary units) (from Glasser et al., 2018) with MD average map (beta estimates). Top: rest tICA component 12. Bottom: task tICA component 4. The borders of extended MD regions are coloured in green. Data available at https://balsa.wustl.edu/87P3x and https://balsa.wustl.edu/Klv5g

2.3.4 Task profiles across the multiple-demand cortex

By definition, every MD area showed a significant positive result in each of our 3 behavioural contrasts. Across areas, nevertheless, we examined the relative preferences for one contrast over another. To evaluate this quantitatively, **Figure 2.9a** shows the mean response of each area (averaged across hemispheres) for each contrast. Predominantly, the picture is one of consistency. For nearly all areas, activation was strongest for the Math>Story contrast, and weakest for Relational H>E contrast. Against this general background, however, there was also differentiation between profiles, with varying patterns of peaks and troughs.

To test the robustness of these patterns, we compared activation profiles in the two independent groups of subjects (210P and 210V). As shown in **Figure 2.9b**, the activation profile for each contrast is almost identical for the two groups. **Figure 2.9c** quantifies this by correlating activation profiles **(in Figure 2.9b)** for the two subject groups. Very high correlations on the diagonal ($r > 0.98$) highlight how the precise pattern of activation for a given contrast is very stable when averaged over many individuals. Off-diagonal correlations are much lower (r=~0.5-0.6). A closely similar pattern was seen when extended MD regions were defined in the 210P subgroup, and correlations computed between two halves of the 210V subgroup (diagonals $r>0.94$, off-diagonals $r=0.25$-0.60). Although all tasks engage all MD areas, there remains considerable and highly consistent inter-areal diversity in precise activation patterns.

To illustrate this inter-areal diversity between the three contrasts, we plotted the normalized profile for each contrast **(line plots in Figure 2.9d).** For each contrast and each subject, we z-scored activations across MD regions, then averaged the z-scores across subjects. For each region, bar heights **(Figure 2.9d, bottom)** show the standard deviation of these normalized z-scores across tasks, separately calculated for each subject and then averaged over subjects. Bars were also coloured to highlight the relative task preferences (see **Figure 2.9e**, where the same colours are projected onto the cortical surface).

The results reveal a diversity of relative task preferences across the extended MD network. Relative preference for relational reasoning (green) occurs in a cluster of anterior frontal areas inferior to the core region a9-46v, as well as in 8C. Dorsal frontal regions (e.g. i6-8 and s6-8) show relative preference

for working memory, whereas dorsal parietal regions (AIP/LIPd/MIP, and POS2) show relative preference for math. Other relative preferences occur across most regions.

Task preferences were also present across hemispheres (**Figure 2.10**). Most MD regions showed stronger activations in the right hemisphere for both working memory and math contrasts, with more variable results for relational reasoning. Across both hemispheres, however, almost all contrasts were positive, in line with a pattern of largely bilateral MD activation.

Despite relative consistency across the entire extended MD network – with the strongest activation for Math>Story, and weakest for relational reasoning – there is also clear evidence of relative functional specialization, with each area showing modest but consistent relative preference for one contrast over another.

Figure 2.9 (next page) Task profiles across the MD system. **(a)** Raw activation estimates (betas) for each contrast. Areas are sorted from left to right according to the strength of their MD response (average across the 3 contrasts). Error bars represent SEM. Core MD areal labels are colored in orange (survived in all 3 contrasts) and red (survived in 2 out of 3 contrasts). **(b)** Task profiles for two independent groups of subjects (210P and 210V). **(c)** Correlation of task profiles between groups. **(d)** Normalized task profiles across the MD system as line plots. Bar heights represent between-task standard deviation, separately calculated for each subject and averaged over subjects. Bar colors indicate relative preferences between tasks. Color wheel indicates red for working memory (WM), green for relational reasoning (Rel), and blue for math. Intermediate colors show mixed preferences. Brighter and darker colors reflect stronger and weaker MD activation, respectively. **(e)** Cortical projection of the RGB color weighted normalized task profiles. Data available at http://balsa.wustl.edu/4m747

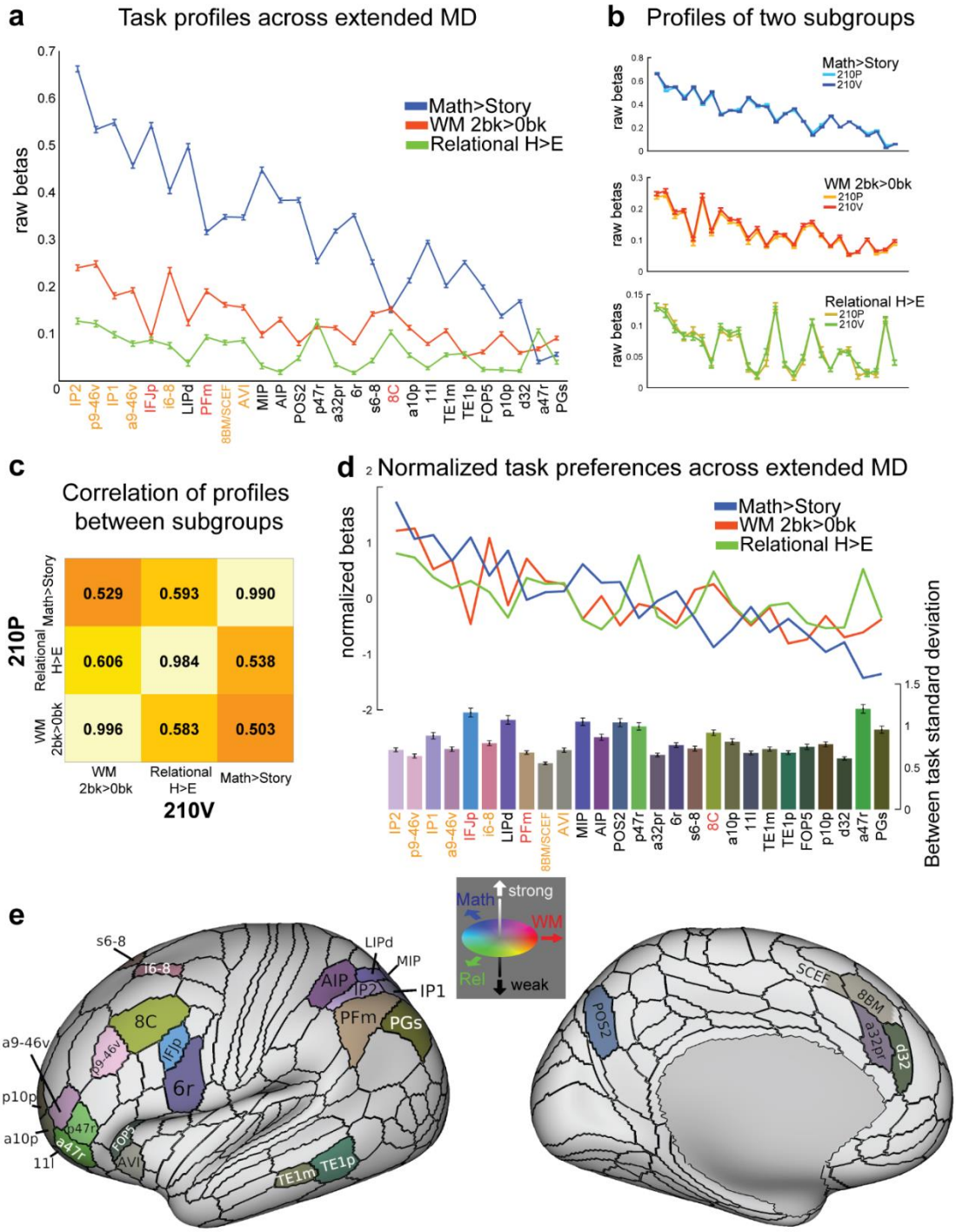
a
Task profiles across extended MD
raw betas
Math>Story
WM 2bk>0bk
Relational H>E
IP2 p9-46v IP1 a9-46v IFJp i6-8 LIPd PFm 8BM/SCEF AVI MIP AIP POS2 p47r a32pr 6r s6-8 8C a10p 11l TE1m TE1p FOP5 p10p d32 a47r PGs
b
Profiles of two subgroups
Math>Story
210P
210V
WM 2bk>0bk
Relational H>E
c
Correlation of profiles between subgroups
210P
210V
Math>Story
Relational H>E
WM 2bk>0bk
0.529 0.593 0.990
0.606 0.984 0.538
0.996 0.583 0.503
d
Normalized task preferences across extended MD
normalized betas
Between task standard deviation
e
strong
weak
Math
WM
Rel
s6-8
i6-8
LIPd
MIP
AIP
IP2
IP1
8C
PFm
PGs
a9-46v
p9-46v
IFJp
6r
p10p
p47r
a10p
a47r
FOP5
11l
AVI
TE1m
TE1p
SCEF
8BM
a32pr
d32
POS2

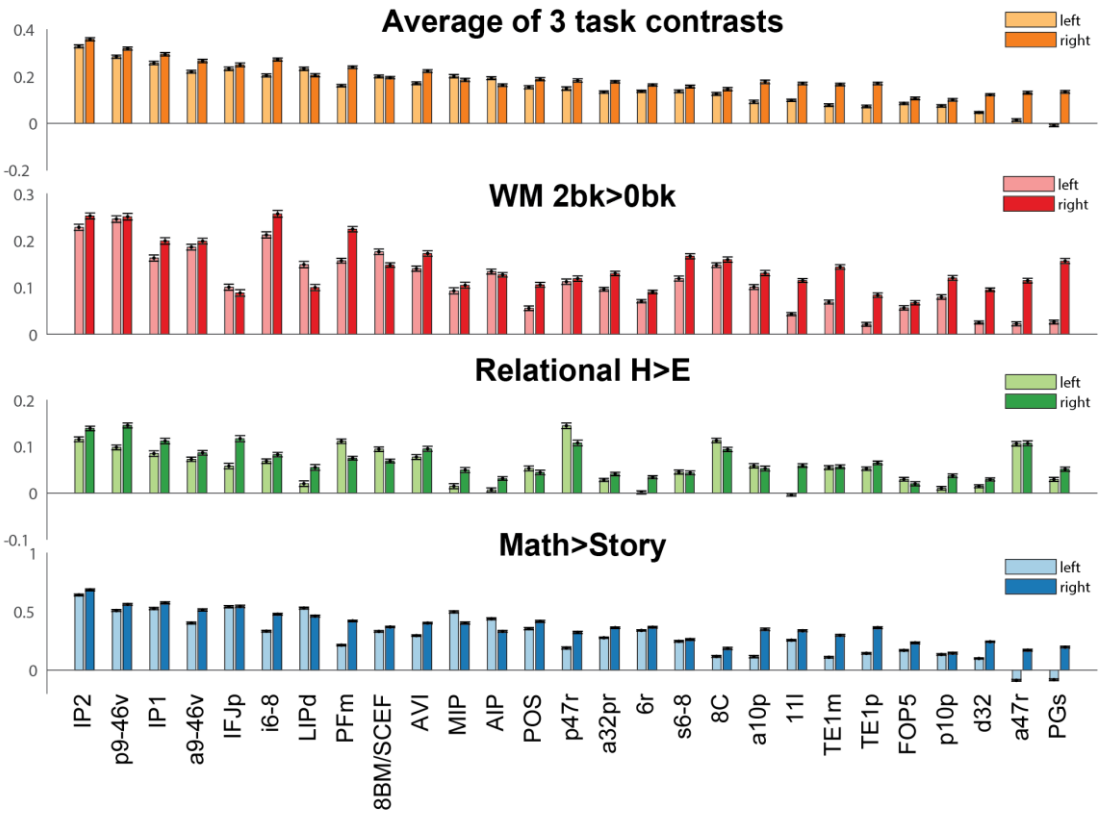

Figure 2.10 Extended MD for each hemisphere. Group average responses for the MD areas of both hemispheres (beta estimates). First row: average of the 3 HCP contrasts. Second row: Working memory. Third row: Relational reasoning. Fourth row: Math>story. Error bars are SEMs.

2.3.5 Multiple-demand regions during weak cognitive demands

A potential limitation of our main analysis is that we might have missed MD regions that are already active even in easy task conditions, and therefore absent in our task contrasts. To investigate this, we examined the group average maps for weak cognitive demands compared against periods during which subjects visually fixated on a cross hair in the middle of the screen. We used the 0bk WM versus fixation contrast (0bk>fix) and easy relational reasoning versus fixation

contrast (Relational E>fix) **(Figure 2.11)**. The Math task did not include any fixation periods and was thus excluded from this analysis.

As expected, the activated regions overlap substantially with the extended MD network, but also include visuo-motor regions as predicted when contrasting task with fixation. In comparison to our previous group MD map **(Figure 2.2)**, however, there are shifts in the easy vs fixation maps. Dorso-lateral frontal activation shows a posterior shift, with strong activation near the intersection of FEF, 6a and i6-8 areal borders. Premotor frontal activation is strongest around IFJp, spreading towards the premotor eye field (PEF) area dorsally and inferior frontal sulcus regions (IFJa and IFSa) ventrally. Frontal pole activation peaks within penumbra region p47r and also weakly engages area 9-46d in addition to previously identified adjacent MD regions. Dorso-medial frontal activation is strongest within the anterior half of SCEF, spreading anteriorly into 8BM. Lateral parietal activations are strongest around penumbra regions AIP, LIPd and MIP and the adjacent LIPv. Dorso-medial parietal activation overlaps with 7Pm sparing POS2. All previously mentioned regions as well as all core MD regions (except for PFm) were significantly activated in both 0bk>fix and Relational E>fix contrasts ($p<0.05$; Bonferroni corrected for 180 regions after averaging across hemispheres).

The comparison with fixation-only periods limits the interpretation of activation in the above highlighted regions, as visuo-motor related activation presumably dominates the pattern. For example, activation in FEF and PEF may largely reflect eye movements, especially in the relational task. Tentatively, however, these results suggest that our main task contrasts may miss additional MD regions, extending from those identified in the main analysis, but with strong activation even in the easier version of each task.

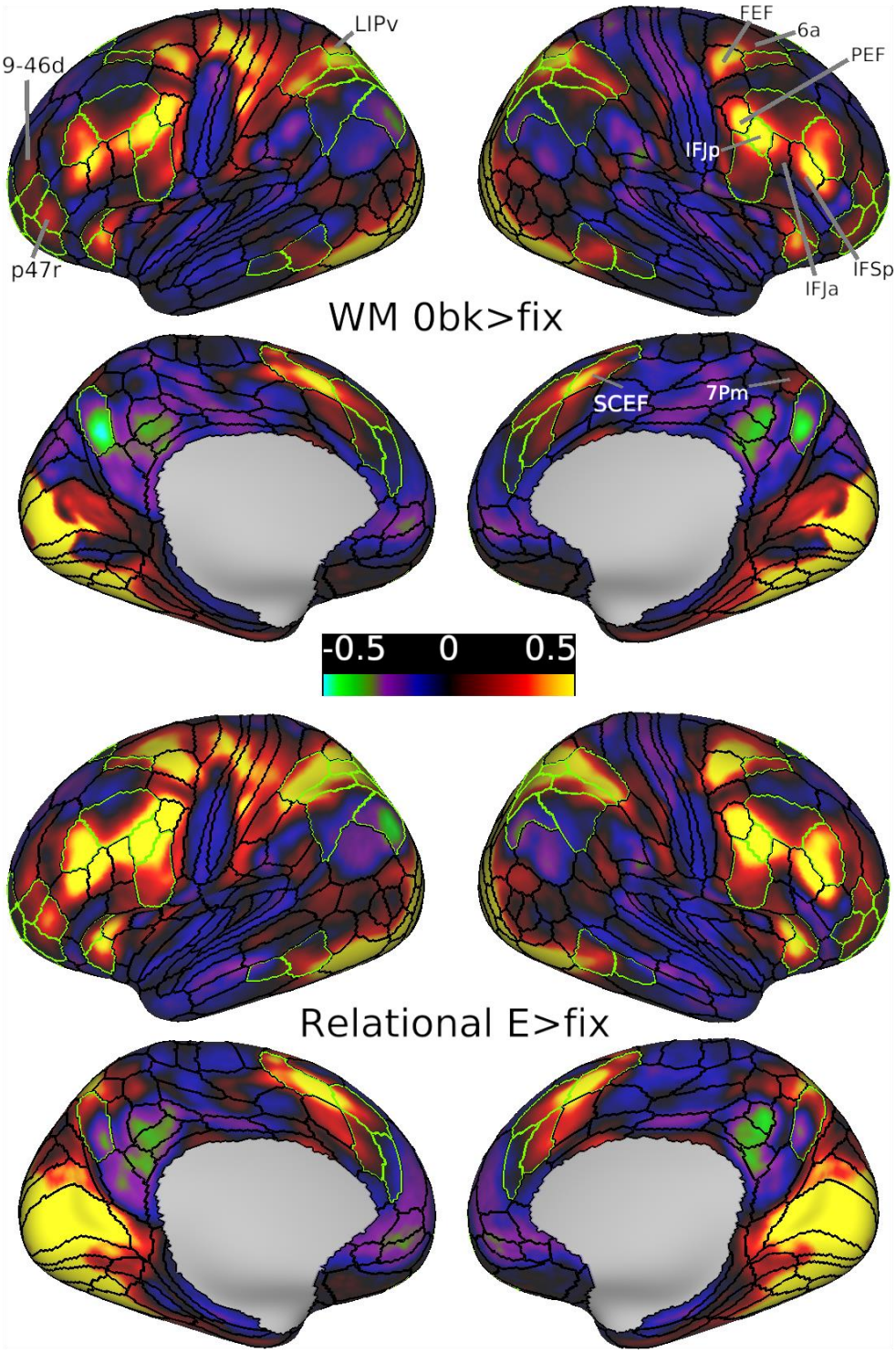

Figure 2.11 Group average beta estimates maps for the WM 0bk>fix contrast (upper) and Relational E>fix contrast (lower). The borders of extended MD regions are colored in green. Data available at http://balsa.wustl.edu/mDkgN

2.3.6 Subcortical and cerebellar components of the multiple-demand system

To identify subcortical and cerebellar components of the MD system we used the same 3 behavioural contrasts used for cortical areas. FreeSurfer's standard segmentation of 19 subcortical/cerebellar structures (left and right caudate, putamen, globus pallidus, thalamus, cerebellum, hippocampus, amygdala, ventral diencephalon, nucleus accumbens; plus whole brainstem) was carried out separately for every subject (see **section 2.2.4**), thus avoiding mixing signals from nearby structures or white matter. For each structure, we first identified significantly activated voxels for each contrast separately (one sample t-test, FDR corrected for each structure separately, $p<0.05$, Bonferroni corrected for 19 structures) and then identified the conjunction of significant voxels across the three contrasts. We analyzed the P210 and V210 groups separately. This revealed activation regions bilaterally mainly in the caudate nucleus and cerebellum. Caudate activation was in a circumscribed region in the head, which was modestly replicable between 210V and 210P groups (r=0.37, Dice=0.60 across all caudate voxels) **(Figure 2.12a, left panel)**. Cerebellar activations, mapped to a cerebellar surface model (Diedrichsen and Zotow 2015) and displayed on a cerebellar flatmap, included separate medial and lateral portions of crus I and II (on dorsal and ventral lateral surface). The pattern was largely symmetrical across hemispheres and was strongly replicable across both groups (r=0.88, Dice=0.88) **(Figure 2.12a, right panel)**.

The analysis showed no significant regions in the thalamus, putamen or globus pallidus **(Figure 2.12a)**. Interestingly, larger bilateral portions of the thalamus (anterior dorso-medial), putamen (dorso-anterior/mid portion) and globus pallidus (dorso-anterior portion) were significantly activated in only two contrasts (working memory and math) and were deactivated in the relational reasoning contrast **(Figure 2.13)**.

In a separate analysis using resting state data, we aimed to identify the subcortical and cerebellar voxels showing significant functional connectivity with the cortical core MD areas. For this analysis we used the group average dense FC matrix for each group **(see section 2.2.7). Figure 2.12b** shows the

statistically significant subcortical/cerebellar voxels (FDR corrected, $p<0.05$, Bonferroni corrected for 19 structures). The patterns were highly replicable (caudate r=0.84, Dice=0.94; cerebellum r=0.97, Dice=0.93) and follow closely the task-identified regions in the caudate nucleus and cerebellum bilaterally. In addition, FC analysis identified significant voxels in bilateral portions of the thalamus (anterior dorso-medial) and putamen (dorso-anterior/mid portion), similar to the regions activated in the working memory and math contrasts **(Figure 2.13)**. We also note that a similar overlapping thalamic region is activated in the Relational E>fix contrast **(Figure 2.13).**

We also compared the MD cerebellar regions with the fronto-parietal network (FPN) identified by resting state data from two studies: Buckner et al. 2011 (7 networks parcellation results from 1000 subjects) and CAB-NP (Ji et al., 2019; results from 339 HCP subjects). **Figure 2.12c** illustrates the strong similarity between the FPNs from both studies and the cerebellar MD hotspots in crus I and II (Dice=0.62-0.70).

Next we measured the similarity between the task and rest identified subcortical and cerebellar MD regions (after conjunction of 210P and 210V maps). With the exception of the left caudate, task and rest fMRI data showed modest overlap (left caudate r=0.01, Dice=0.07; right caudate r=0.18, Dice=0.26; left cerebellum r=0.65, Dice=0.68; right cerebellum r=0.60, Dice=0.62). Thus, together, task and rest fMRI data converge on identifying subcortical, especially caudate, and cerebellar regions related to the cortical MD core.

Figure 2.12 (next page) Subcortical and cerebellar MD components. (a) Left: Conjunction of significant voxels across the three tasks for the 210P (top) and 210V (bottom). Right: Cerebellar activity is displayed on a flat cerebellum with lines representing anatomical borders (Diedrichsen and Zotow 2015). Data available at http://balsa.wustl.edu/Z4NXp (b) Left: Subcortical voxels with significant connections to the cortical core MD areas. Right: Cerebellar MD connectivity displayed on a flat map. Data available at http://balsa.wustl.edu/VjwZg (c) FPN from Buckner et al. (2011) (left) and Ji et al. (2019) (right). Data available at http://balsa.wustl.edu/3g7wv

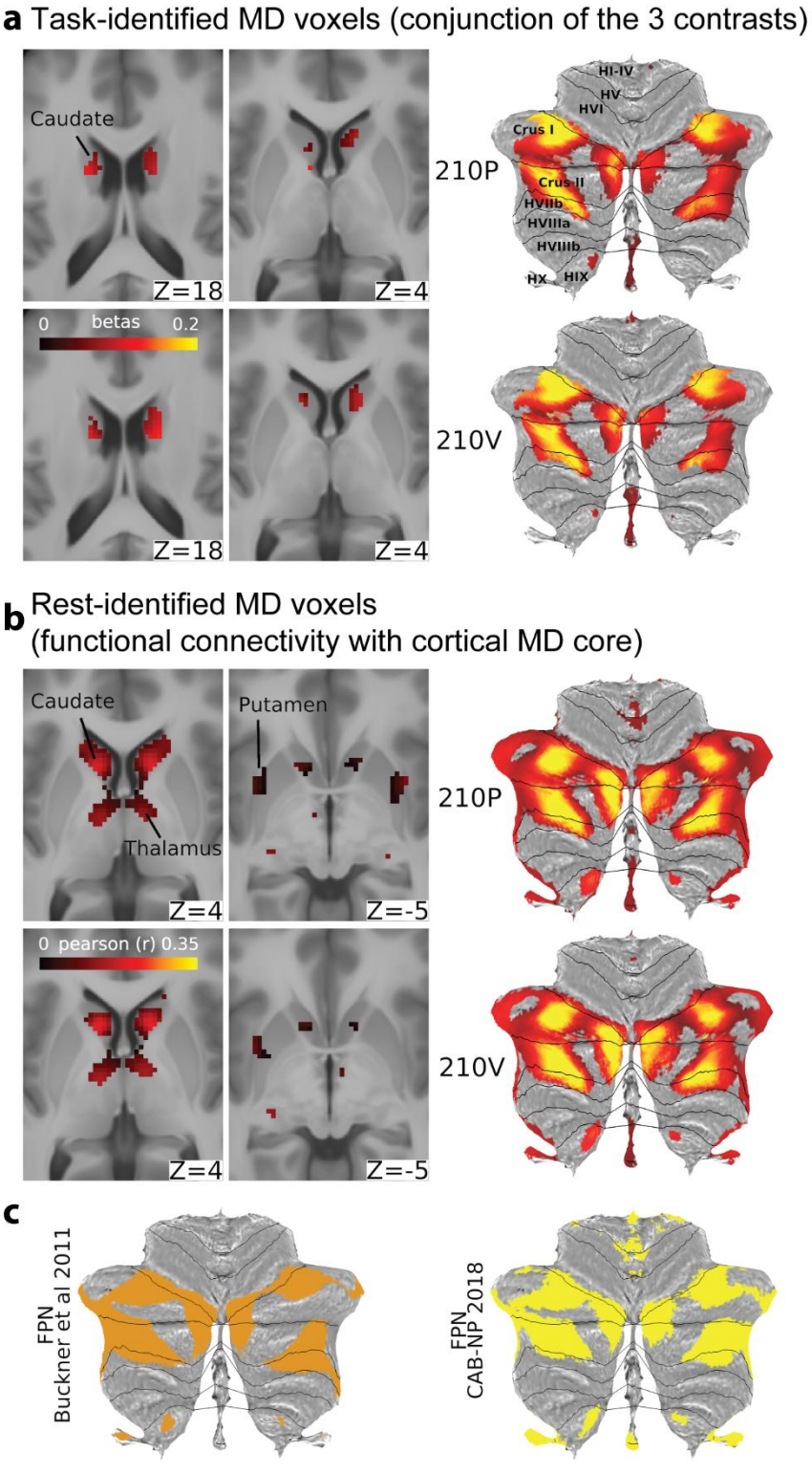
a Task-identified MD voxels (conjunction of the 3 contrasts)
Caudate
Z=18
Z=4
0 betas 0.2
Z=18
Z=4
HI-IV
HV
HVI
Crus I
Crus II
HVIIb
HVIIIa
HVIIIb
HX
HIX
210P
210V
b Rest-identified MD voxels
(functional connectivity with cortical MD core)
Caudate
Thalamus
Putamen
Z=4
Z=-5
0 pearson (r) 0.35
Z=4
Z=-5
210P
210V
c
FPN
Buckner et al 2011
FPN
CAB-NP 2018

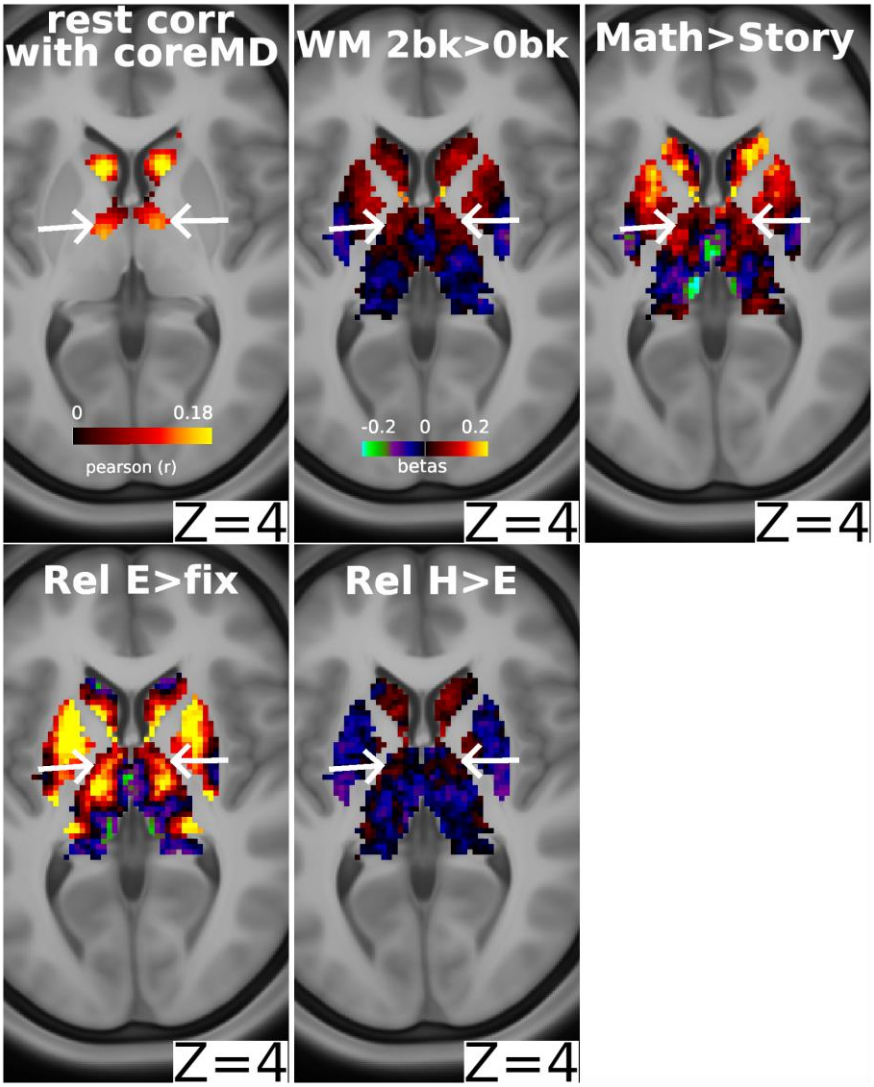

Figure 2.13 Top left: Subcortical voxels with significant connections to the cortical core MD areas. All other panels: Group average activity for each task contrast. Arrows highlights that the thalamic hotspot in the top row panels is also activated in the Relational E>fix contrast (bottom left). Data available at https://balsa.wustl.edu/Nw1MK

2.4 Discussion

Thousands of brain imaging studies have identified regions of frontal and parietal activation crossing multiple cognitive demands. In this study, we used HCP's high quality multimodal MRI data and improved brain registration methods to demonstrate that diverse cognitive tasks from different sensory modalities engage widely distributed but tightly delineated foci of multiple-demand (MD) activation **(Figure 2.2a)**. The network of twenty-seven extended MD areas is organized into nine larger patches **(Figure 2.2a, b)**: three distributed in an anterior-posterior chain running along the lateral frontal surface, a fourth in and above the anterior insula, a fifth on the most dorsal part of the lateral frontal surface, a sixth on the dorsomedial frontal surface, a seventh within and surrounding the intraparietal sulcus, an eighth in the dorsomedial parietal cortex, and a ninth in posterior temporal cortex. Within these larger patches, we identified a set of core areas, characterized by their strong activation and FC-based interconnectivity, surrounded by a penumbra having relatively weaker activations and interconnectivity. We also identified localized MD regions in the caudate nucleus and cerebellum that share strong connectivity with the cortical core MD. These data provide strong evidence for the existence of highly specific MD regions in the human brain. The improved anatomical precision offered by the HCP methods revealed novel findings regarding the anatomical and functional organization of the MD network, as well as the functional connectivity of its components.

Why should the brain contain this precise network of MD regions, co-activated during many cognitive activities? Within the extended MD system, we propose that the core regions, most strongly active and interconnected lie at the heart of information integration and exchange mediating cognitive operations. Surrounding penumbra regions, with their connectivity into multiple cortical networks, feed diverse information into and out of the core. Across the entire MD system, co-activation reflects rapid information integration and exchange, while modest functional preferences reflect differential connectivity and information access. Together, these properties allow MD regions, with associated subcortical regions, to build integrated cognitive structures suited to

current behavioural requirements. These proposals are developed and extended in the following sections.

2.4.1 Broad anatomical distribution and relative functional preferences

Similar activation patterns crossing many cognitive domains, roughly corresponding to our current MD findings, has been documented in a large body of previous work. At the same time, there have been many suggestions of functional differentiation between MD-like regions, albeit with little consensus emerging across studies (Dosenbach et al. 2007; Champod and Petrides 2010; Hampshire et al. 2012; Yeo et al. 2015; Lorenz et al. 2018). Our fine-grained anatomical findings illustrate the challenges in interpreting studies that are based on traditional neuroimaging analyses. For example, when coarsely-analysed data suggest functional dissociation between MD-like regions, the dissociation might concern penumbra or core MD regions, or even nearby non-MD regions that are more task specific. (See **Figure 2.1** for task specific activations for each of the 3 contrasts extending beyond MD parcels; also see Coalson et al. 2018 for a quantification of the uncertainties involved in mapping between volumetric activations and surface activations.) The finer-grained anatomy of the current study helps clarify issues of functional differentiation within the MD system. On one side is strong evidence for a network of co-activated MD regions, broadly distributed across the cortex. On the other is strong evidence for relative functional differentiation, often somewhat corresponding to previous proposals in the literature. Below we summarize concrete functional questions that are clarified by the present data.

Much prior work (see **Figure 2.2b**) has suggested MD-like activation in the posterior dorsal prefrontal cortex, in a region close to the FEF. Though a reasonable interpretation might be increased eye movements in more demanding conditions, we show that the main focus of MD activation is localized anterior and dorsal to the FEF, including regions i6-8 (core) and s6-8. These results strongly suggest that MD activation is distinct from activations driven simply by eye movements in complex tasks. Our results match an early demonstration of

working memory activation immediately anterior to FEF (Courtney 1998); in our data, the strong MD response of i6-8 and s6-8 is supplemented by relative preference for the working memory contrast (see **Figure 2.9d**).

Near the frontal pole, we localized MD activation in one core region (a9-46v) and 5 surrounding penumbra regions. There has been much debate concerning an anterior-posterior gradient of activation on the lateral frontal surface. On the one hand, many tasks produce activation near to the frontal pole, suggesting an MD-like pattern (Ramnani and Owen 2004). On the other hand, many studies suggest selective activation in this region, for example associated with abstract reasoning (Bunge 2004; Christoff et al. 2009) or hierarchically-organized cognitive control (Badre 2008; Badre and Nee 2018). Our results indicate that a9-46v is almost as strongly co-activated as more posterior core regions, arguing against a simple gradient of activation. Its adjacent penumbra regions (a47r, p47r) also show clear MD activation but with relative functional preference for the abstract relational reasoning task, matching previous reports of reasoning activation in this region.

The combined 8BM/SCEF MD area on the medial frontal surface showed the least functional preference (**Figure 2.9d**). Our findings show MD activation rising to and peaking at the border between 8BM and SCEF, with similar patterns also visible in other task contrasts and fine-grained analysis of functional connectivity (**Figure 2.4**). In our group-average map, hints of peak task activation near areal borders can also be seen at the borders of 8C/IFJp and POS2/7Pm (**Figure 2.2a**). Though detailed analysis of these functional transitions is beyond our scope here, it is possible that here too MD activation peaks near areal borders. Borders between these areas were defined using robust multiple overlapping functional, architectural and/or topological criteria (Glasser, Coalson, et al. 2016). Thus, we speculate that our data may reflect close interaction between areas sharing a common border, reflecting the general principle of spatial proximity between brain regions that are in close communication.

Previously, many studies have reported a band of occipito-temporal activation accompanying activation of fronto-parietal MD regions **(see Figure 2.2b)**. As most tasks used in these studies were visual, a plausible interpretation might be top-down input into higher visual areas. In our data we identified two

penumbra regions, TE1m and TE1p, in posterior temporal cortex. Since these regions were activated by the auditory as well as the visual contrasts, the interpretation of top-down input into higher visual areas is less plausible. The location of these regions midway between higher visual areas, auditory areas and language and semantic areas (Pobric et al. 2007; Visser et al. 2010; Fedorenko et al. 2011) suggests a genuine MD region, situated to integrate higher visual, auditory and semantic/language processing. Similar to previous findings in Broca's area (see Fedorenko et al., 2012), these data highlight an MD area with close proximity to language regions.

Previous studies employing math tasks identify an MD-like pattern that is commonly interpreted as a domain-specific "math network" (Amalric and Dehaene 2017). Our results show that the math contrast engages all extended MD regions, but with relative preferences among dorsal parietal areas (AIP, LIPd, MIP; and POS2 on the medial surface) and dorsal frontal region IFJp. We note that in our data, math preferences are potentially confounded with auditory preferences (Michalka et al. 2015).

Our selected task contrasts might have led us to miss MD regions that were already active in the easier tasks. Indeed, comparison of easy tasks with fixation suggested extension of MD activation into adjacent regions, including FEF, PEF, 9-46d, 7Pm and LIPv. Evidence that even easy tasks produce strong activation in posterior regions of the lateral frontal cortex fits a number of previous reports (Badre 2008; Crittenden and Duncan 2014; Shashidhara et al. 2019). At present, the limited number of suitable contrasts in the HCP data and the difficulty of interpreting contrasts with fixation preclude strong conclusions on these additional putative MD regions. For example, while activation of FEF and PEF might simply reflect eye movements, this interpretation could be incomplete given that one easy task (0bk) used only stimuli placed in the center of the visual field. Future studies utilizing HCP methods and examining a broader range of task contrasts should provide clearer answers.

In line with much current thinking, relative functional specializations might suggest that different MD regions are specialized for different cognitive operations. Though this interpretation is reasonable, it leaves open the question of why these regions are active in such a diversity of tasks, how they communicate and coordinate their activities, why their representations show

such flexibility, and why they have such consistently strong functional connectivity. Instead of strong functional specialization, we suggest that distributed MD regions serve to combine and relate the multiple components of cognitive operations. While data from macaques show that putative MD regions share many anatomical connections (Hampson et al. 2006; Mitchell et al. 2016), each also has its own unique fingerprint of connections to and from other brain regions (Petrides and Pandya 1999; Markov et al. 2014). Thus the wide distribution and diverse connections of MD regions likely provides the necessary anatomical skeleton for access to different kinds of information from different brain systems. Different tasks, emphasizing different kinds of information, then lead to quantitatively different patterns of activation across the MD system. At the same time, rich interconnections between MD regions allow information to be rapidly exchanged and integrated.

While core MD regions were more consistently strongly activated than penumbra MD across the current 3 tasks, the core/penumbra distinction is likely more graded than absolute. Indeed, some penumbra MD, in some tasks, show equally strong or stronger activations when compared to core MD (**Figure 2.9**). Our proposal suggests that the activation strength of any one MD region is guided by its unique local and distributed connectivity as well as by the specific integrative demands of the ongoing task. Accordingly, strong penumbra MD activations likely reflect more specialized demands. This is because of penumbra MD's weaker interconnectivity and their membership to different, more specialized RSNs (**Figure 2.6**). Strong core MD activations, on the other hand, likely reflect more diverse integrative demands, owing to core MD's anatomical distribution and stronger interconnectivity. Thus, contrasts with strong and diverse integrative demands, like our current 3 contrasts, will tend to highlight stronger core MD activations. Individual demanding contrasts are more likely to highlight strong activations in specific penumbra MD regions. These ideas are discussed in further detail in **chapter 5**.

To extend the present results, a wider range of task contrasts would be valuable. Though the 3 contrasts used here are already quite diverse, a wider range of contrasts could establish boundary conditions on MD recruitment, and add more detailed understanding of relative functional preferences. One open question concerns strong manipulations of cognitive demand that produce little

MD activation. Most conspicuously, some studies (e.g. Han and Marois 2014; Wen et al. 2018) – though certainly not all (e.g. Jiang and Kanwisher 2003; Crittenden and Duncan 2014) – suggest little MD activation for demanding visual discriminations limited by the quality of sensory data. Though we would contend that any task requires integration of its components, we might speculate that integration demands do not limit performance in simple sensory tasks. Such exceptions to the MD pattern remain an important topic for future work.

2.4.2 MD cortex and resting state networks

In this study we identified the extended MD system using a conjunction of three task contrasts. Using MD regions identified from task data, we proceeded to demonstrate strong within-network functional connectivity at rest. As expected, our analysis of resting state data shows much convergence with canonical functional networks derived from the same data (Ji et al. 2019), but we also found additional fine-grained structure. MD core regions constitute a subset of areas within the canonical FPN that are distinguished by especially strong mutual connectivity. This strong connectivity includes widely separated areas. In contrast to the MD core, penumbra regions are distributed across four canonical networks. Again, compared to other regions within those networks, they are distinguished by especially strong connectivity with the MD core. These results support the picture of MD regions as a strong communication skeleton, with penumbra regions in particular drawing together information from several distinct large-scale networks.

In some prior work (Dosenbach et al. 2006, 2007, 2008), insula, dorsomedial frontal and anterior lateral frontal regions have been combined into a CON network, separate from other control regions forming the FPN. In line with CAB-NP, our precise delineation suggest a slightly different picture, with specific regions of anterior insula (AVI), dorsomedial frontal (8BM) and anterior lateral frontal cortex (a9-46v) included in the MD core, and closely adjacent regions included in a separate CON.

Our conclusions are reminiscent of extensive recent work using network science approaches (e.g., graph theory) to identify putative cortical communication hubs (Sporns 2014; Petersen and Sporns 2015; Bassett and

Sporns 2017; Bertolero et al. 2018). In this graph theoretic approach, hubs are defined by broad connectivity and/or spatial proximity with multiple cortical networks. Typically they include a set of regions resembling the current MD system, but also others including the temporo-parietal junction, extensive regions of the mid- and posterior cingulate and more (Power et al. 2013; Gordon et al. 2018). These connectional findings are broadly consistent with our proposal that MD regions act as an integrative skeleton for cognitive activity, but they leave open the question of precise relations between the MD pattern, defined with converging task contrasts, and the definition of hubs based solely on functional connectivity. Because hubs are defined by connectivity with multiple cortical networks, their identification depends on the granularity with which these networks are separated and by other factors, including the threshold used to define network 'edges' and by potential methodological biases that are commonly overlooked, such as regional differences in receive coil sensitivity that may impact FC values. Such limitations do not apply to definition of MD regions based on converging task contrasts. Further work may help to contrast the functional role of MD regions relative to hubs defined by connectivity but not showing robust activation across multiple diverse tasks.

2.4.3 Subcortical and cerebellar MD regions

We found MD activation and strong functional connectivity with the cortical MD core in the head of the caudate nucleus. In nonhuman primates, the anterior portion of the caudate receives projections from all prefrontal regions (Averbeck et al. 2014). Tracer studies have established that the dorso-lateral prefrontal, dorso-medial prefrontal and parietal cortices, in addition to strong mutual interconnections, also share converging projections to the caudate, mainly targeting its head (Kemp and Powell 1970; Alexander et al. 1986; Yeterian and Pandya 1991; Middleton and Strick 2000; Haber 2003; Hampson et al. 2006; Choi et al. 2016). Within the striatum, overlap in the projection zones of nearby cortical areas may in part be mediated by interdigitating dendrites and axons that cross functional boundaries (Haber 2003; Averbeck et al. 2014). These anatomical findings are consistent with the identified MD activations in the head of the caudate and strongly support its putative role in information integration.

We also identified distributed MD regions in the cerebellum. Tracer studies identify polysynaptic connections between the prefrontal cortex and the lateral portions of crus I and II as well as vermal lobules VII and IX (Bostan et al. 2013), largely overlapping with our MD cerebellar regions. In addition, previous studies have implicated similar cerebellar regions in several aspects of complex cognitive activity (King et al. 2019) as well as encoding task-relevant information (Balsters et al. 2013). Importantly, MD cerebellar regions do not overlap with motor-related regions (Diedrichsen and Zotow 2015). Not surprisingly, there is strong overlap between the cerebellar regions identified here using converging task contrasts and strong connectivity with the MD cortical core, and the FPN-related cerebellar network defined in previous studies (Buckner et al. 2011; Ji et al. 2019). Importantly, the cerebellar MD regions were identified by connectivity with the more spatially restricted cortical MD core in comparison with the cortical FPN, further suggesting a central role for the cortical MD core.

Based on resting state connectivity, we also identified putative MD regions in the anterior portion of the thalamus. The connectivity-identified thalamic regions are in line with numerous studies reporting strong anatomical and functional connectivity between thalamic nuclei (especially medio-dorsal portions) and fronto-parietal cortex (Haber 2003; Halassa and Kastner 2017). A similar thalamic region was also identified by the conjunction of working memory and math contrasts; for relational reasoning, however, this thalamic region was already active in the contrast of easy task vs rest, with no further increase in the harder task version.

Further work at higher field MRI strength (e.g., 7T) may help clarify the role of these and other subcortical regions associated with the cortical MD system. Meanwhile, in agreement with known anatomy, our data suggest extensive cortical-subcortical interaction in control of complex cognitive activity.

2.4.4 A precisely-localized neural system supporting complex cognition

For continued progress in understanding brain functional organization, a basic step is delineation of an accepted set of component regions. In the case of MD activation, progress has been slow because we lack such a precise definition, leading to many thousands of studies showing similar activation patterns, but little agreement over questions such as functional similarity/differentiation. Based on the HCP multi-modal parcellation, our work defines a precise network of core MD regions and their surrounding penumbra, and establishes a pattern of widespread co-recruitment, relative functional differentiation, and strong functional connectivity.

These properties support a central role for the MD system in supporting complex cognition. The richness of even a simple cognitive event, and the precise relations that must be established between its different components, call for a widely-connected system, able to access any kind of cognitive content. Owing to their differential anatomical and functional connections, different MD regions may be preferentially recruited as different cognitive contents are accessed. However, strong interconnection between MD regions likely allows different information to become quickly integrated and exchanged, leading to a dominant pattern of co-activation. Extensive MD connections with other regions also suggest a broad role in coordinating brain activity in service of the task at hand. This proposal conforms with the finding that the MD system, among different brain networks, is the most striking in changing its global brain connectivity during different task states (Cole et al. 2013).

CHAPTER 3

VISUAL AND AUDITORY PREFERENCES OF DOMAIN-GENERAL BRAIN REGIONS

3.1 Introduction

The previous chapter identified domain-general or Multiple-demand (MD) regions that co-activate in association with different cognitive tasks. Against this co-activation background, however, the results also provided the strongest evidence yet of functional preferences or biases (i.e. stronger/weaker activations) for specific tasks (or task components). Mapping the anatomical organization of these functional preferences and uncovering their underlying causes is critical for understanding how MD regions can coordinate whole-brain activity. Chapters 1 and 2 proposed that differential MD anatomical connections underlie these preferences. But the lack of a consensus map of functional preferences remains a barrier to properly validate this proposal. One of the most basic preferences, yet still unclear, concerns MD sensory modality biases. A system concerned with coordinating whole brain activity is expected to communicate with different sensory areas. Indeed MD regions share anatomical connections with and respond to stimuli from different sensory areas (Markov et al. 2014; Noyce et al. 2017). But many details remain unclear. For example, are sensory connections unequal in density? Perhaps to help a division of labour in which some MD regions are more responsive to one modality over another? Could MD

multi-sensory responses be an artefact of finer grained neighbouring modality-selective regions (Michalka et al. 2015)? Or do all MD regions respond equally to all sensory modalities? This chapter attempts to answer some of these questions by using the Human Connectome Project (HCP) multi-modal MRI protocols to scrutinize with unprecedented anatomical resolution MD visual vs auditory preferences during a working memory task.

3.1.1 MD regions: multimodal or unimodal?

Numerous human fMRI studies provide evidence that overlapping regions within frontal, parietal and temporal cortices are activated during tasks presented through visual, auditory or tactile modalities (Downar et al. 2000; Szameitat et al. 2002; Piazza et al. 2006; Vohn et al. 2007; Tombu et al. 2011; Braga et al. 2013; Noyce et al. 2017; Assem et al. 2020; Diachek et al. 2020). For example, chapter 2 demonstrated that all MD regions responded to the visual tasks (working memory, reasoning) and to the auditory task (math). These results align with the generally accepted view of association cortices as convergence zones for anatomical projections from primary and secondary sensory regions (Pandya and Yeterian 1985; Mesulam 1998). Accordingly, studies in non-human primates (NHPs) have shown that neurons in putative homologous MD regions respond to more than one modality (Watanabe 1992; Fuster et al. 2000; Miller and Cohen 2001; Romanski 2007; Stein and Stanford 2008; Gu et al. 2016).

Against this background of multi-modal responses, however, there is evidence for sensory specializations within association cortices. For example, anatomical and physiological studies identified distinct frontal regions receiving afferents from auditory and visual areas [see (Romanski 2007) for a review]. Single cell studies also identify frontal neurons that selectively respond to auditory, visual or somatosensory stimuli (Azuma and Suzuki 1984; Romanski 2007). In line with these findings, studies using resting-state fMRI (rfMRI) connectivity have also stratified association cortices based on their differential connectivity with primary auditory and visual areas (Michalka et al. 2015; Mayer et al. 2016; Braga et al. 2017; Tobyne et al. 2017). In one study, rfMRI and structural connectivity suggested a spatially coarse dorsal (visual) to ventral (auditory) gradient across fronto-parietal regions (Braga et al. 2017). Another

study used HCP's rfMRI data (with brains aligned using multi-modal MRI features; MSMAll) to show that frontal regions spatially overlapping with MD cortex share strong connectivity with posterior-visual regions, strongly suggesting that MD frontal regions are visually biased (Tobyne et al. 2017).

One account to reconcile multi-sensory and sensory-selective results is that some or all MD regions have relative rather than absolute sensory preferences for one or more modalities. But the evidence for this is mixed. On the one hand, a number of fMRI studies that contrasted visual vs auditory versions of a cognitive task (usually tapping executive functions) failed to find modality preferences across all (Piazza et al. 2006; Kirschen et al. 2010) or some MD cortex (Lewis et al. 2000; Braga et al. 2013). On the other hand, since the early days of neuroimaging (Bushara et al. 1999), several studies have identified sensory biases within MD regions. One study contrasted a visual vs auditory Stroop-like task and identified a caudal (auditory) to rostral (visual) gradient throughout lateral, medial frontal and medial parietal cortices (Mayer et al. 2016). Another study contrasted a visual vs auditory attention task and identified two distinct (i.e. modality biased) fronto-parieto-temporal networks (Braga et al. 2013). In more posterior lateral frontal regions, Michalka et al. (2015) contrasted visual and auditory attention tasks and identified four interdigitated sensory-biased regions; two visual-biased regions along the superior and inferior precentral sulcus interleaved with two auditory-biased regions, one in between the visual regions and another antero-ventral to the inferior visual region. To estimate the overlap of these sensory-biased regions with the HCP multi-modal parcellation (Glasser, Coalson, et al. 2016), Tobyne et al. (2017) applied a surface transformation approach and estimated they overlap with FEF (visual), 55b (auditory), PEF (visual) and IFJa (auditory) all of which are, interestingly, just outside frontal MD regions (see **Figure 3.2a**). It is important to note, though, that these sensory biases were relative and not absolute i.e these regions did respond to both the visual and auditory modalities but each region was biased to respond more strongly to one modality over the other (Michalka et al. 2015; Noyce et al. 2017; Lefco et al. 2020). That said, the inherent inaccuracies in transforming ROIs across surfaces (Coalson et al. 2018) leaves the question open on an accurate delineation of MD sensory preferences. Further, recent indications suggest more anterior and widespread visual and auditory biases and

their spatial extent is yet to be clearly delineated (Tobyne et al. 2017; Lefco et al. 2020).

Outside of the cerebral cortex, the evidence for sensory biased responses is also mixed. Single cell studies in animals identify both multisensory and sensory selective neurons in the basal ganglia and the thalamus (Nagy et al. 2005; Klemen and Chambers 2012). Some fMRI studies have failed to find subcortical modality preferences (Bushara et al. 1999; Mayer et al. 2016). While in the cerebellum, evidence for selective visual and auditory responses was reported in Cruses I and II where MD cerebellar regions where previously identified (Petacchi et al. 2005; Kirschen et al. 2010).

3.1.2 The current study

While the previous studies provide some evidence for both sides of the story (i.e. multi-modal as well as sensory-biased responses), it is clear that their anatomical delineations are far from complete. An important observation from recent studies is that traditional imaging approaches will miss out on strong evidence of sensory-biased regions (Noyce et al. 2017; Lefco et al. 2020). Such traditional approaches rely on suboptimal brain alignment procedures (i.e. using sulci only) which fail to capture individual differences in areal topographies (different sizes and shapes) (Coalson et al. 2018). In this study, we use state-of-the-art HCP pipelines which utilize multi-modal MRI features (Glasser, Smith, et al. 2016; Robinson et al. 2018) for sharper brain alignment to compare anatomical distribution of our identified extended MD system (**Figure 3.2a**) and sensory biases, previously identified in the literature, by contrasting a visual and an auditory version of a working memory task, each with two levels of difficulty, performed by the same set of subjects.

3.2 Methods

3.2.1 Subjects

Thirty-seven subjects participated in this study (age=25.9±4.7, 23 females, all right-handed). Originally fifty subjects were scanned over two sessions; thirteen subjects were excluded either due to incomplete runs from both sessions (n=5), excessive head movement during scanning (n=4), technical problems during scanning (n=2) or during analysis (n=2). All participants had normal or corrected vision (using MRI compatible glasses). Informed consent was obtained from each subject and the study was approved by the Cambridge Psychology Research Ethics Committee.

3.2.2 Task Paradigms

Each subject performed five tasks in the scanner over two sessions. The current study used data from two tasks: visual n-back (session 1), auditory n-back (session 2). Each n-back task was performed for four runs, and each run consisted of four 1-back (easy) and four 3-back blocks (hard). Each task block (30 s) started with a cue (4 s) followed by 12 trials (24 s, 2 s each) and ended with a blank screen (2 s) as an inter-block interval. Task blocks were paired (easy followed by hard, or hard followed by easy) and the order was counterbalanced across runs and subjects. A fixation block (16 s) followed every two paired task blocks. In the visual session, each run consisted of 36 blocks: 8 visual n-back blocks, 12 fixation blocks, 8 blocks for each for two other visual tasks. In the auditory session, each run consisted of 8 auditory n-back and 4 fixation blocks. In the auditory session, n-back runs were alternated with runs of another visual task not analysed here.

Each trial lasted for 2 s. The visual stimulus was presented for 1500 ms (auditory stimuli had a median duration of 1250 ms and ranged between 1250-1520 ms), followed by 500 ms (480-750 ms) of a blank screen. Responses were accepted at any moment throughout the trial. For the 3-back condition, subjects were instructed to press right for the target stimulus (i.e. current stimulus was the same as the one 3 steps back), and left for all non-target presentations. Similarly, for the 1-back condition, subjects were instructed to press right for the target stimulus (i.e. current stimulus was an exact repetition of the immediate previous stimulus) and press left for all non-target stimuli. In each block there were 1-2 targets, and in the case of the 3-back task 2-4 non-target lures (repeated items in

the wrong n-back position, either 2-back or 4-back). For the visual n-back, stimuli consisted of pictures of faces and houses. Face stimuli were selected from the Developmental Emotional Faces Stimulus Set (Meuwissen et al. 2017). Faces were either males or females, children or adults, making a happy or sad face (**Figure 3.1**). House stimuli were pictures of houses or churches, old or new, from inside or outside. There were 32 faces and houses each, counterbalanced across each of the three categories within it. These categories were necessary for other visual tasks during the session and have no bearing here. Auditory n-back stimuli consisted of animate (e.g. a human's cough, a lion's roar) and inanimate (e.g. a musical instrument, a bell ringing) sounds. There were 9 animate and inanimate sounds each. Each stimulus type was presented in a separate block and all stimulus features were counterbalanced across blocks and runs. Subjects were encouraged to use their right hand and respond to targets using a middle finger press and to non-targets using an index finger press but this was not enforced and several subjects found it more comfortable to use both hands for responses responding with index fingers or thumbs.

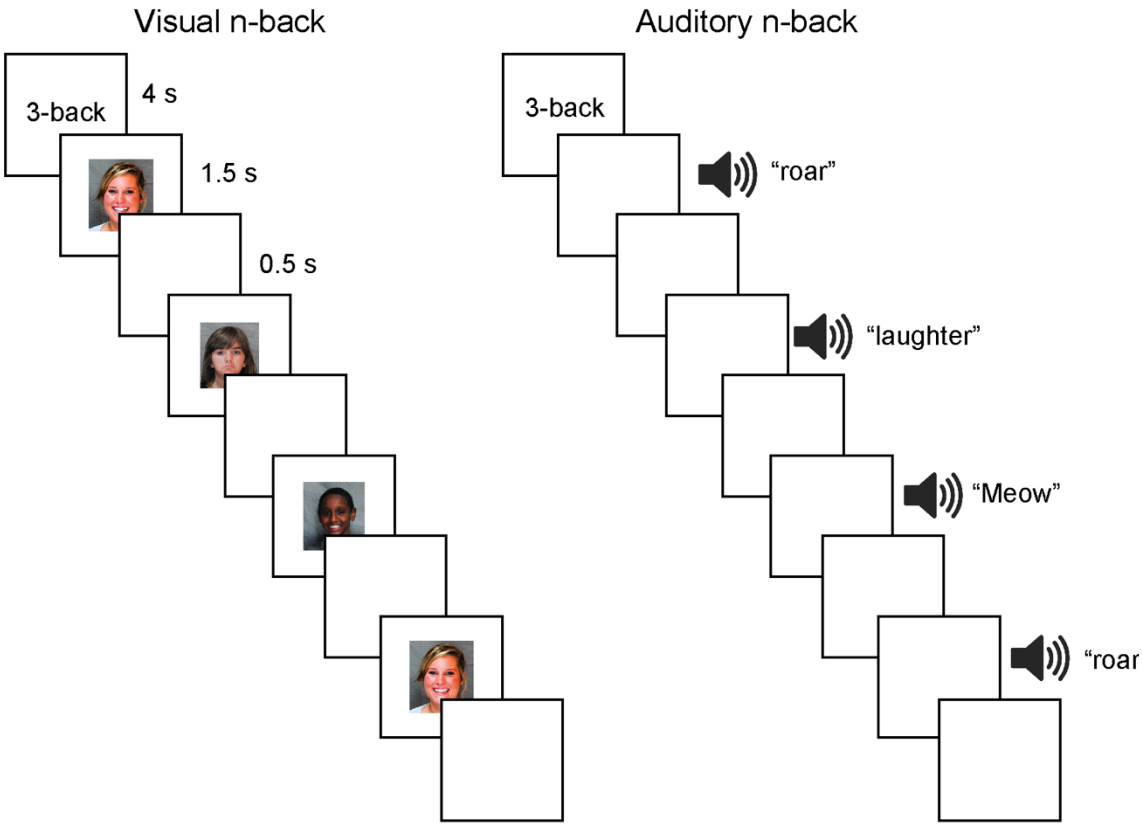

Figure 3.1 Task paradigms. Illustration of a stimulus sequence from each n-back task. Each trial lasted for 2 s during which participants pressed left for every non-target stimulus and right for a target stimulus.

3.2.3 Image Acquisition

Images were acquired using a 3T Siemens Prisma scanner with a 32-channel RF receive head coil. MRI CCF acquisition protocols for HCP Young Adult cohort were used (package date 2016.07.14; https://protocols.humanconnectome.org/CCF/). These protocols are substantially similar to those described in the methods section of chapter 2 and in previous studies (Glasser et al. 2013; Smith et al. 2013; Uğurbil et al. 2013) but do differ in some regards; All subjects underwent the following scans over two sessions: structural (at least one T1w MPRAGE and one 3D T2w SPACE scan at 0.8-mm isotropic resolution), rest fMRI (2 runs × 15 min), and task fMRI (5 tasks, 4 runs each, approx. 100 min total). Whole-brain rest fMRI and task fMRI data were acquired using identical multi-band (factor 8) EPI sequence parameters of 2-mm isotropic resolution (TR = 800 ms, TE=37 ms). Both rest and task EPI runs were acquired in pairs of reversed phase-encoding directions (AP/PA). Spin echo phase reversed images (AP/PA) were acquired during the structural and functional (after every 2 functional runs) scanning sessions to (1) correct T1w and T2w images for readout distortion, (2) enable accurate cross-modal registrations of the T2w and fMRI images to the T1w image in each subject, (3) compute a more accurate fMRI bias field correction and (4) segment regions of gradient echo signal loss.

3.2.4 Data preprocessing

Data preprocessing was also substantially similar to the HCP's minimal preprocessing pipelines (Glasser et al. 2013) detailed previously in the methods section of chapter 2. Differences are noted here. HCP pipelines versions 3.27.0 and 4.0.0 were used (https://github.com/Washington-University/HCPpipelines). Briefly, for each subject, structural images (T1w and T2w) were used for extraction of cortical surfaces and segmentation of subcortical structures. Functional images (rest and task) were mapped from volume to surface space and combined with subcortical data in volume to form the standard CIFTI grayordinates space. Data were smoothed by a 2mm FWHM kernel in the

grayordinate space that avoids mixing data across gyral banks for surface data and avoids mixing areal borders for subcortical data.

Rest and task fMRI data were additionally identically cleaned up for spatially specific noise using spatial ICA+FIX (Salimi-Khorshidi et al. 2014). To improve its performance, ICA+FIX was applied separately to each of the following concatenated runs: rest-state runs (2x15 mins), visual runs from session one (4x15 mins), auditory runs (4x5 mins). An improved FIX classifier was used (privately provided by M. Glasser and HCP team) for more accurate classification of noise components in task fMRI datasets. After manual checking of ICA+FIX outputs for 10 subjects, a threshold of 50 was determined for "good" vs "bad" signal classification. In contrast to chapter 2, global structured noise was not removed using temporal ICA as the scripts have not been made public yet due to ongoing optimizations.

For accurate cross-subject registration of cortical surfaces, MSMAll (i.e. "sulc" (cortical folds average convexity), myelin, resting-state network and rfMRI visuotopic maps) were used to optimize the alignment of cortical areas (Robinson et al. 2014). In this study, 30 mins of resting state were used (cf. ~1 hour for chapter 2 dataset).

3.2.5 Task fMRI analysis

Task fMRI analysis steps are detailed in Barch et al. (2013) and are similar to those mentioned in chapter 2. Briefly, autocorrelation was estimated using FSL's FILM on the surface (default parameters in HCP's task fMRI analysis scripts were used). Activation estimates were computed for the preprocessed functional time series from each run using a general linear model (GLM) implemented in FSL's FILM (Woolrich et al. 2001).

For each of the n-back tasks, 4 regressors were used (2 stimulus category x 2 task difficulty). Each predictor covered the period from the onset of the cue to the offset of the final trial (28 sec). All regressors were convolved with a canonical hemodynamic response function and its temporal derivative. The time series and the GLM design were temporally filtered with a Gaussian-weighted linear highpass filter with a cutoff of 200 seconds. Finally, the time series was prewhitened within FILM to correct for autocorrelations in the fMRI data.

Surface-based autocorrelation estimate smoothing was incorporated into FSL's FILM at a sigma of 5mm. Fixed-effects analyses were conducted using FSL's FEAT to estimate the average effects across runs within each subject.

For further analysis of effect sizes, beta 'cope' maps were generated using custom built MATLAB scripts after moving the data from the CIFTI file format to the MATLAB workspace. Unless mentioned otherwise, parametric statistical tests were used.

For parcellating the cerebral cortex, the group-average HCP multi-modal parcellation (MMP1.0) was used (Glasser, Coalson, et al. 2016) as the individual-specific areal classifier has still not been made public. Values of vertices sharing the same areal label were averaged together to obtain a single value for each area.

For subcortical and cerebellar analysis, an MD mask covering regions of the caudate, thalamus and cerebellum was used. In chapter 2, two versions of the subcortical/cerebellar MD masks were defined: One based on a conjunction of task activations and one based on rfMRI connectivity with cortical MD core. In this study, the mask based on rfMRI was utilized because (1) it includes putative thalamic MD regions that are not included in the task-based mask (2) task and rest fMRI masks show substantial overlap in the remaining caudate and cerebellar regions.

3.3 Results

3.3.1 Behavioural performance

Performance on target trials showed that participants were more accurate on the visual than the auditory task during both the easy and hard conditions (**Table 3.1**). Though note that there was no significant visual vs auditory difference for the drop in target detection between the easy and hard versions. As expected, performance on non-target trials was much better than target trials though with a similar visual vs auditory trend. Also, as expected, performance on the easy condition was better and faster than the hard condition for both visual and auditory tasks [with an exception for reaction time (RT) of auditory non-targets].

It is worth noting that reaction times between visual and auditory conditions were not compared as the auditory stimulus takes a longer time to be presented.

Table 3.1 behavioural performance on the visual (V) and auditory (A) n-back tasks for target and non-target trials. $p<0.05$ are in bold.

	Accuracy (%)		V>A	RT (s)	
	visual	auditory	t_{36} (p)	visual	auditory
Targets					
easy	92.5 ±9.2	86.2 ±12	**3.2 (0.003)**	0.62 ±0.08	1.3 ±0.1
hard	78.8 ±10.6	67.2 ±13.7	**4.3 (0.0001)**	0.82 ±0.1	1.39 ±0.14
hard>easy t_{36} (p)	**-6.6 (1.1×10^{-7})**	**-7.3 (1.3×10^{-8})**	1.6 (0.1)	**13.8 (6.5×10^{-16})**	**3.1 (0.004)**
Non-Targets					
easy	98.4 ±2	97.9 ±2.4	1.2 (0.2)	0.61 ±0.1	1.29 ±0.1
hard	94.5 ±3.2	89.6 ±5.5	**5.3 (5.5×10^{-6})**	0.75 ±0.12	1.3 ±0.1
hard>easy t_{36} (p)	**-8.1 (1.1×10^{-9})**	**-9.3 (3.6×10^{-11})**	**5.0 (1.4×10^{-5})**	**11.4 (1.6×10^{-13})**	0.5 (0.6)

3.3.2 No sensory preferences across MD cortex during hard cognitive demands

We first sought to investigate sensory biases with the hard>easy contrast. This is because, as demonstrated in chapter 2, this contrast is commonly associated with strong MD activations. For an initial overview, we examined the group average activations for each modality separately. **Figure 3.2 b, c** show the resulting overview. As expected, both visual and auditory hard>easy activations show substantial overlap with extended MD regions (green borders). Unexpected, though, is the striking similarity between the visual and auditory hard>easy contrasts (correlation between both maps' cortical vertices r=0.96). This similarity was not an artefact of averaging activations across subjects as it was also evident in individual subject activation maps (average r=0.71, range 0.43-0.82).

To quantify hard>easy activations across the 28 extended MD regions (here SCEF and 8BM were considered as separate regions), for each region we averaged the beta estimates for all vertices and performed a one-sample t-test across subjects against a mean of zero. For this analysis, we have also probed hard>easy activations across the 4 regions estimated to overlap with the inter-digitated sensory-biased frontal regions [visual-biased: FEF, PEF, auditory-biased: 55b and IFJa (Tobyne et al. 2017)]. As expected from chapter 2, all extended MD regions were significantly activated in at least one hemisphere (23/28 on both hemispheres) during both the visual and auditory hard>easy contrasts (**Figure 3.3;** $p<0.05$, Bonferroni corrected for n=64 regions). Extended MD activations in the right hemisphere were slightly stronger than the left hemisphere, replicating the findings of the visual n-back task in chapter 2. Sensory-biased regions (FEF, 55b, PEF, IFJa) were significantly activated for both the visual and auditory tasks in at least one hemisphere (**Figure 3.3;** $p<0.05$, Bonferroni corrected for n=64 regions), except for 55b which showed a trending significance for the visual contrast (uncorrected p=0.001). These results confirm recent indications that sensory biases in regions neighbouring the MD system are relative and not absolute (Noyce et al. 2017).

Next to investigate MD sensory preferences, we subtracted the group average activations for the auditory hard>easy contrast from the visual hard>easy contrast. The resulting overview in **Figure 3.4a** showed little to no sensory preferences throughout the extended MD regions and no signs of inter-digitated sensory-biased regions apart from a potentially small auditory biased region in an anterior ventral frontal region (IFSa). To statistically investigate any sensory preferences within those regions, for each subject we subtracted the visual hard>easy map from the auditory hard>easy map and extracted a single value for each region by averaging across its vertices. A one-sample t-test across subjects, for each region, again failed to find any significant sensory preferences for extended MD regions or the potentially sensory biased regions (i.e. FEF, 55b, PEF and IFJa) on either hemispheres (as this was an exploratory test, Bonferonni correction was performed for all cortical parcels n=360; **Figure 3.4b**). We did, however, find a significant auditory preference for IFSa, which is a much more anterior than previously reported frontal auditory biased regions (Tobyne et al. 2017) and lies in between two MD regions p9-46v (caudal) and p47r (rostral).

To uncover potential finer grained regions with sensory preferences, we repeated the one-sample t-test on each cortical vertex (FDR corrected $p<0.05$). This analysis again failed to identify any contiguous sets of significant vertices within extended MD regions (**Figure 3.4c**). Confirming the previous results, we identified a bilateral set of auditory preferring vertices overlapping with IFSa (**Figure 3.4c**). Further, we identified several small sets of significant vertices that overlap with early auditory regions (e.g. A4 and A5) and visual extrastriate regions (e.g. V5), each showing preferences to their corresponding sensory modality (**Figure 3.4c**).

Taken together, these results failed to find any evidence for MD sensory biases during high cognitive demands (hard>easy). This contrast also failed to identify previously reported interdigitated pattern of sensory-biased regions in the frontal cortex. The results, however, did identify a novel anterior ventral frontal region (IFSa) with a relative preference for the auditory modality.

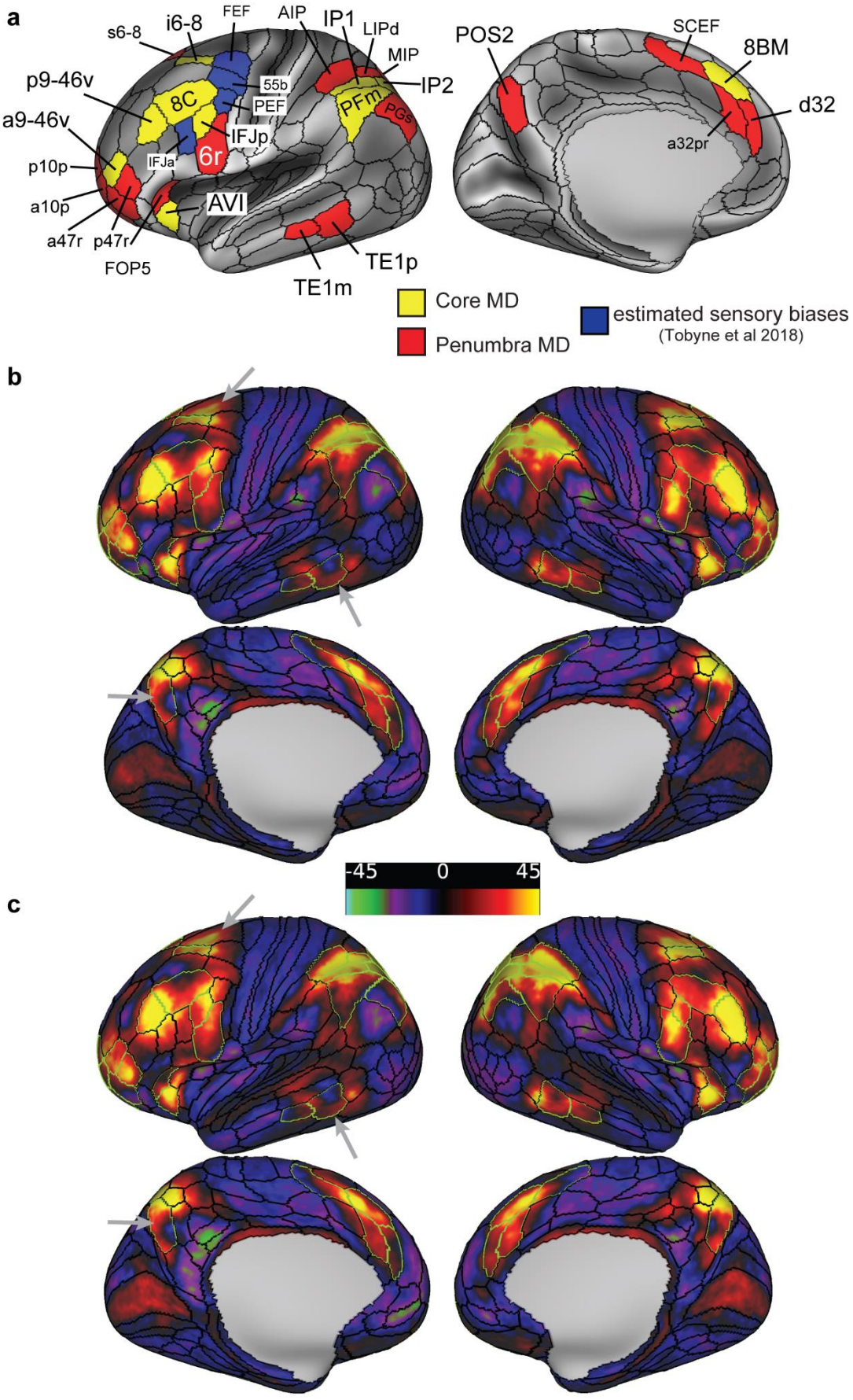
a
s6-8
i6-8
FEF
AIP
IP1
LIPd
MIP
IP2
p9-46v
a9-46v
8C
55b
PEF
IFJp
PFm
PGs
6r
IFJa
p10p
a10p
a47r
p47r
FOP5
AVI
TE1m
TE1p
POS2
SCEF
8BM
d32
a32pr
Core MD
Penumbra MD
estimated sensory biases
(Tobyne et al 2018)
b
-45
0
45
c

Figure 3.2 (above) Group average hard>easy n-back activation maps. (a) Core (yellow) and penumbra (red) MD regions labels. Blue parcels are Tobyne et al 2018 estimate of HCP_MMP 1.0 regions that overlap with sensory biases identified in Michalka et al 2015 (b) visual n-back and (c) auditory n-back hard>easy contrasts. Activation values are beta estimates. Black contours correspond to the HCP_MMP 1.0 areal borders and green contours correspond to extended MD areal borders. Grey arrows highlight some of the remarkably similar activation topographies between the visual and auditory contrasts.

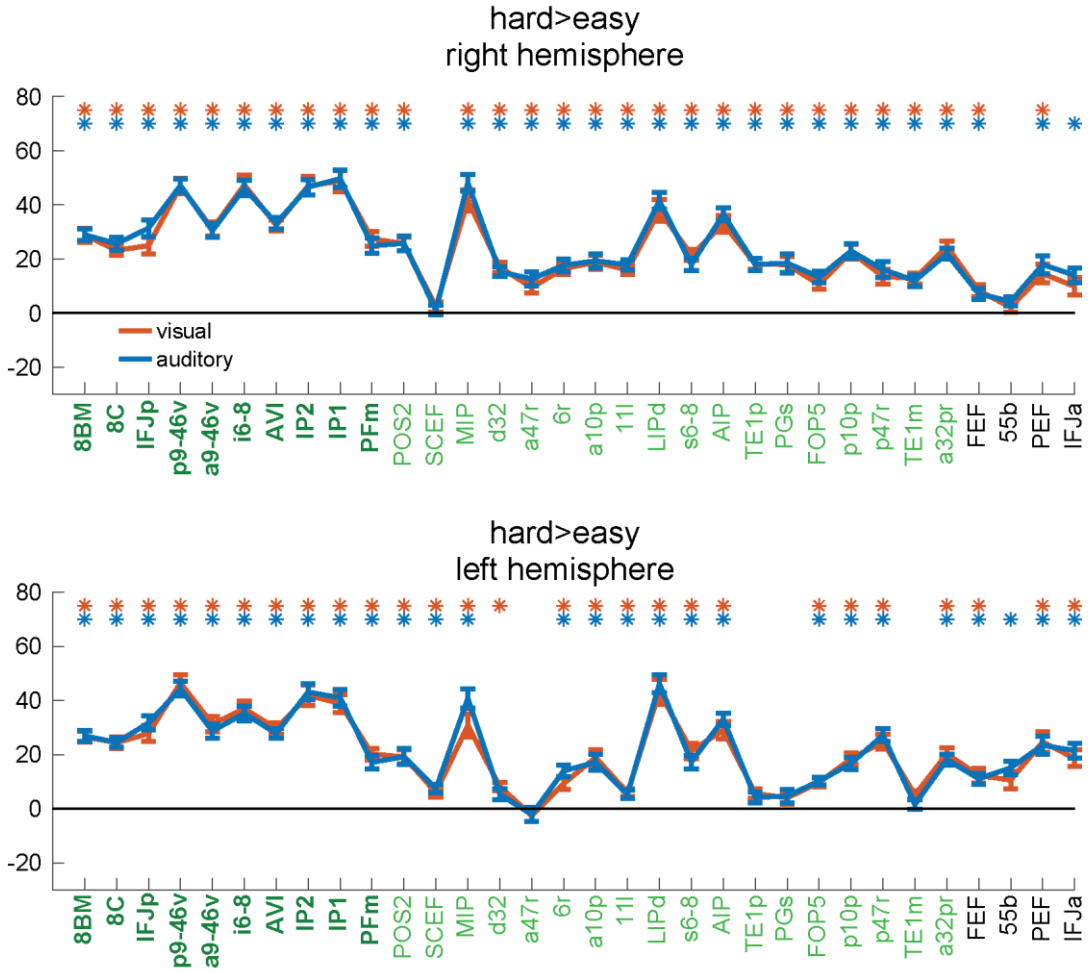

Figure 3.3 Hard>easy contrast activations. (top) right and (bottom) left hemisphere activations (beta estimates) for each of the visual (orange) and auditory (blue) n-back hard>easy contrasts. Error bars represent SEM. Extended MD regions labels are coloured in green (core MD in dark green and bold, penumbra MD in light green). The four regions in black labels correspond to Tobyne et al (2017) estimated sensory-biased regions. Asterisks denote $p<0.05$ bonferroni corrected for n=64 regions.

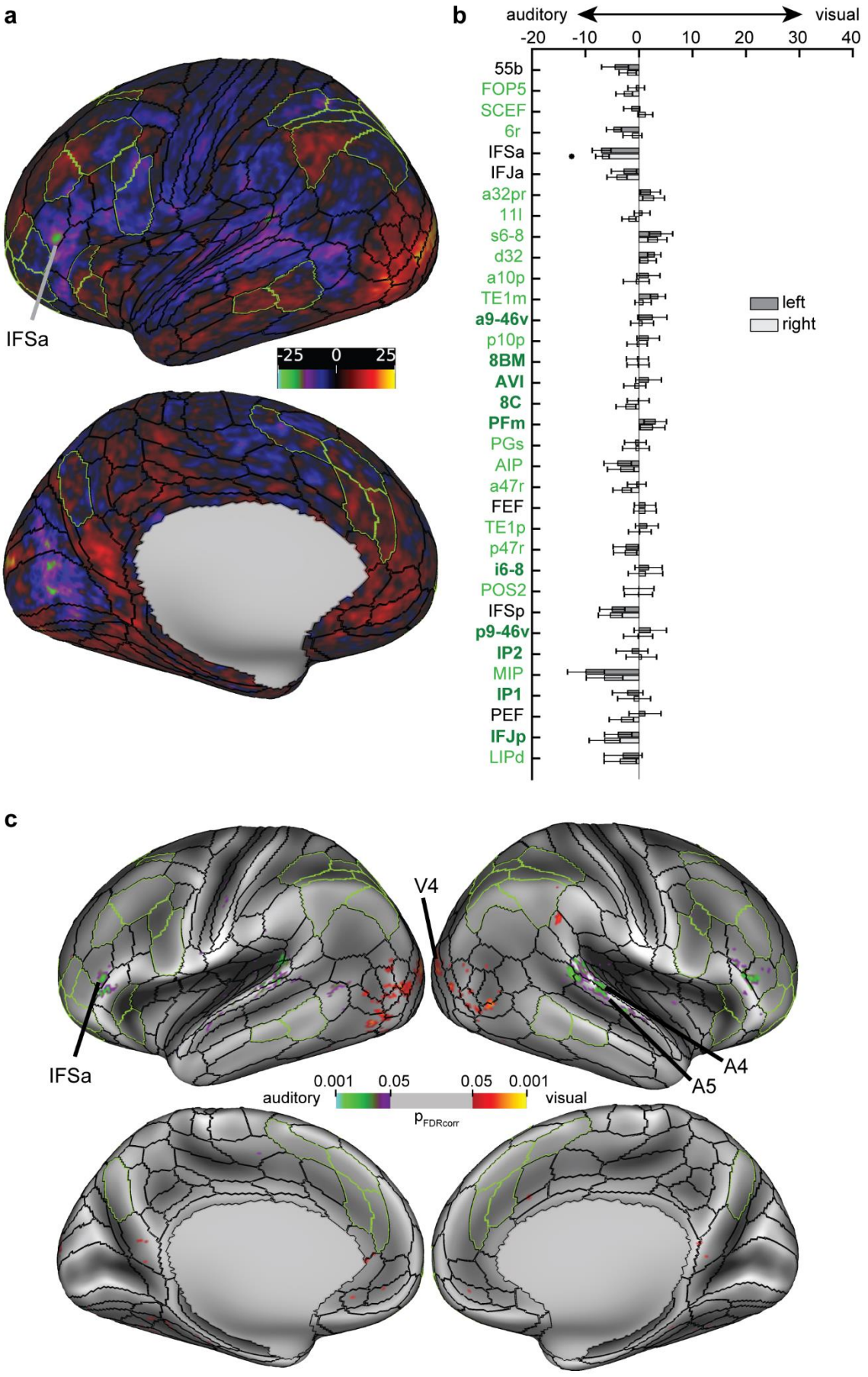
a
IFSa
-25 0 25
b
auditory
visual
-20 -10 0 10 20 30 40
55b
FOP5
SCEF
6r
IFSa
IFJa
a32pr
11l
s6-8
d32
a10p
TE1m
a9-46v
p10p
8BM
AVI
8C
PFm
PGs
AIP
a47r
FEF
TE1p
p47r
i6-8
POS2
IFSp
p9-46v
IP2
MIP
IP1
PEF
IFJp
LIPd
left
right
c
V4
IFSa
A4
A5
0.001 0.05 0.05 0.001
auditory
visual
$p_{FDRcorr}$

Figure 3.4 Hard>easy visual vs hard>easy auditory preferences. (a) Raw beta activations of the left hemisphere for this contrast. Extended MD regions are surrounded by green borders (b) Bar heights represent average activations for each region across subjects. Error bars represent SEM. Asterisks denote p<0.05 bonferroni corrected for n=360 regions. Positive values mean a visual preference, while negative values mean an auditory preference. Regions are sorted according to their sensory preferences in Figure 3.5. Light colored bars represent regions of the right hemisphere. Extended MD regions labels are coloured in green (core MD in dark bold green, penumbra MD in light green). (c) Significant vertices with sensory preferences (FDR corrected p<0.05).

3.3.3 Cortical MD sensory preferences revealed during easy cognitive demands

Why did the hard>easy contrast fail to replicate sensory biases, robustly identified in previous studies, across much of the frontal and parietal cortices (Michalka et al. 2015; Noyce et al. 2017; Tobyne et al. 2017)? In an attempt to reproduce these sensory-biased regions, we sought to investigate visual and auditory activations for the easy>fix contrast. One possibility could be that the hard>easy contrast overlooked sensory-biased regions that are already strongly engaged during the easy task. For an initial inspection, we subtracted the group average auditory easy>fix contrast from the visual easy>fix contrast. The resulting overview in **Figure 3.5a** revealed several hotspots with prominent sensory preferences. To test the statistical significance of these preferences, we repeated the same analysis mentioned in the previous section using the easy>fix contrast. For each subject we subtracted the visual easy>fix map from the auditory easy>fix map then we performed a one sample t-test, across subjects for each region (after averaging across each region's vertices, p<0.05, Bonferroni corrected n= 360; **Figure 3.5b**) and for each vertex (FDR corrected p<0.05; **Figure 3.5c**).

On the lateral frontal surface, the results replicated the interdigitated pattern of visual vs auditory biases though with a crisper anatomical delineation. In line with Noyce et al.'s estimation, FEF and PEF showed relative visual preferences. In between FEF and PEF, a small posterior region within 55b

showed a significant auditory preference (**Figure 3.5a, c**) which is stronger in the right hemisphere (**Figure 3.5b**). Further anterior, PEF's visual preference extended towards IFJp and IFJa. Within IFJa, we found that its dorsal segment had a visual preference, while its ventral segment had an auditory preference. This division was more prominent on the left hemisphere (**Figure 3.5a, c**). Because of this sensory division, IFJa as a region shows no overall sensory preferences (**Figure 3.5b**). Further anteriorly, we identified two more interdigitating regions: IFSp with a relative visual preference, confirming previous indications of a new anterior visually-biased region (Lefco et al. 2020). More anteriorly, IFSa had an auditory preference replicating our hard>easy findings in the previous section. Even more anteriorly near the frontal pole, we identify a visual preferring hotspot mostly overlapping with p47r (penumbra MD), just ventral to core MD region a9-46v. It is worth pointing out how all the previously mentioned sensory-biased regions surround core MD regions (**Figure 3.5a, c**).

Interestingly, almost all MD regions showed significant relative visual-preferences (**Figure 3.5**). For core MD, IFJp is the most visually biased and a9-46v is the least. In penumbra MD, LIPd showed the strongest visual preferences. Around left anterior insula, FOP5 had the strongest auditory preferences, adjoining AVI (core MD) which had a visual preference. Both 6r and SCEF showed no overall preferences likely due to the antagonistic finer grained visual and auditory biases (**Figure 3.5**).

As observed in the hard>easy analysis, early auditory and visual regions showed sensory biases though here they were more prominent and more spatially extensive. (**Figure 3.5a, c**). Within visual regions, foveal/central patches had strong visual preferences while patches related to peripheral visual field had auditory preferences (**Figure 3.5a, c**). These results could be thought to reflect that attention to auditory stimuli suppresses foveal vision but it might also suggest a functional role for peripheral visual regions in auditory processing. One more finding is worth mentioning, on the medial parietal surface, we identified a novel non-MD small auditory preferring region overlapping with area PCV.

In summary, most MD regions had relative visual preferences. These visual preferences cannot be explained by task difficulty because behavioural

data suggested the auditory task was more challenging, thus on the contrary, the auditory task should have engaged MD regions more strongly than the visual task. We further delineated six interdigitated visual and auditory biased regions on the lateral frontal surface, two of which exist further anterior to previous reports. Previously it was not clear whether these regions overlapped with MD regions. Here we show that they are located right outside the borders of core MD regions. Importantly, these results demonstrate that MD sensory preferences do not scale with cognitive demand, but likely reach a ceiling level (at least as measured by fMRI) during easy cognitive demands.

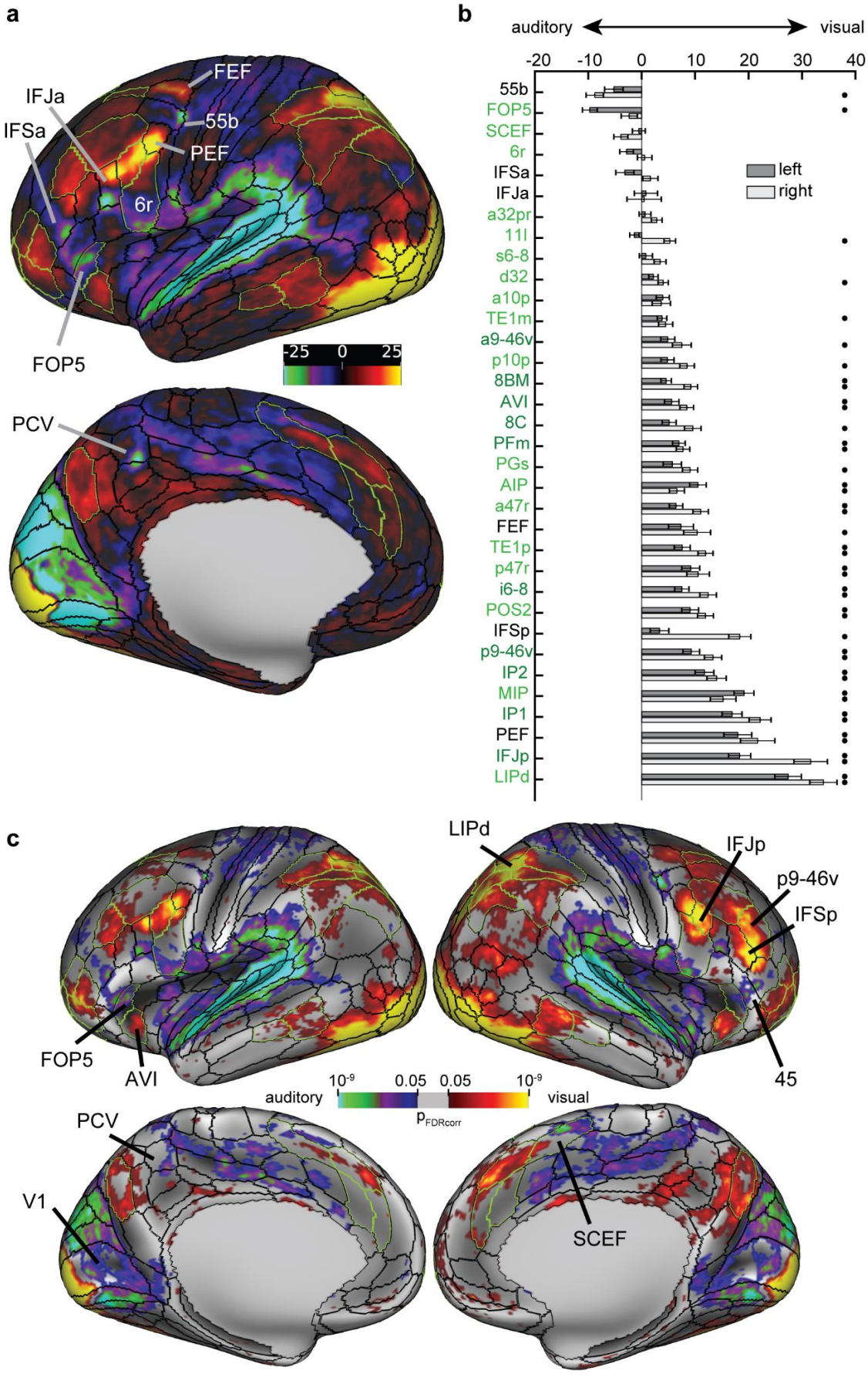
a
FEF
IFJa
IFSa
55b
PEF
6r
FOP5
-25 0 25
PCV
b
auditory
visual
-20 -10 0 10 20 30 40
55b
FOP5
SCEF
6r
IFSa
IFJa
a32pr
11l
s6-8
d32
a10p
TE1m
a9-46v
p10p
8BM
AVI
8C
PFm
PGs
AIP
a47r
FEF
TE1p
p47r
i6-8
POS2
IFSp
p9-46v
IP2
MIP
IP1
PEF
IFJp
LIPd
left
right
c
LIPd
IFJp
p9-46v
IFSp
FOP5
AVI
45
auditory
10-9 0.05 0.05 10-9
visual
pFDRcorr
PCV
V1
SCEF

Figure 3.5 Easy>fix visual vs easy>fix auditory preferences. (a) Raw beta activations of the left hemisphere for this contrast. Extended MD regions are surrounded by green borders (b) Bar heights represent average activations for each region across subjects. All details are the same as in Fig 3.4b (c) Significant vertices with sensory preferences (FDR corrected $p<0.05$).

3.3.4 Sub-cortical and cerebellar MD sensory preferences

In this section, we investigated whether MD sensory preferences extend outside the cerebral cortex. In chapter 2, MD regions were identified in the head of the caudate and in localized cerebellar regions (mainly cruses I and II). Their definition was based on a conjunction of co-activation during diverse cognitive tasks and strong functional connectivity with the cortical core MD. A further putative anterior thalamic MD region was also identified, though in this case, it was based only on its strong functional connectivity with cortical core MD.

First we sought to confirm that the previously identified MD regions (bilateral caudate, thalamus and cerebellum; green borders in **Figure 3.6b**; see Methods section) were activated during each of the visual and auditory hard>easy contrasts. For each region, we obtained a single estimate for the hard>easy activations (by averaging across all MD voxels within a region) and performed a one-sample t-test across subjects. This test indeed confirmed that all bilateral caudate, thalamic and cerebellar MD regions were significantly activated ($p<0.05$, Bonferroni corrected for 6 regions; **Figure 3.6a**).

Next to unveil regions with statistically significant sensory preferences, we repeated the cortical analysis detailed above (i.e. for each subject we subtracted the visual map from the auditory map, once using the hard>easy contrast and once using the easy>fix contrast). First, we focused on the previously identified MD regions. For each MD region we obtained a single visual vs auditory value per subject then we performed a one-sample t-test across subjects. For the visual hard>easy minus auditory hard>easy contrast, none of the MD regions showed any sensory preferences ($p>0.05$, Bonferroni corrected for 6 structures; **Figure**

3.6a), similar to the absent cortical MD sensory preferences for the hard>easy contrast. Meanwhile, the visual easy>fix minus auditory easy>fix revealed visual preferences in MD cerebellar regions bilaterally and the right MD thalamic region ($p<0.05$, Bonferroni corrected for 6 structures; **Figure 3.6b**). Left MD thalamic and bilateral MD caudate regions failed to show any sensory preferences. These results again broadly align with the predominantly visual cortical MD preferences in the easy>fix contrast.

To also explore sensory preferences outside of MD regions (and any finer grained preferences within MD regions), we performed a one-sample t-test on each voxel ($p<0.01$, FDR corrected). For the visual hard>easy vs auditory hard>easy contrast, we failed to identify any interpretable contiguous set of voxels with sensory preferences either subcortically or in the cerebellum (not shown in figure). In contrast, for the visual easy>fix vs auditory easy>fix contrast, we identified a cluster of voxels in the posterior thalamus overlapping with the lateral geniculate nucleus (LGN) with visual preferences (**Figure 3.6b**). We also identified a smaller set of voxels with auditory preferences immediately medial to LGN, the expected location of the medial geniculate nucleus (not shown in figure) which is the relay station for the auditory pathway. In cerebellum, as expected, large clusters of voxels within MD borders in cruses I and II (medial and lateral hotspots) showed visual preferences. Medially, outside MD borders the visual preferences extended both dorsally (into lobule VI) and ventrally (into lobule VIIb), in line with previous studies identifying visual retinotopic responses in these regions (van Es et al. 2019). Laterally, there is some evidence that MD borders are surrounded by clusters of voxels with auditory preferences both ventrally (VI) and dorsally (VIIb).

On the whole, these subcortical and cerebellar results mirror the cortical MD sensory preferences. During high cognitive demands (i.e. hard>easy), no significant sensory preferences were identified, while during easy cognitive demands (easy>fix), MD regions in the right thalamus and cerebellum showed relative visual preferences.

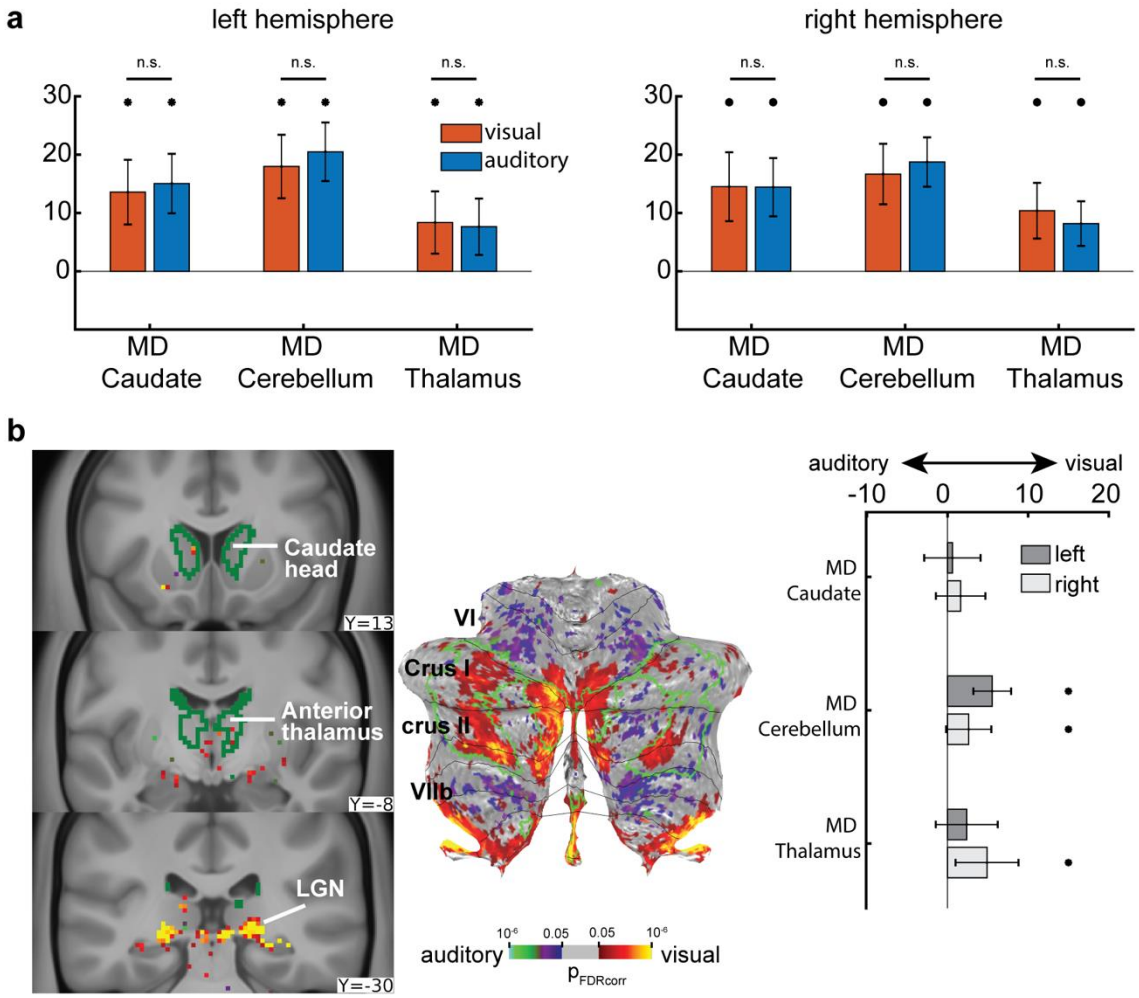

Figure 3.6 Subcortical and cerebellar MD sensory preferences. (a) Raw hard>easy beta activations for the visual and auditory tasks. Error bars are SEM. Asterisks denote significant hard>easy activations ($p<0.05$; Bonferroni corrected n=6 regions). n.s. denotes non-significant differences between visual hard>easy and auditory hard>easy ($p<0.05$; Bonferroni corrected n=6 regions). (b) Significant voxels with sensory preferences for the visual easy>fix vs auditory easy>fix contrast (FDR corrected $p<0.05$). *Left:* subcortical regions. *Middle*: Cerebellar significant voxels are displayed on a flat cerebellum with lines representing anatomical borders. *Right:* Sensory preferences of subcortical and cerebellar MD regions (delineated by the green contours in left and middle)

3.4 Discussion

Previous brain imaging studies painted a mixed picture about the generality/selectivity of sensory-modality responses in association cortices. This study utilised HCP's state-of-the-art multi-modal brain imaging methods to accurately delineate the anatomical and functional organisation of visual vs auditory preferences during a working memory task across the whole brain. The same subjects were scanned over two sessions, performing a visual n-back task in one and an auditory n-back task in the other (each with an easy and a hard version). Although MD regions are activated by both auditory and visual tasks, during low/easy cognitive demands, almost all cortical, subcortical and cerebellar MD regions showed *relative* (rather than absolute) visual preferences. The results also replicated, with a crisper anatomical delineation, a previously reported set of interdigitated visual and auditory biased regions on the lateral frontal surface but localize them just outside core MD regions. The results further identified several novel sensory biases throughout the brain. Importantly, as cognitive demand/task difficulty increased, sensory preferences were dwarfed by demand related activations. In other words, MD regions showed no sensory preferences with additional cognitive demands. We discuss how these new findings potentially reconcile many of the previous conflicting results. We further propose a neural circuit model that predicts load-dependent domain-general and domain-specific responses within MD regions. Further, these results demonstrate the remarkable anatomical precision and replicability of the new HCP pipelines (**Figure 3.2**).

3.4.1 Cognitive load-dependent sensory preferences in MD regions

A striking finding is how, in most MD regions (cortical, subcortical and cerebellar), visual responses were stronger than auditory ones during the easy cognitive demand (easy>fix; **Figure 3.5**, **Figure 3.6**). This is despite the auditory task being harder, suggesting it should have elicited stronger MD activations. The visual biases were more pronounced in penumbra MD (e.g.

LIPd) than in core MD regions, with the exception of IFJp (core MD) which showed strong visual biases. Importantly, a recent fMRI study showed that MD insular and anterior cingulate regions did not show any sensory biases (Noyce et al. 2017). Here we show a clear visual preference for 8BM (cingulate) and AVI (insular) regions. Subcortically, only the right MD thalamus showed a visual preference. Cerebellar MD regions mirrored cortical MD and showed a dominant visual preference. It is worth emphasising, however, that all MD sensory preferences are *relative* and not absolute. MD regions showed clear responses to both auditory and visual tasks (**Figure 3.3, Figure 3.6a**).

An exception for MD visual preferences is peri-insular area FOP5 (penumbra MD) which had relative auditory preferences, while its adjoining AVI (core MD) had relative visual preferences. This observation fits with the broader literature on insular involvement in auditory, language and speech processing (Bamiou et al. 2003; Remedios et al. 2009). A recent invasive electrophysiology study in humans in the left hemisphere separated anterior opercular from anterior insular activity during a reading task with opercular electrodes responding more strongly (Woolnough et al. 2019). Interestingly, in our study auditory preferences were located within FOP5 on the left hemisphere but it was shifted more dorsally outside of the peri-insular region (area 45) on the right hemisphere. This matches findings from a recent fMRI study that found articulation-related responses within the left MD anterior insula but not on the right hemisphere (Basilakos et al. 2018). Our study extends these findings by delineating these preferences between a penumbra and a core MD region. Subcortical (caudate, thalamus) and cerebellar MD regions did not show any auditory biases.

The visual bias for MD regions aligns with a previous rfMRI connectivity study which found that posterior visual regions showed stronger connections (than auditory regions) with frontal patches that broadly overlap with MD areas (Tobyne et al. 2017). Some previous task fMRI studies did highlight visual preference for fronto-parietal activations (Braga et al. 2013; Mayer et al. 2016), though with a coarser spatial resolution. The underlying mechanisms for this visual bias remain unclear. One possibility could be richer MD connections with visual than auditory regions but systematic studies directly comparing visual and auditory systems are lacking (Markov et al. 2014; Donahue et al. 2016).

During high cognitive demand (hard>easy), a different picture emerged: visual and auditory MD activations were remarkably similar with no apparent modality preferences (**Figure 3.2, Figure 3.4**). These results suggest that modality-specific responses constitute a part, but not all, of the variance in MD responses and could account for previous mixed results in the literature as discussed in the introduction.

How is it possible to observe modality preferences at one cognitive load but not the other within the same MD region? One possible neural circuit model is illustrated in **Figure 3.7** that attempts to reconcile the three main findings from this study: (1) MD regions respond to both visual and auditory stimuli (2) Most MD regions show a stronger response during the visual task (3) MD sensory biases are absent during the hard>easy contrast. One can start by considering a putative MD region with a heterogeneous arrangement of visually- and auditory-sensitive neurons interspersed with a larger number of neurons with more complex responses related to cognitive-operations. Similar arrangements have already been observed during audio-visual tasks from invasive studies in NHPs (Watanabe 1992). This arrangement obviously predicts an MD response to both auditory and visual modalities. Critically, however, assuming the visual and auditory cognitive demands are equal, the response strength of modality-selective neurons will determine the sensory-preference of this MD region. While "strength" of a response is likely determined by complex physiological processes (e.g. duration of response or population dynamics), here we consider the simplest case which is the number of modality-sensitive neurons. If our model MD region has more visual than auditory-selective neurons, then an equally demanding task should elicit stronger visual than auditory responses (**Figure 3.7a**). Cognitive-operation neurons will undoubtedly also contribute to this response. During low task demands, activity in these neurons might reflect specific processes operating on information communicated by the modality-specific neurons. (**Figure 3.7a**). As task (integrative) demands increase, more cognitive-operation neurons are expected to be recruited, much of which might reflect mixed selectivity properties, because of the requirements for more complex conjunctions that modality-specific neurons likely cannot support (e.g. binding more items in working memory, linking them to more response rules and temporal information, previous knowledge etc…). Thus, during an increased

cognitive demand, most of the MD region's increased response could be attributed to non-modality specific integrative demands (**Figure 3.7b**). Thus, contrasting high vs low cognitive demands activation, will only highlight the increased recruitment in mixed-selectivity neurons (i.e. integrative demands) without detecting any sensory preferences (**Figure 3.7c**) just like the hard>easy contrast failed to reveal MD sensory preferences (**Figure 3.4**).

One more point is worth noting. While MD visual preferences were stronger in the right hemisphere (**Figure 3.5**), this likely reflects the right hemispheric dominance for the n-back task. Language studies, for example, have shown that MD visual and auditory responses are stronger in the left hemisphere (Diachek et al. 2020).

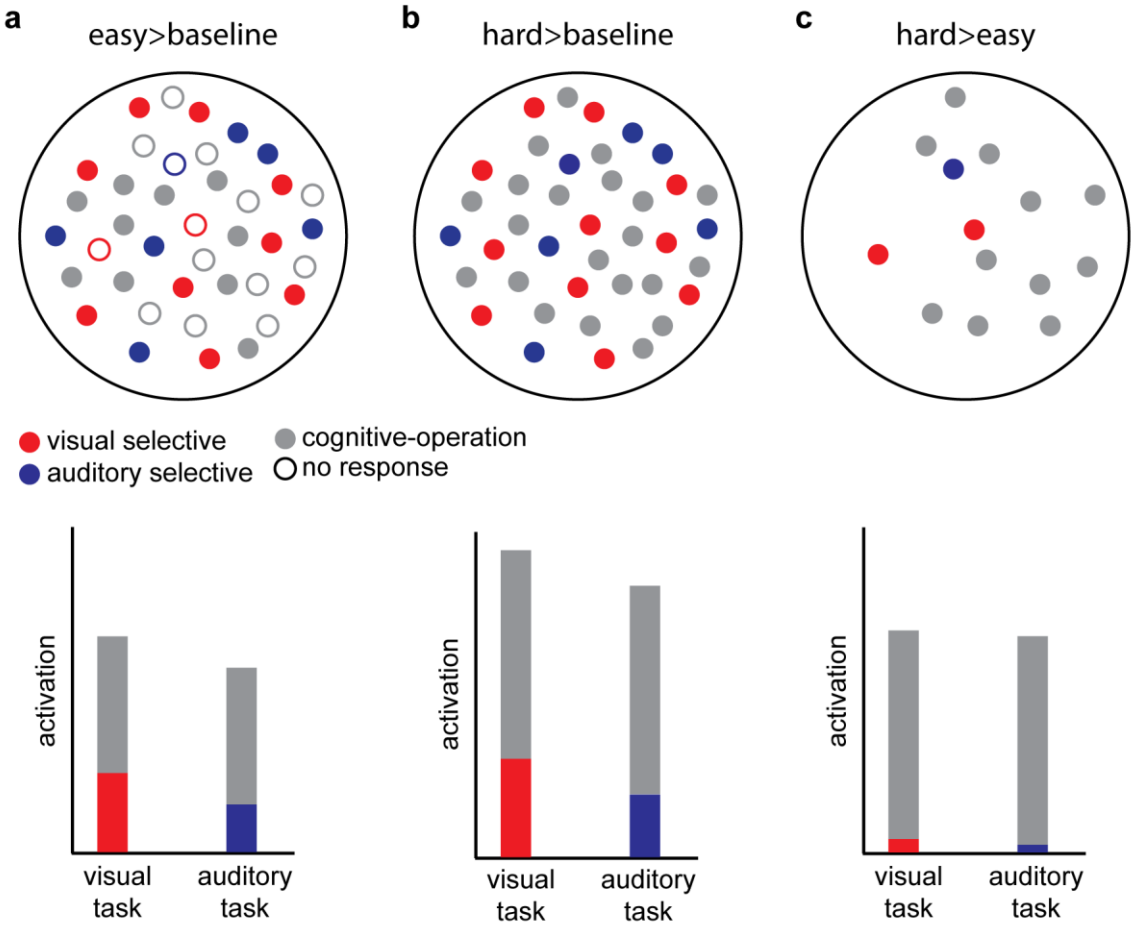

Figure 3.7 A neural model for load-dependent sensory preferences in a putative MD region. (a) *Top:* Responses of individual neurons (small circles) during a low demand task (easy>baseline). Interspersed in the region are neurons with selective responses to visual stimuli (solid red), auditory stimuli (solid blue) and cognitive-operation related neurons (solid grey). Here visual neurons are larger in number than auditory neurons (see Discussion). Neurons with no responses are depicted as hollow circles. *Bottom:* A bar plot of the average neural responses and variance contributed by the different neuron types. During a visual task, visual selective and cognitive-operation neurons are the main contributors while during an auditory task, auditory selective neurons replace the visual selective neurons. Note how auditory neural responses are weaker than visual ones due to their lower number. (b) As task demand increases, visual/auditory selective neural responses increase only slightly while most of the increased response variance is due to increased recruitment of mixed-selective neurons. (c) Subtracting (a) from (c) will mainly highlight the increased recruitment of cognitive-operation neurons. If this recruitment was similar across the visual and auditory tasks, their hard>easy overall responses will look very similar as shown in the bar plot.

3.4.2 Sensory biases surrounding core MD regions

The current study clearly delineates MD regions from nearby regions with generally stronger and more mixed sensory biases (**Figure 3.5**). On the lateral frontal surface, we confirm previous evidence that inter-digitated auditory and visual regions lie immediately outside MD regions (Michalka et al. 2015; Tobyne et al. 2017). One exception is core MD region IFJp which seems to constitute one of the visually-biased interdigitated regions, especially in the right hemisphere (**Figure 3.5**). We found that these interdigitations also extend much more anteriorly than previously thought. Specifically, we identified an anterior frontal auditory preferring hotspot within IFSa which was the only exception for a sensory-biased region to survive the hard>easy contrast. This matches sporadic reports of anterior frontal regions with an auditory preference (Bushara et al. 1999; Mayer et al. 2016). These findings suggest IFSa might play an important role for cognitively demanding auditory stimuli. Near the frontal pole we also identify a visually preferring hotspot mostly overlapping with p47r (penumbra MD).

The sharper anatomical delineation in our study separates one of the inter-digitated regions (IFJa) into a ventral auditory preferring region and a dorsal visual preferring region. This ventral/dorsal division extends along further anterior regions. Relatedly, on the medial frontal surface a caudal-rostral division was visible in SCEF, with its posterior preferring the auditory task while its anterior portion preferred the visual task, further supporting the functional dissociation previously observed across SCEF (Chapter 2). These ventral/dorsal and caudal/rostral divisions broadly align with previous rfMRI connectivity indications of a spatially coarse ventral/caudal (auditory) to dorsal/rostral (visual) gradient (Braga et al. 2017).

Two more findings are worth noting. The first regards area PCV, on the medial parietal surface, which we identified as a novel non-MD small auditory preferring region. A recent HCP rfMRI study found that PCV forms a part of a novel “posterior multi-modal network” that includes regions around the temporo-parietal junction close to language and theory of mind activations (Ji et al. 2019). Second, in early visual regions (V1, V2, V3), peripheral visual regions showed a strong preference for the auditory task while foveal/central regions

were predominantly visual preferring. This aligns with previous fMRI reports showing strong engagement of peripheral visual regions during auditory tasks (Cate et al. 2009) and aligns with anatomical evidence of direct connections between the primary auditory region and peripheral V1 regions (Falchier et al. 2002; Cappe and Barone 2005). This further supports a potential role for peripheral visual regions in auditory processing.

An interesting observation is how some of the previously noted regions with the strongest sensory biases (FEF, PEF, IFJa, IFSp, IFSa, p47r, posterior SCEF, LIPd) surround core MD regions, raising a question about their role in communicating with the MD core. We have previously identified some of them (e.g. p47r and LIPd) as penumbra MD but it is clear that the rest of these regions are also activated by multiple tasks (e.g. during the easy>fix contrasts in chapter 2) and are multi-sensory as the current study shows [see also (Noyce et al. 2017)]. These regions are characterized by their strong initial engagement during easy cognitive demands as well as their membership of different resting-state networks [chapter 2; (Ji et al. 2019; Assem et al. 2020)]. Depending on task demands, their activations "spread" into the nearby core MD regions suggesting they might be important communication points between their affiliated networks and MD core.

These findings also have implications for fMRI studies implementing multivariate analysis methods comparing audio-visual stimuli as multivariate differences might be reflecting strong local univariate differences between these modalities.

Finally, it is important to note that because the visual and auditory stimuli in our tasks are not well-matched, the relative sensory biases identified using the easy>fix contrast could reflect stimulus specific processing instead of modality preferences. For example, it has been previously argued that frontal visual-biased regions are more sensitive to spatial demands while auditory-biased regions are sensitive to temporal demands (Michalka et al. 2015). While our matched cognitive demand (n-back) minimizes the likelihood of this interpretation, the temporal structure of the auditory stimuli could be a driving factor for auditory-biases. Thus, the novel sensory-biases we identified remain to be replicated using better matched visual and auditory stimuli. That said, our replication of sensory-biased regions, identified in previous studies based on

different tasks and task-free rfMRI (Tobyne et al. 2017), attest to the fitness of this contrast.

In summary, this study demonstrated that MD regions show *relative* rather than absolute sensory preferences with almost all MD regions having a visual bias. The sharper anatomical delineation of this study places the strongest sensory biases in regions surrounding the core MD regions suggesting multiple entry points for sensory information into the MD core. This anatomical arrangement might thus provide MD regions with broader integrative abilities to suit relevant task demands.

CHAPTER 4

INTRAOPERATIVE FUNCTIONAL MAPPING OF CONTROL-RELATED REGIONS USING ELECTROCORTICOGRAPHY

4.1 Introduction

The previous chapters investigated the anatomical and functional organization of multiple-demand (MD) brain regions using fMRI. In this chapter I explore their organisation using electrophysiological data acquired by placing electrodes on the brain surface, an approach called electrocorticography (ECoG), from human patients undergoing awake neurosurgeries. There are two important motivations for this study. First, it helps to bridge the worlds of fMRI and electrophysiology. Little is known about MD electrophysiology, especially in humans. Their rapid and adaptive neural dynamics uncovered by invasive animal studies (Stokes et al. 2013) are hidden behind the temporally slow fMRI signal (Logothetis 2008; Dubois et al. 2015). Further, our interpretation of fMRI signals can improve by relating it to its underlying electrophysiological processes (Logothetis 2012).

Second, ECoG is a clinically useful tool for mapping the function of brain regions during tumour surgeries as it assists neurosurgeons to minimize the loss of healthy tissue and preserve brain function (Bertani et al. 2009). This is

important as the recovery of patients with certain brain tumours, such as Low Grade Glioma (LGG), improves as the tumour resection zone becomes larger (Sanai et al. 2010). However, this poses a challenge for neurosurgeons who need to delicately balance between maximising the resection zone and preserving healthy brain tissue. The risks become compounded with tumours like LGG which preferentially emerge in association cortices (Mandal et al. 2020) rich in MD regions. Previous work has informed us that damage to MD regions (e.g. from stroke) is detrimental to the organisation of behaviour and is associated with significant losses in broad measures of intelligence (Roca et al. 2010; Woolgar et al. 2018). Coupled with individual variability in the size and location of functional brain regions (Glasser, Coalson, et al. 2016; Fedorenko and Blank 2020; Shashidhara et al. 2020), intraoperative functional mapping approaches were developed to assist neurosurgeons in navigating the brain functional territories (Sagar et al. 2019).

The study in this chapter investigates whether electrophysiological signals recorded from the lateral surface of the frontal lobe can identify localized control-related regions similar to the frontal MD activations observed in fMRI. The approach of this study is to use a task difficulty manipulation similar to that used in fMRI studies, i.e. by contrasting a cognitively demanding task with an easier version of the task. The spatial distribution of spectral analysis will then be compared to a canonical fMRI fronto-parietal network. Overlap between both will provide converging evidence from electrophysiology and fMRI for the existence of localized control-related regions in the frontal lobe. The identified signal can then be further explored for its clinical potential to extend functional mapping in neurosurgeries to the domain of cognitive control.

4.1.1 Direct electrical stimulation for functional mapping

The most popular mapping approach used in standard clinical care is direct electrical stimulation (DES) (Szelényi et al. 2010; Sagar et al. 2019). Typically, during an awake craniotomy, the patient is asked to perform a behavioural task relevant to the brain region the neurosurgeon is interested in. A probe then

delivers short electrical pulses to the underlying brain region under the assumption that it will temporarily disrupt its function (Szelényi et al. 2010). For example, if the brain tumour is next to a region of the motor cortex suspected to be involved in hand movement, the patient is asked to move their hand while the suspected region is stimulated. Disrupted hand movement is taken as a causal sign of the involvement of that region in hand movement. This level of high spatial accuracy offered by DES has earned it a place as part of standard clinical care and it is commonly applied for mapping the somatotopic organisation of the motor cortices (Suess et al. 2006) as well as language regions in the temporal and frontal cortices (Ojemann et al. 1989). Extensions are developed for other functions, for example to map the fusiform face areas (Parvizi et al. 2012), and higher cognitive functions (Birba et al. 2017) but are not yet established as a standard in clinical practise. That said, DES is a time-consuming process during a time-sensitive surgery; the probe (around 1 cm in diameter) is used to *sequentially* map small sections of a cortical patch tens of times the size of the probe and sometimes multiple stimulation trials of the same section are needed. DES could also induce seizures due to neuronal after discharges, and if the seizures are frequent, it could cut the mapping procedure short (Szelényi et al. 2010). Further, a lack of understanding of how stimulation affects processing in a cortical area makes it difficult to interpret its results, especially for higher cognitive functions (Borchers et al. 2012). DES effects have also been found to spread for a few centimetres beyond the stimulated area (Blume et al. 2004; Matsumoto et al. 2004). Thus, stimulation of a functionally irrelevant area might cause behavioural disruptions overestimating and/or underestimating functionally critical cortex (Crone et al. 2006). Despite these limitations, and in the absence of other established tools, stimulation remains widely regarded as the gold standard for functional mapping.

4.1.2 ECoG for functional mapping

ECoG involves placing electrodes on the cortical (pial) surface to detect electrophysiological signals assumed to be related to the behavioural task the patient is performing. These signals could then either be exclusively used to guide the tumour resection or, more frequently, combined with DES to constrain

the mapping region (Crone et al. 2006). ECoG measures local field potentials (LFPs), the voltage changes resulting from all ionic movements in the extracellular medium (Wang 2010; Buzsáki et al. 2012). LFPs are complex signals, consisting of both irregular (non-oscillatory) and rhythmic (oscillatory) components across a broad range of frequencies (Miller et al. 2009; Wang 2010; Buzsáki et al. 2012). One LFP component popular for functional mapping is signal in the high frequency range (gamma; >30 Hz). Gamma's spatial precision aligns well with established functional anatomy (Crone et al. 2006; Lachaux et al. 2012). For example, increases in gamma power (energy or amplitude of voltage fluctuations) can accurately map the motor somatotopic organization (Miller et al. 2007; Vansteensel et al. 2013), can localize the FFA when seeing faces (Parvizi et al. 2012), and can map language areas in the temporal lobe (Miller et al. 2011). The spatial specificity of gamma is also supported by non-invasive brain imaging studies finding a decent overlap between gamma responses and fMRI activations, especially in early sensory and motor regions (Logothetis et al. 2001; Nir et al. 2007; Engell et al. 2012; Hermes et al. 2012). The temporal resolution of gamma signals has also proved fruitful for tracking the timing of cognitive processes. For example, the onset of gamma activity in primary sensory and motor areas aligns well with the onset of stimuli or movement initiation, respectively (Crone et al. 2006; Lachaux et al. 2012). In language studies, gamma dynamics were also shown to track consecutive stages involved in word production (Pei et al. 2011). These properties make gamma signals an attractive general index of local cortical activity for functional mapping (Crone et al. 2006).

It is still unclear, however, how gamma properties change across brain areas with different cytoarchitectures, connections, and functions (Lachaux et al. 2012). This poses a challenge for their use to understand functional anatomy. Gamma is not a homogenous band and consists of at least two subcomponents: a low gamma band (LG; ~30-70 Hz) and a high gamma band (HG; >70 Hz) (Ray, Crone, et al. 2008; Ray and Maunsell 2011; Buzsáki and Wang 2012). While most of the previous results implicate both components, HG findings have been more robust across cortical regions and studies (Crone et al. 2006; Lachaux et al. 2012). The high spatial fidelity of gamma signals is likely due to the low-pass filtering properties of cortical dendrites, which restrict the spread of high

frequency signals, thus linking their detection to local processes (Buzsáki and Wang 2012). Further, gamma signals have been found to correlate with local spiking activity (Ray, Crone, et al. 2008; Ray and Maunsell 2011; Buzsáki and Wang 2012), suggesting an oscillatory process to synchronize the firing rates of local populations of neurons (Engel et al. 2001; Fries 2015). On the opposite end of synchronized origins, gamma signals were found to be associated with asynchronous firing rates and post-synaptic currents (Miller et al. 2009; Wang 2010; Buzsáki and Wang 2012). Different physiological origins of gamma signals could thus reflect different processes across cortical areas.

To better understand the role of gamma signals in different cortical areas, it is important to consider its accompanying lower frequency LFP components (<30 Hz). Increases in gamma power are usually associated with decreases in power of lower frequencies (Podvalny et al. 2015). Functional mapping studies have long demonstrated that, compared to gamma band, low frequency signals are less spatially and temporally specific (Crone et al. 2006; Lachaux et al. 2012). For example, in a motor mapping study, high gamma activity was able to separate regions related to hand movement from mouth movement. In contrast, beta band (12-30 Hz) was less spatially specific (Miller et al. 2010). Recent results, however, show that cortical areas can exhibit low frequency decreases at distinct frequencies or not exhibit any low frequency decreases in association with gamma increases (Fellner et al. 2019). Thus, combining information about high and low frequency modulations could be utilized as a spectral fingerprint for areal mapping (Siegel et al. 2012). More generally, lower frequency dynamics have been related to spatially distributed large-scale cortical networks (Betzel et al. 2019). In summary, despite unclear physiological origins, the spatial and temporal specificity of gamma signals have facilitated their growing use for mapping cortical regions.

4.1.3 ECoG for mapping MD regions

So far, I have discussed mapping studies utilizing cognitive tasks with overt behaviour (e.g. speech or movement). But how can ECoG map MD functions? To briefly recap relevant information from earlier chapters, MD regions refer to a set of cortical areas distributed in frontal, parietal and temporal lobes. A

functional signature of MD regions arises from increased cognitive demand, with thousands of fMRI studies showing increases in MD activations with increased task difficulty across many types of cognitive domains. MD regions are strongly interconnected (as indexed by correlation of their timeseries), forming a core part of the canonical resting-state fronto-parietal network (FPN) (Duncan 2010, 2013; Fedorenko et al. 2013; Assem et al. 2020; Shashidhara et al. 2020).

Much of our understanding of the electrophysiological properties of MD regions comes from invasive animal and human studies based on concepts of cognitive or executive control. Cognitive control is an umbrella term for processes such as selective attention, working memory, set shifting, response inhibition, conflict monitoring, problem solving, and goal-directed behaviour (Rabbitt 2004; Diamond 2013). Brain imaging studies have long associated executive control tasks with MD co-activations (Duncan 2010, 2013; Fedorenko et al. 2013; Assem et al. 2020; Shashidhara et al. 2020). In this section I review the main MD related electrophysiological findings that are relevant for using ECoG as a functional mapping approach.

Since their discovery, increases in gamma power have been thought to reflect a heightened attentive state (Bouyer et al. 1981). Attended stimuli, whether in early sensory or fronto-parietal regions, will elicit stronger gamma responses than unattended stimuli (Fries 2001; Ray, Niebur, et al. 2008; Szczepanski et al. 2014; Helfrich and Knight 2016). Frontal gamma responses are also stronger for unpredicted vs predicted events (Crone et al. 2006; Dürschmid et al. 2016). In working memory (WM) tasks, increases in WM load lead to parametric increases in frontal gamma power (Howard 2003). Gamma increases are also sustained during WM delay periods (Howard 2003; Mainy et al. 2007). Sustained gamma responses were also observed in lateral frontal regions in eight tasks that varied in difficulty and sensory modality (Haller et al. 2018). However, recent analysis at the single trial level argues sustained responses are artifactual due to averaging multiple trials with discrete gamma bursts (Miller et al. 2018). Increases in task demands as indexed by more abstract rules have also been associated with frontal gamma increases (Voytek et al. 2015). Fronto-parietal gamma responses have generally been interpreted to reflect control or top-down signals. For example, in a visual WM task, enhanced

gamma responses in frontal eye field (FEF) temporally precedes those in visual area V4, suggesting that a top-down attention signal leads to enhanced gamma synchrony (Gregoriou et al. 2009). Collectively, these results show that gamma increases in fronto-parietal regions are observed during a broad range of executive tasks.

Cognitive control tasks are also associated with power modulations in lower frequency bands. For example, improved synchrony in the beta band (12-30 Hz), compared to pre-trial baseline period, was observed between frontal and parietal areas in delayed matched-to-sample and guided search tasks (Buschman and Miller 2007; Saalmann et al. 2007). In contrast, beta power increases were detected in the right inferior frontal gyrus when a habitual motor response was inhibited during a stop-signal task (Swann et al. 2009). In selective attention tasks, alpha band activity (8-12 Hz) decreases in power in the hemisphere contralateral to the attended hemifield (Helfrich and Knight 2016; Sadaghiani and Kleinschmidt 2016). In a switching task, fronto-parietal regions were synchronized in the theta band (4-8 Hz) and this was interpreted to reflect a preparatory state (Phillips et al. 2014). Theta power increases with WM load (Meltzer et al. 2008) and systematically tracks the duration of WM delay periods (Raghavachari et al. 2001). Clearly this sample of studies demonstrates that in fronto-parietal cortices, power modulations in lower frequencies are complex and reflect more than the straightforward decreases in power accompanying gamma increases seen in early cortical regions (Crone et al. 2006; Lachaux et al. 2012).

One framework to understand how high and low frequencies interact for the implementation of cognitive control considers the laminar structure of the cortex. High frequency modulations are prominent in superficial layers while lower frequencies dominate in deeper ones (Wang 2010; Bastos et al. 2018). Feedforward bottom-up signals are carried through the superficial layers by gamma, and feedback top-down signals are carried through deeper layers by low frequencies (Buschman and Miller 2007; Wang 2010; Miller et al. 2018). A complementary framework considers a hierarchical relationship between low and high frequency bands where the phase of the lower frequencies controls the precise timing of high frequency power modulations. This coupling between gamma and lower frequencies has been observed in cognitive control tasks. For

example, demand related increases in gamma power in the frontal cortex were accompanied by enhanced theta synchrony (Voytek et al. 2015). In another study, delta (1-4 Hz)/theta and gamma coupling predicted reaction times in an attention task on a trial by trial basis (Szczepanski et al. 2014).

Finally, it is worth noting that a common limitation for most of the above-mentioned studies is that recording locations are assigned broad labels such as pre-frontal cortex. As explained in chapter 1, such association cortices are rich in functionally heterogenous regions including MD regions. This limits comparison and integration of results across studies. Nevertheless, these results consistently highlight that cognitive control tasks are associated with gamma increases across broad frontal and parietal regions.

4.1.4 The current study

This study used ECoG during awake craniotomies to identify an electrophysiological signature related to MD regions as a first step towards its potential use for clinical functional mapping. The patients involved in this study were undergoing surgery for LGG tumours. In conventional ECoG studies involving epilepsy patients, electrodes are implanted for a few days/weeks to localize epileptic foci and experimental testing occurs during this period. Electrodes locations in such studies are determined based on pure clinical considerations. In contrast, the electrodes in the current study were temporarily placed for a short duration during the surgery and their locations were chosen based on research considerations (limited by the craniotomy).

The approach to localize frontal control-related regions in this study was motivated by fMRI studies of MD regions which contrasts brain activity of a difficult task with an easier version. The tasks in this study were an easy counting task (from 1 to 20) and a harder version requiring alternate counting between letters and numbers (1 a 2 b 3 c….20). The hard task shares some features with the Trail task which is commonly used to assess executive functions as part of standard neuropsychological assessment. The tasks were designed to be easily administered in an intraoperative setting but also as matched as possible across cognitive components (i.e., counting), presentation form (verbal instructions), and response modality (verbal response). The

expected outcome from this difficulty manipulation is that it will be associated with localized increases in gamma power. This stems from evidence that cognitively demanding tasks elicit localized fMRI BOLD increases and the previously discussed decent spatial correlation between BOLD and localized gamma signals.

4.2 Methods

4.2.1 Patient recruitment

Out of twenty-one patients who underwent awake craniotomies (at the Department of Neurosurgery at Addenbrooke's hospital, Cambridge, UK), thirteen participated in this study (age range 22-56; 6 males; see **TABLE 4.1** for patient demographics). The other eight patients were excluded either due to technical difficulties or inability to perform the tasks during the surgery. Patients were recruited from the same pool of glioma patients that are normally evaluated for awake neurosurgeries by the adult neuro-oncology multidisciplinary team at Addenbrooke's hospital (Cambridge, UK). All study procedures were approved by the East of England - Cambridge Central Research Ethics Committee (REC reference 16/EE/0151). Patients gave informed consent to participate and were aware that the research will not benefit themselves but that it also would not impact their clinical care before, during or after surgery.

4.2.2 Experimental procedures

All patients were familiarized with the tasks during standard pre-operative clinic visits. During the surgery, the testing was performed after the patient has been awakened and prior to tumour resection (except for one patient where the experiment was performed after partial resection due to clinical considerations). **Figure 4.1a,b** illustrate the intraoperative setup and cognitive tasks. During the awake craniotomy, patients performed one baseline task and two cognitive tasks. For the baseline task, the patients were asked to stay calm and remain silent for a period of 2-3 mins (rest). All personnel in the surgical theatre were asked to limit

their conversations to minimize disruptions. The baseline task was immediately followed by alternating trials of two tasks: counting forward (1 to 20; easy) and alternate counting and reciting the alphabet (1, a, 2, b, 3, c, up to 20; hard). Task onsets were cued either verbally by the experimenter saying "start now" or by an audio bleep. The task was stopped when the patient finished counting or after around 1 minute if the patient needed more time during the hard task. Each task condition was repeated for 2-5 trials (median for both = 4 trials) based on each patient's ability and time constraints during the surgery. Easy trials took on average 20.1±7.4s, while hard trials were longer 29.4±9.4s. Most patients were instructed to alternate between the easy and hard conditions, though on a few occasions some easy/hard trials were performed in succession (in some cases this could highlight some perseverative behaviour from the patients). Only correctly performed trials (i.e. no errors in forward or alternate counting) were included in the analysis (e.g. a failed hard trial that was excluded: 1, a, 2, b, 3, b, 4, b, 5, b, 6, b…).

4.2.3 MRI acquisition

MRI data were acquired pre-operatively using a Siemens Magnetom Prisma-fit 3 Tesla MRI scanner and 16-channel receive-only head coil (Siemens AG, Erlangen, Germany). Structural anatomic images were acquired using a T1-weighted (T1w) MPRAGE sequence (FOV 256 mm x 240 mm x 176 mm; voxel size 1 mm isotropic; TR 2300 ms; TE 2.98 ms; flip angle 9 degrees).

4.2.4 Electrode mapping

The extent of craniotomy of all patients was determined by clinical considerations to allow for the tumour resection. Based on the craniotomy size, one to three electrode strips were placed on the cortical surface in regions judged by the neurosurgeon to be healthy. Strips placed on the tumour or outside of the frontal and motor cortices were excluded from this study. Each strip was composed of four electrodes. Two types of strips were used with electrode diameter either 5 mm (MS04R-IP10X-0JH, Ad-Tech, Medical Instruments

corporation, WI, USA) or 3 mm (CORTAC 2111-04-081, PMT Corporation, MN, USA). For both strip types, electrodes spacing was 10 mm centre to centre.

Electrode locations were determined either using (1) an automated method with a probe linked to a stereotactic neuronavigation system (StealthStation® S7® System, Medtronic, Inc, 24 Louisville, CO, USA) or (2) a semi-manual "Grid method" using intraoperative photographs and a grid-like delineation of cortical sulci and gyri. Most electrodes (51/79) were localised using the automated method but due to occasional technical limitations, 28 electrodes were localized using the Grid method. Both methods are illustrated in **Figure 4.1c** and are detailed below.

(1) Stereotactic neuronavigation: A hand-held probe was placed at the centre of each electrode, automatically registering its physical coordinates, using the neuronavigation system, to the subject's native high resolution preoperative T1w scan. In some cases, coordinate data were available for only two or three out of the four electrodes in each strip. This was due to either time constraints during the surgery or because an electrode was located underneath the skull, not allowing the placement of the probe on it. Each subject's native T1w scan was linearly co-registered with the MNI template volume at 2 mm resolution using FLIRT as implemented in the FSL using 12 degrees of freedom (full set affine transformation) and the correlation ratio cost function. The resulting native-to-MNI transformation matrix was then used to convert electrodes native coordinates to MNI coordinates.

(2) The Grid method: This follows the method described in (Havas et al. 2015) and (Ojemann et al. 1989). (a) Visible major sulci were delineated from the intraoperative photographs: precentral sulcus, sylvian fissure, inferior and superior frontal sulci. Spaces between these sulci were populated by vertical lines (1.5 cm apart) to create a grid-like structure (b) A grid was created in the same way on a template cortical reconstruction of the MNI volumetric map (reconstructed using the HCP structural preprocessing pipeline 4.0.0; https://github.com/Washington-University/HCPpipelines) (c) MNI coordinates for each electrode were extracted by manually marking its approximate location on the template cortical grid while it was visualized using the Connectome Workbench v1.4.2 (https://www.humanconnectome.org/software/get-connectome-workbench). As the template cortical reconstruction is co-registered

with its MNI volumetric version, it facilitated the automatic transformation of any point marked on the surface back to its MNI volumetric coordinates.

Electrode displacements due to brain shifts (caused by pressure changes related to craniotomy) were compensated by back-projecting onto the cortical surface along the local norm vector (Hermes et al. 2010) as implemented in the fieldtrip (v20160629) protocol for human intracranial data (Stolk et al. 2018). Electrode activations were projected on the template cortical surface using a weighted sphere method with 10 mm surface smoothing as implemented in fieldtrip.

4.2.5 Electrophysiological data acquisition and analysis

Data were recorded using a 32-channel amplifier (Medtronic Xomed, Jacksonville, FS, USA) sampled at 10 KHz. Potential sources of electrical noise such microscope, patient warming blanket, and IV pumps were identified and repositioned to avoid signal contamination. The data were recorded via dedicated channels on the acquisition system and two Butterworth online filters were applied: a high-pass filter at 1 Hz and a low-pass filter at 1500 Hz. A ground needle electrode was connected to the deltoid muscle and the electrodes were referenced to a mid-frontal (Fz) spiral scalp EEG electrode.

Data were analysed offline using EEGLAB (v13.6.5b) and custom MATLAB scripts. The data were downsampled to 2 kHz then re-referenced using a bipolar scheme to detect any changes with the highest spatial resolution as well as to avoid contamination of high frequency signals by scalp muscle artifacts detected by the Fz electrode. The last electrode on the strip was excluded from the following analysis i.e. for a four-electrode strip, electrode pairs 1-2, 2-3 and 3-4 were used and assigned to electrode positions 1, 2 and 3, respectively. The location of electrode 4 was discarded. Thus out of the original 79 electrodes, re-referenced data from 59 was used for further analysis (**Figure 4.1**; 55 left, 24 right, 32 MFG, 39 IFG, 8 on motor cortex).

A notch filter was applied at 50 Hz and its harmonics to remove line noise. Notch filtering was also applied at 79 Hz and its harmonics to remove additional noise observed in the data, probably due to equipment in the surgical theatre. Data were then bandpass filtered into 6 classical frequency bands (delta:1-4,

theta: 4-8, alpha: 8-12, beta: 12-30, low gamma (LG): 30-70, high gamma (HG): 70-250). Power of the timeseries was obtained by squaring the absolute amplitude envelope of the Hilbert transformed data.

Data were then segmented into separate conditions and trials. Because trial onset and offset markers were manually recorded, 2s from the beginning and end of the rest trial and 1 s from each task trial were excluded to account for human reaction time related error. For the hard trials (alternate numbers/letters), a further 3s from the beginning of each trial was excluded to discard the initial easy phase of this task (1, a, 2, b, 3, c, 4, d). One power value for each task was obtained by concatenating data across trials of that task. To compare power across conditions (i.e. hard>easy or easy>rest) the power ratio between two conditions was calculated (i.e. simple division of power in condition 1 vs power of condition 2).

For each electrode, a permutation testing approach was used to statistically compare power across conditions. All task trials from both conditions were concatenated serially to form a loop: the end of the last trial from condition 1 was concatenated to the beginning of the first trial from condition 2. And the end of the last trial of condition 2 was concatenated to the beginning of the first trial of condition 1. Thus the concatenated trials from both conditions formed a "circular loop". Trial onset/offset markers were then shifted using a random jitter, allowing them to "rotate" along the data loop. This rotation approach was used to generate surrogate data while preserving trial lengths and the temporal correlations in the data. After each rotation, we computed the mean power (for each condition) and power ratio (across conditions) based on the new trial markers. This process was repeated 100,000 times to create a surrogate distribution against which two-tailed statistical significance could be calculated (percentile ranks 97.5 and 2.5) for each electrode.

To relate electrode locations with control-related regions identified by fMRI studies, a canonical resting-state fronto-parietal network (FPN) volumetric mask was used (Yeo et al. 2011b). The volumetric mask was resampled to 2mm MNI space (then binarised to include any voxel with a non-zero probability) to match the original resolution of electrode localization using the grid method. Ideally, the electrodes localization and comparison with fMRI data would have

utilized a surface based approach. However, the presence of cortical lesions (i.e. the tumour) prevented accurate cortical surface extraction.

Table 4.1 Patient demographics

Patient	**Age**	**Gender**	**Tumour**	
			hemisphere	location
1	24	Male	Left	Frontal
2	25	Male	Left	Frontal
3	41	Female	Left	Frontal
4	26	Male	Left	Temporal
5	55	Female	Left	Frontal
6	22	Female	Right	Frontal
7	29	Male	Right	Frontal
8	38	Female	Right	Frontal
9	29	Male	Left	Frontal
10	33	Female	Left	Temporal
11	27	Female	Left	Temporal
12	56	Female	Left	Temporal
13	27	Male	Left	Frontal

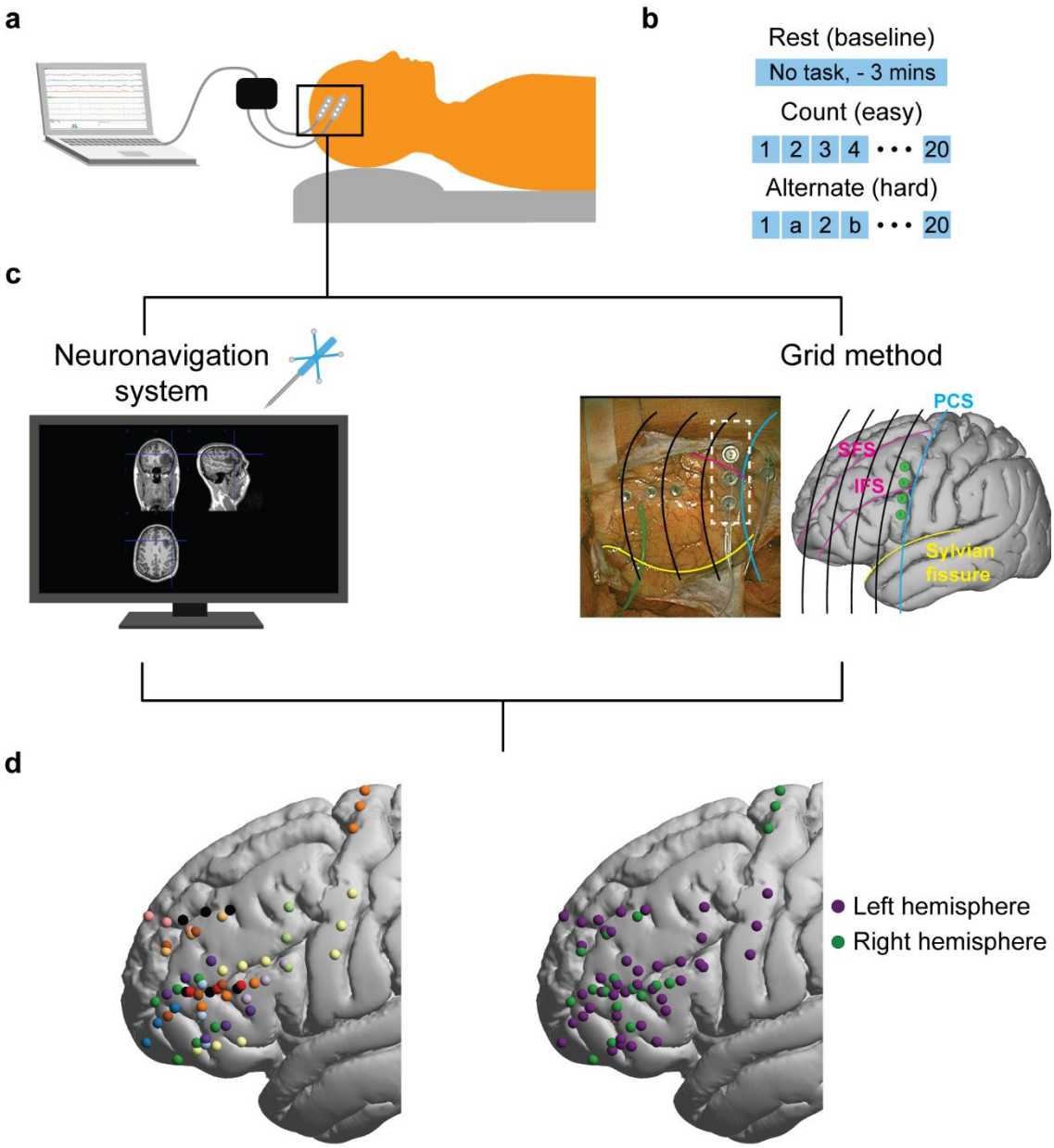

Figure 4.1 Intraoperative setup and electrode localization. (a) Intraoperative setup: Patient is awake while performing the cognitive tasks and the electrophysiological signals are simultaneously recorded (b) Cognitive tasks: one rest task and two verbal tasks. (c) Two approaches for electrode localisation: *Left*: a probe linked to a neuronavigation system co-registered with the patient's native T1w scan *Right*: an example of localising a strip of electrodes (white dotted box) using the grid method. The major anatomical sulci (coloured) are identified on both the intraoperative photograph and the template brain: precentral sulcus (PCS, blue), inferior frontal sulcus (IFS, pink), superior frontal sulcus (SFS, pink, not visible for this patient), and the sylvian fissure (yellow). To form the grid, parallel lines (black) spaced 1.5 cm were added starting from the PCS. (d) Left: Electrodes distribution (shown: n=59 after bipolar referencing, original n=79) for each patient (13 in total) in a separate colour *Right*: hemispheric distribution of electrodes.

4.3 Results

4.3.1 Frequency specific power modulations associated with cognitive demand

To identify contacts sensitive to increased cognitive demand, we calculated the percentage signal change for the hard>easy contrast (power_hard/power_easy – 1*100) in each frequency band separately. Significant power changes ($p<0.05$, uncorrected; see section 4.2.54.2.5 above) in the HG and LG bands were predominantly increases [HG 45.8% (27 out of all 59 electrodes), LG 22% (13/59)] while fewer electrodes showed power decreases [HG 5.1% (3/59), LG 13.6% (8/59)] (**Figure 4.2a**). In contrast, the beta band was dominated by power decreases [55.9% (33/59)] with only one electrode showing a significant power increase (1.7%) (**Figure 4.2a**). Next, we assessed the spatial overlap across frequency bands. Most electrodes showing significant LG increases also showed HG increases [92.3% (12/13)]. Further, electrodes showing HG and LG increases were highly likely to show beta decreases [HG 85.1% (23/27), LG 76.9% (10/13)]. However, these results could simply reflect that almost all the significant electrodes in the beta band showed power decreases. A follow up correlation analysis showed a decent spatial correspondence between electrodes showing HG increases and beta decreases (r=0.64, p<0.0001). However, there was weaker spatial correlation between electrodes showing LG increases and beta decreases (r=0.32, p=0.005). Thus, consistent with previous reports (Lachaux et al. 2012), power increases in HG band, but interestingly not the LG band, co-occurred with power decreases in the beta band (**Figure 4.2a**, right).

To further evaluate whether gamma power modulations were more localized than beta modulations, we compared (unpaired t-test) the Euclidean distances between all pairs of electrodes showing significant increases for HG and LG vs those showing significant decreases in beta (HG vs beta t=-7.8, $p=1.5\text{x}10^{-14}$, LG vs beta t=-2.24, p=0.03). These results confirmed that HG and LG increases were spatially localized in anterior frontal regions while beta power decreases were more spatially distributed (**Figure 4.2a**).

Are the spatially localized HG and LG increases specific for cognitive demand increases (hard>easy) or could a weak demand elicit similar results? To answer this, we explored power modulations for the easy>rest contrast. Few electrodes with significant power increases for easy>rest contrast also showed significant increases for the hard>easy contrast (HG 31.8% (7/22), LG 8.3% (1/12)) (**Figure 4.2b**). In other words, the two contrasts engage mostly non-overlapping sets of electrodes. Critically, easy>rest gamma increases were shifted posteriorly to hard>easy increases (**Figure 4.2b;** Wilcoxon rank sum test comparing hard>easy vs easy>rest y-coordinates (anterior-posterior axis) for electrodes with significant power increases: HG p=0.02, LG p=0.07). These results are consistent with fMRI studies showing an anterior-posterior demand gradient across frontal control regions (Badre and Nee 2018; Shashidhara et al. 2019; Assem et al. 2020).

For completeness, **Figure 4.3** shows that the remaining lower frequency bands (delta, theta, alpha) showed a similar picture to the beta band, with predominantly power decreases though with a patchier spatial arrangement. Overall, these results show that the common finding of better spatial specificity for higher vs lower frequencies extends into lateral prefrontal cortex.

Taken together, these results show that, along the lateral frontal cortex, increases in cognitive demand are associated with (1) a spatially localized increase in high frequency power and (2) a spatially distributed decrease in low frequency power. Further, a shift from an easy to a difficult cognitive demand was tracked by a corresponding posterior to anterior shift in high frequency power increases.

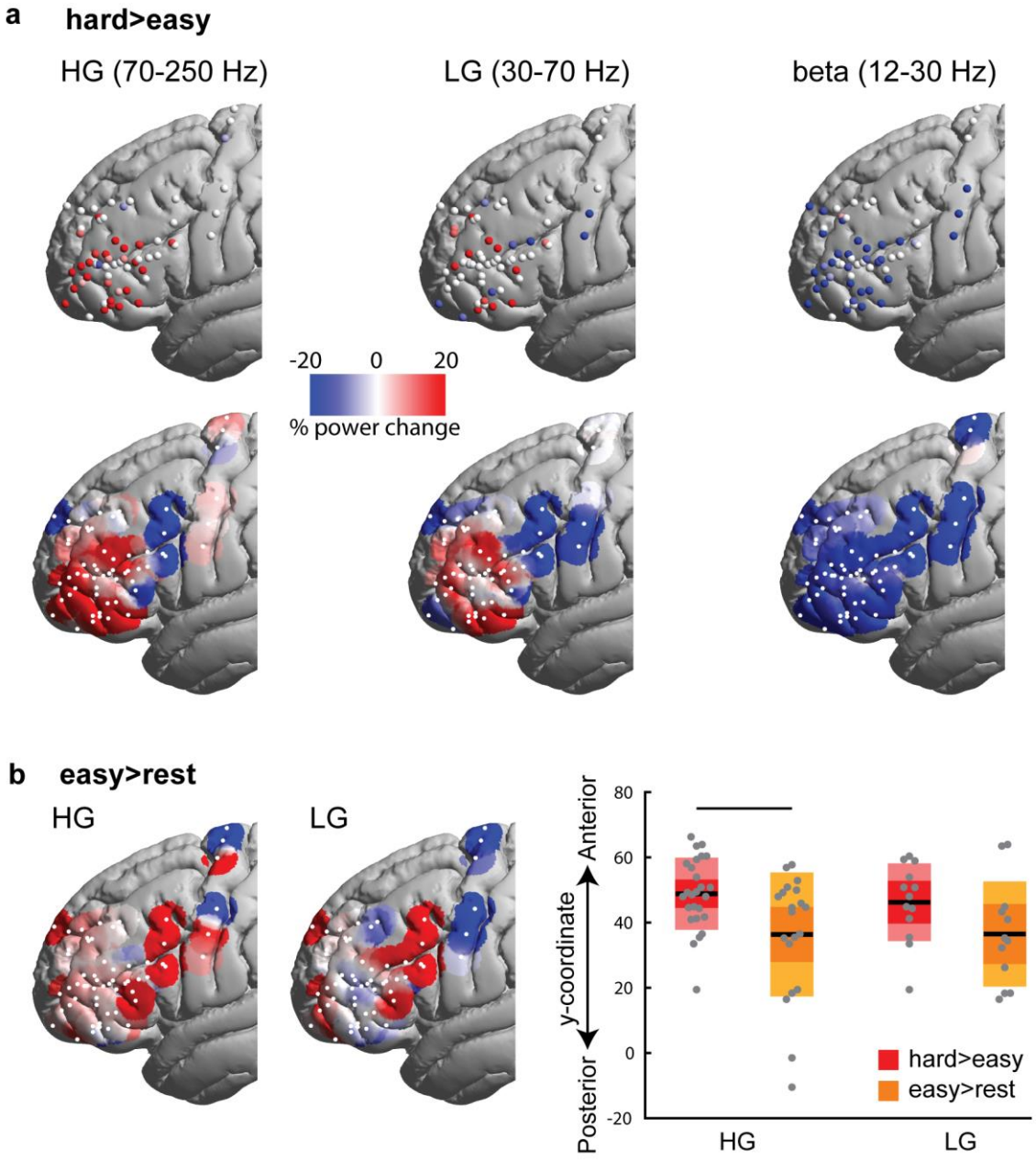

Figure 4.2 Cognitive demand related power modulations. (a) Power modulations for the hard>easy contrast. *Top*: Electrodes with significant ($p<0.05$, uncorrected) power increases (red), decreases (blue) and non-significant changes (white). *Bottom*: Projection of all electrodes' (white dots) unthresholded average power change on the template's surface. Power for each electrode (white dots; including electrodes with non-significant power changes) was spatially smoothed by 10 mm and the value at each surface vertex is the average of the overlapping powers. (b) *Left:* Surface projection of power modulations for the easy>rest contrast. Note how the anterior cluster of HG and LG power increases in (a) is now weaker and shifted posteriorly. *Right*: Box plots of significant electrodes' y-coordinate. Middle black line: mean, lighter box limits (95% CI), darker box limits (1 SD). Top black line: $p<0.05$ using Wilcoxon rank sum test.

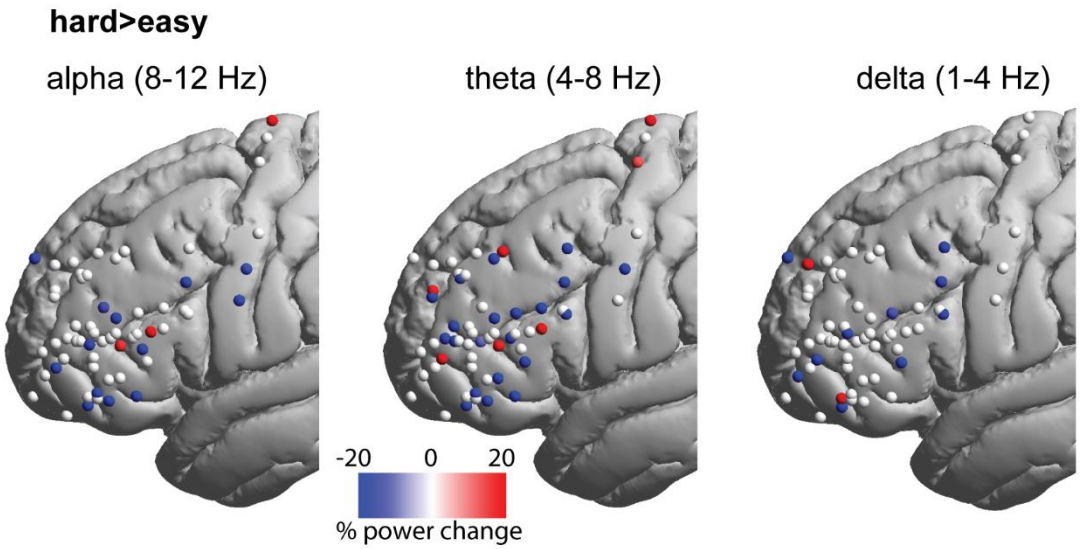

Figure 4.3 Cognitive demand related power modulations in lower frequency bands. Power modulations for the hard>easy contrast. Electrodes with significant ($p<0.05$, uncorrected) power increases (red), decreases (blue) and non-significant changes (white).

4.3.2 High frequency power increases overlap with fMRI-defined fronto-parietal network

The results so far have highlighted a localized group of electrodes with increases in gamma power surrounded by dorsal and posterior electrodes that show little to no power modulations (**Figure 4.2a**). This spatial pattern is reminiscent of fMRI studies identifying localized frontal control-related patches. Here we predicted that a task difficulty manipulation would produce spatially overlapping gamma increases (in ECoG) and BOLD increases (in fMRI). To this end, we used a canonical mask of the control-related FPN as defined from fMRI (see section 4.2.5).

First, we identified the electrodes that overlap with the FPN (**Figure 4.4a)**. Then we found that, for the hard>easy contrast, electrodes showing significant HG power increases were more likely to be located within the FPN (63.6% of all electrodes within the mask: 21/33) than outside of it (23.1% 6/26) (**Figure 4.4b)**. LG increases showed a similar trend [27.3% (9/33) vs 15.4% (4/23)]. In contrast, electrodes showing significant beta power decreases had equal probabilities of

being located within and outside the FPN [57.6% (19/33) vs 53.8% (14/26)], further confirming the spatially distributed nature of beta decreases.

In a complementary analysis, electrodes within the FPN showed significantly stronger HG and LG power increases compared to those outside of the FPN **(Figure 4.4c;** HG t_{57}=2.8, p=0.0036, LG t_{57}=2.9, p=0.0026, p-values are one-tailed due to our directional prediction of gamma increases). Again, there was no significant difference between FPN and non-FPN electrodes for beta power decreases (t_{57}=1.1, p=0.14, one tailed) nor for any of the lower frequency bands (ps>0.05, uncorrected).

A limitation of the previous analysis is that most effects could be driven by a subset of subjects. To address this, we selected 9 out of the 13 patients who each had electrodes overlapping with both FPN and non-FPN regions to perform a within-subjects analysis. Despite the low number of subjects available for this analysis, the results again showed that within the same patient, FPN electrodes showed statistically stronger LG power increases compared to non-FPN electrodes (Wilcoxon signed rank test; p=0.02, one tailed). However, differences for HG and beta powers were non-significant though trending (both ps=0.08, one tailed).

Collectively, these results suggest that power increases in high frequency bands related to increased cognitive demand are likely to co-localize with the fMRI-identified FPN. Excitingly, results from two different modalities (ECoG and fMRI) show converging parcellation evidence for a localized region within the lateral frontal lobe related to cognitive control.

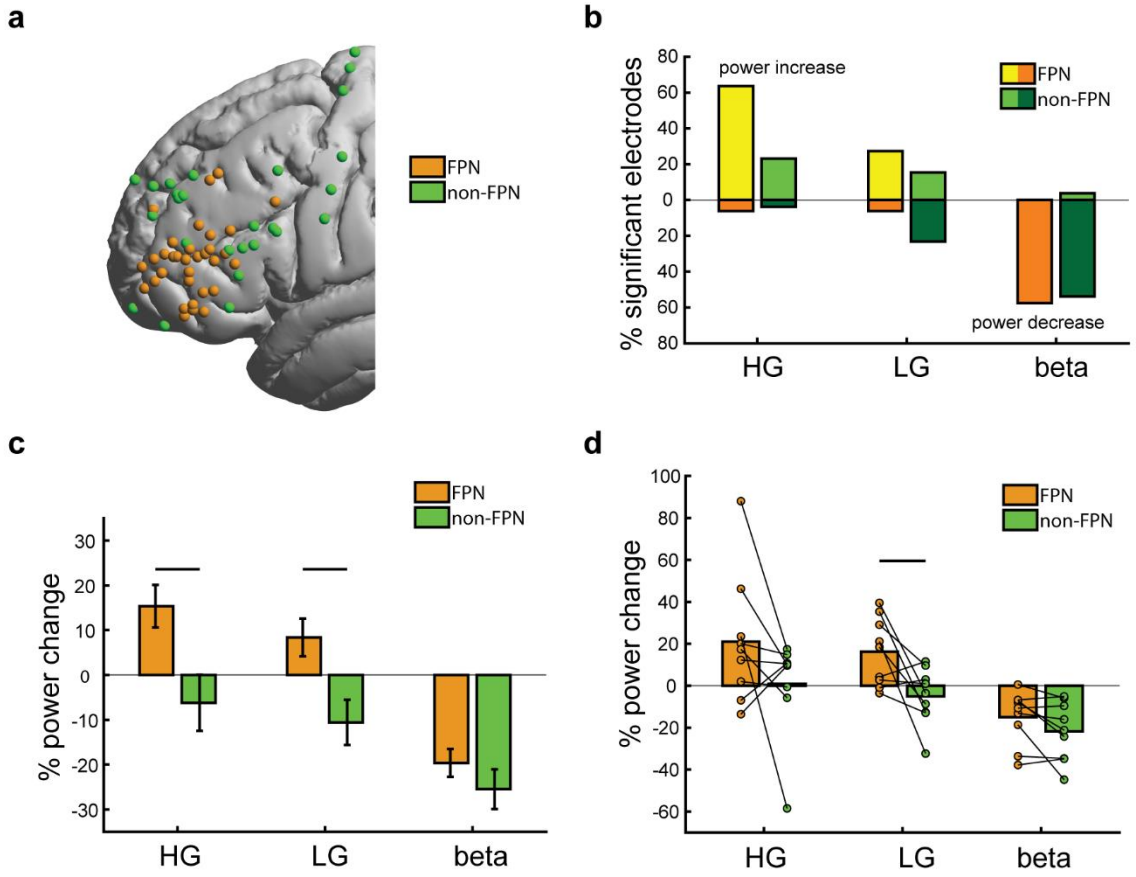

Figure 4.4 Power changes overlap with FPN. (a) Electrodes coloured based on their overlap with a canonical fMRI FPN mask (Yeo et al. 2011b) (b) Percentage of significant electrodes out of all electrodes contained within each mask (FPN and non-FPN). Darker colours (below zero) refer to percentage of electrodes showing power decreases. (c) Bar plots comparing powers of all electrodes within each mask for each frequency band. Top black lines: $p<0.05$. (d) A within-subjects comparison of power changes between masks. Each dot represents average power within a mask for one patient. Top black line: $p<0.05$ for a Wilcoxon signed rank test.

4.4 Discussion

Thousands of fMRI studies document increased co-activations of fronto-parietal regions during cognitively demanding tasks. However, little is known about their corresponding electrophysiological markers, especially from invasive human studies. In this unique dataset, LFP signals were recorded from the lateral frontal surface from human patients undergoing awake craniotomies for tumour resections. The results revealed a circumscribed frontal region that shows increases in HG and LG powers during a cognitively demanding counting/switching task. Localised gamma increases were accompanied by spatially broad beta power decreases. Regions showing gamma increases overlapped with a canonical mask of the fMRI defined FPN, linking increased fMRI activations with increased gamma power in the FPN.

4.4.1 Lateral frontal cortex parcellation using converging evidence from ECoG and fMRI

There is a consensus from previous electrophysiology studies that gamma power increases in frontal regions are associated with multiple executive processes. However, invasive human studies rarely systematically assessed the anatomical distribution of gamma increases, with most studies reporting isolated findings in individual electrodes (Lachaux et al. 2012; Helfrich and Knight 2016). The current study demonstrates that a circumscribed region along the lateral frontal surface robustly shows increases in gamma power during an executive task. Although some previous studies have reported different reliabilities and putative physiological origins for HG and LG (Crone et al. 2006; Ray and Maunsell 2011; Buzsáki and Wang 2012; Lachaux et al. 2012), here both bands were broadly in agreement.

Excitingly, gamma increases co-localized with a canonical mask of the FPN derived from independent resting-state fMRI data. Previous studies have linked localized gamma increases with corresponding fMRI activations in early cortical regions (Nir et al. 2007; Engell et al. 2012; Hermes et al. 2012).

Accordingly, gamma increases were generally interpreted to reflect localized task-relevant processing. The current results extend these reports to the domain of cognitive control in frontal regions and suggest a link between increased fMRI fronto-parietal activations during demanding executive tasks and increases in gamma power. More generally, task difficulty manipulations provide converging evidence from ECoG and fMRI modalities for control-related parcellation of the lateral frontal cortex.

These findings open the door for extending clinical functional mapping to the domain of cognitive control. This is a matter of importance because damage to control regions is associated with disorganized behaviour (Woolgar et al. 2010) and poorer recovery from neurosurgeries (Romero-Garcia et al. 2019). Current mapping approaches to assess executive regions are limited. On the one hand, DES is useful for mapping motor and language functions. However, on its own, DES effects in higher association are much more difficult to interpret. On the other hand, ECoG could provide a complementary approach to DES. However, ECoG studies investigating cognitive control usually employ complex computer-based tasks that would not be suitable in a surgical setting. Here we employed a simple behavioural manipulation based on task difficulty. The behavioural task was well tolerated by most patients and the whole experiment was performed in under 10 minutes (including time for electrodes placement). Further, the detected gamma signals are characterized by spatial specificity of a few mm. For example, near-by electrodes on the same strip can show differential gamma responses. This level of neuroanatomical precision is vital for guiding neurosurgeons during tumour excision.

Two further findings from this study are worth noting. First, beta (and lower frequencies) showed spatially broad decreases in power which were not confined to the FPN. It is important to note that these results are not necessarily inconsistent with findings of improved synchronization in lower frequency bands between fronto-parietal regions during executive tasks e.g. (Voytek et al. 2015), since power and synchrony modulations could change independently. One framework to relate gamma increases and beta decreases is to think of them as two faces of the same process (e.g. a rotated power spectrum around a middle range frequency) (Helfrich and Knight 2016). Recent evidence, however, argues against this simple interpretation, showing that depending on the cortical region,

increases in high gamma power are not necessarily accompanied by decreases in low frequency power (Fellner et al. 2019). In line with this, the current results also showed that beta decreases were more spatially broad and were not necessarily accompanied by gamma increases. Another framework proposes a hybrid spiking-synaptic plasticity WM model, in which bursts of spikes (gamma increases) in superficial layers serve to encode and maintain WM content, while beta, which is assumed to have an inhibitory role, is suppressed in deeper layers to allow superficial gamma bursts (Lundqvist et al. 2011; Miller et al. 2018). Again such a model fails to predict regions with beta decreases without gamma increases. It is plausible, though, that due to neuronal architectures acting as low pass filters (Buzsáki et al. 2012) they allowed distant spread of beta modulations to regions which are not engaged in the task and thus showed no gamma increases. Pending further experimental and theoretical studies, these results provide an important constraint for theoretical models of executive processes.

A second intriguing finding concerns the posterior shifts of gamma increases for the easy>rest contrast which are also consistent with fMRI studies showing an anterior-posterior cognitive demand gradient across the lateral frontal surface (Badre and Nee 2018; Shashidhara et al. 2019; Assem et al. 2020). The results also suggest that FPN mainly picks up areas modulated by a hard>easy contrast. Chapters 2 and 3 made similar observations, with easy>fix activations mainly highlighting penumbra regions that did not necessarily belong to the FPN. That said, it is important to note that the easy>rest contrast is less controlled for confounds (e.g. easy condition includes speech while the patient remains silent during the rest condition). Hence, posterior gamma increases might also reflect language related processing.

4.4.2 Future directions

This study presents the first step towards scaling up this approach for future functional mapping studies. The results demonstrated here used a group-level approach. However, individual functional localization is vital for guiding neurosurgeries. This could be achieved using larger and denser electrode grids per patient.

While the study aimed to detect an index of cognitive control processing, only one type of cognitive demand was manipulated. A conjunction of activity across several tasks is more likely to zero in on core MD regions. This might require modifying existing paradigms to more surgical theatre friendly versions. One such task could be contrasting verb generation with repeating nouns.

While the analysis performed here was offline, the pipeline was developed with an online testing approach in mind, for example, through optimizing several steps for speedy execution of the scripts. More work is needed to assess the number of trials necessary to detect a statistically reliable increase in gamma power. One approach could involve using the current data to train a statistical model which could then be used for setting appropriate statistical thresholds during online data analysis. Further, only amplitude modulations were investigated in this study. Investigating synchrony (i.e. phase changes) within and across frequency bands (as well as phase-amplitude coupling) could reveal unique markers of FPN dynamics during task execution. Another exciting step is to investigate synchrony between electrodes during the baseline period and its correspondence with fMRI based resting-state networks, which could lead to new insights into the neurophysiological basis of large scale cortical networks. Finally, integrating ECoG with DES and pre-operative multi-modal brain imaging opens up a new exciting phase for comprehensive surgical planning (Hart et al. 2020).

CHAPTER 5

DISCUSSION: TOWARDS A PRECISE ANATOMY OF DOMAIN-GENERAL BRAIN REGIONS

Progress in understanding the role of domain-general or Multiple-demand (MD) brain regions in cognitive control has been hampered by the lack of precise knowledge of their anatomical and functional organization. This was partly due to the blurry spatial localization provided by traditional brain imaging approaches (Coalson et al. 2018). To reveal a crisper delineation of the MD system's anatomy and functional properties, the experiments in chapters 2 and 3 capitalized on novel fMRI methods developed by the HCP. The HCP approach utilizes precise surface-based geometric models of the cortex and areal-feature based surface alignment algorithms that utilize neurobiologically grounded multimodal MRI features (Robinson et al. 2014, 2018; Glasser, Coalson, et al. 2016; Glasser, Smith, et al. 2016).

In chapter 2, using hundreds of subjects from the HCP dataset and a conjunction of working memory, math and reasoning behavioural contrasts revealed 9 widely distributed cortical MD patches per hemisphere. For the most accurate anatomical delineation the study used an areal classifier capable of

identifying individual specific cortical areas, based on a recent state-of-the-art multimodal cortical parcellation (Glasser, Coalson, et al. 2016), which subdivided the 9 patches into an MD core of 10 regions that are most strongly co-activated and functionally interconnected, surrounded by an MD penumbra of 17 additional regions. For the first time, this study allowed a detailed comparison between the MD co-activation pattern and canonical resting-state networks. Core MD was found to constitute a portion of the fronto-parietal network (FPN) with the MD penumbra distributed across FPN, dorsal-attention (DAN), cingulo-opercular (CON), default-mode (DMN) networks. The study is also the first to examine in detail MD activations outside of the cerebral cortex. MD hotspots were identified in the head of the caudate and cerebellar regions (crus I and II) with a putative MD region in the anterior thalamus. Reconciling a 20 year debate, MD activations showed relative rather than absolute functional preferences against a strong background of co-recruitment.

The study in chapter 3 investigated one debated account of MD functional preferences: sensory-modality biases. The study compared matched auditory and visual versions of a working memory task. Comparing easy versions of each task modality revealed strong sensory biases across all MD regions with a predominantly visual preference. Interestingly, regions with the strongest biases (visual or auditory) were located just outside core MD regions. Comparing the difficult vs easy version for each task modality separately highlighted a strong co-recruitment of MD regions. Importantly, comparing sensory-biases related to this increase in cognitive demand found that MD regions no longer showed sensory-modality biases, reflecting joint demand of each task modality on the domain-general MD resources. Similar patterns were observed in subcortical and cerebellar MD regions. Excitingly, this study reconciled several conflicting findings in the literature regarding sensory biases in frontal regions demonstrating the great potential of the precise neuroanatomical localization offered by HCP protocols.

A common way to illuminate MD regions in fMRI studies is to compare brain scans during a hard vs an easy version of a cognitive task. Chapter 4 investigated a similar approach to map out MD regions using electrophysiological data. The data were acquired from electrodes placed on the lateral frontal surface of human patients undergoing awake neurosurgeries. The

aim is to identify an electrophysiological signal related to MD regions that can be used to guide neurosurgeons during tumour resections. By comparing a difficult task (alternating between counting and alphabet) vs an easy task (simple counting), spectral analysis showed that power increases in the higher frequency range (>70 Hz) revealed a circumscribed frontal region, which overlaps with frontal control regions revealed by fMRI. By contrast, power modulations in the lower frequency range (<30 Hz) were broadly distributed and spatially non-specific. These findings present the first step for the potential use of this protocol for extending the process of functional mapping in neurosurgeries to the domain of cognitive control. Importantly, these results provide converging evidence from fMRI and electrophysiology for localized frontal regions related to cognitive control.

Taken together, the distributed anatomical organization, mosaic functional preferences, and strong interconnectivity, suggest MD regions are well positioned to integrate and assemble the diverse components of cognitive operations. In this chapter I further explore the implications of this crisper anatomical delineation, discuss some intriguing findings and future directions.

5.1 A co-activation and functional preferences model

The experiments in chapters 2 and 3 demonstrated that co-activation is a central feature of MD regions. All MD areas were statistically activated during cognitively demanding tasks. However, the results also revealed statistical differences between activations of different tasks. How should these two observations be interpreted? Traditionally, statistically low powered and blurry fMRI studies have biased interpretations towards modular conceptualizations of high cognitive functions like inhibition, monitoring, working memory etc…. However, better powered and crisper studies like the current ones suggest that these functional specializations are relative and statistical, not absolute.

An interpretative model is illustrated in **Figure 5.1a**. The distributed arrangement of MD regions in the brain suggests each MD region is

differentially connected to its local surrounding, in line with recent evidence from monkeys that ~70% of connections to a brain region are local (Markov et al. 2013). The strong MD inter-connectivity suggests a basis for integration of information. Diverse tasks with different behavioural needs will lead to the preferential engagement of the relevant MD regions, giving rise to statistical functional preferences. And the rapid communication between MD regions suggests an explanation for their co-activation. At a finer grained level **Figure 5.1b**, this model predicts a zoo of neural responses in any MD region. Specific information being fed into an MD region predicts the existence of neurons with specialized responses. However, as MD regions are hypothesised to be hubs for information integration and exchange, neurons with mixed responses are expected to be more abundant. Overall, the present results and model offer a basis for reconciling domain-specific and domain-general accounts of fronto-parietal activations. This model would greatly benefit from data on the structural connectivity of MD regions, which will be critical to begin to understand their dynamic activity.

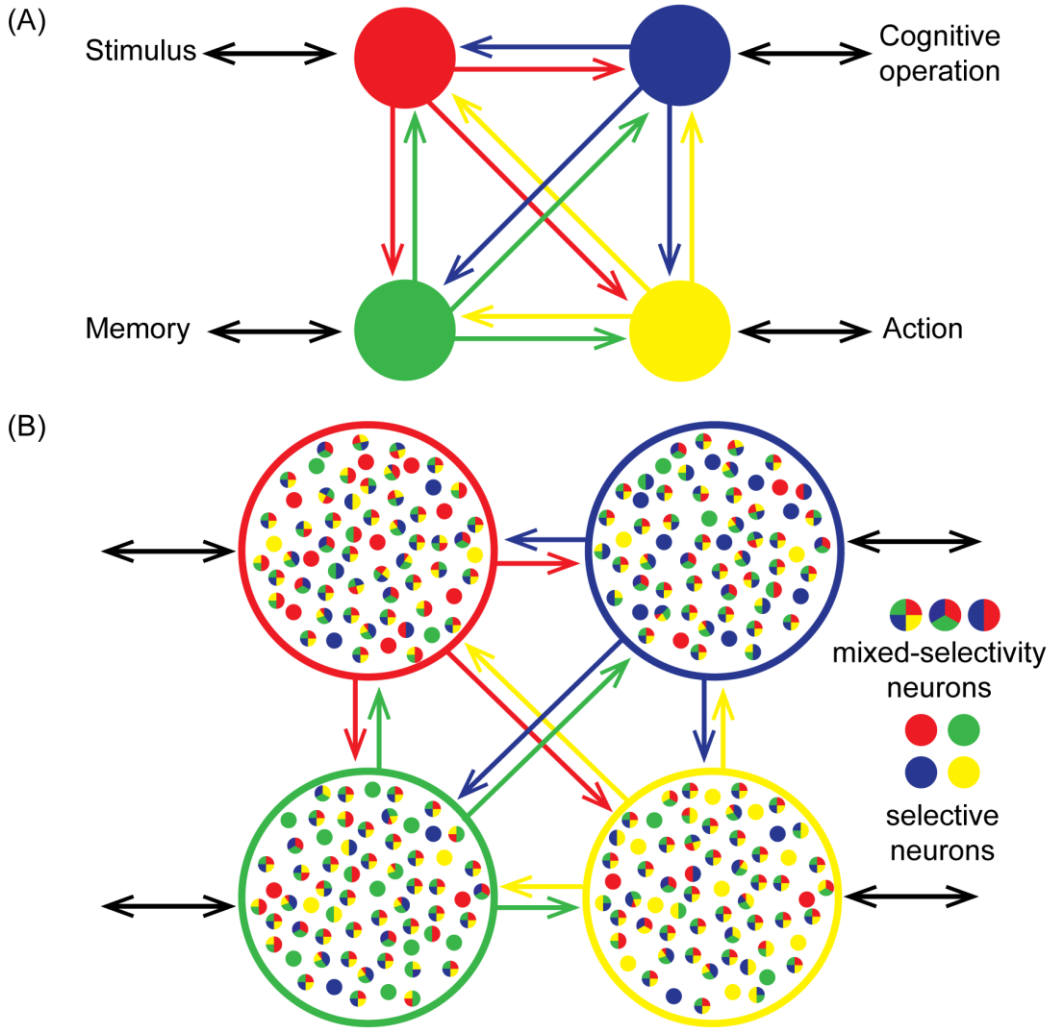

Figure 5.1 (a) Each MD region (coloured circles) has local access to different information and brain operations (illustrated with black bidirectional arrows) suggesting a basis for relative functional preferences. Strong connectivity between MD regions allows rapid exchange and integration of information between MD regions suggesting a basis for coactivation. (b) The local and distributed connectivity of MD regions give rise to a rich and diverse range of neural responses from selective responses to mixed-selectivity responses.

5.2 MD areal heterogeneity and resting state networks

A recurring observation across the fMRI activation maps in chapters 2 and 3 is the spatial heterogeneity of MD activations. For example, chapter 2 briefly touched upon the activations at the border between two medial PFC parcels

SCEF and 8BM. Here I take a closer look at heterogeneity in this region. **Figure 5.2a, b** zooms in on activations for the easy>fix contrast for each of the relational reasoning and working memory tasks used in chapter 2. It is clear that the peak of the activation is initially located in SCEF and is spatially similar in both tasks. **Figure 5.2e, f** shows the hard>easy contrast, where each task elicited different spatial activations within 8BM. More striking examples of heterogeneity within 8BM were also noted from a new set of tasks we acquired using HCP protocols. For example, using task switching and stop signal paradigms, the easy>fix contrast again shows activations starting in SCEF (**Figure 5.2c, d,** unpublished data). However, hard>easy contrast for each of those tasks shows a remarkably different spatial engagement of 8BM (**Figure 5.2g, h,** unpublished data).

An interesting next question is what guides these spatially different profiles of activations? As mentioned previously (**section 5.1**), differential MD local connections likely give rise to functional preferences. A closer look at resting-state connectivity highlights that 8BM, a core MD region and part of the canonical FPN, is surrounded by regions with different connectivity profiles (reflected in their membership of different canonical networks). The proposed mechanism that follows from these observations is that, depending on the task, the distribution of spatial activation within an MD region might be constrained by the canonical rfMRI networks most engaged by the task. This could explain why resting-state connectivity patterns are capable of predicting task-specific activations (Tavor et al. 2016; Ito et al. 2020).

A related observation from recent literature on resting-state networks (RSNs) highlights finer-grained subdivisions of canonical resting-state networks based on connectivity preferences with other networks. For example, a recent study subdivided the DMN based on differential connectivity with control and language/social networks (Gordon et al. 2020). The DMN subdivision related to the FPN network is remarkably similar in topography to areas lying in between core MD regions and nearby DMN regions. These observations suggest another mechanism underlying the relative functional preferences observed in MD regions.

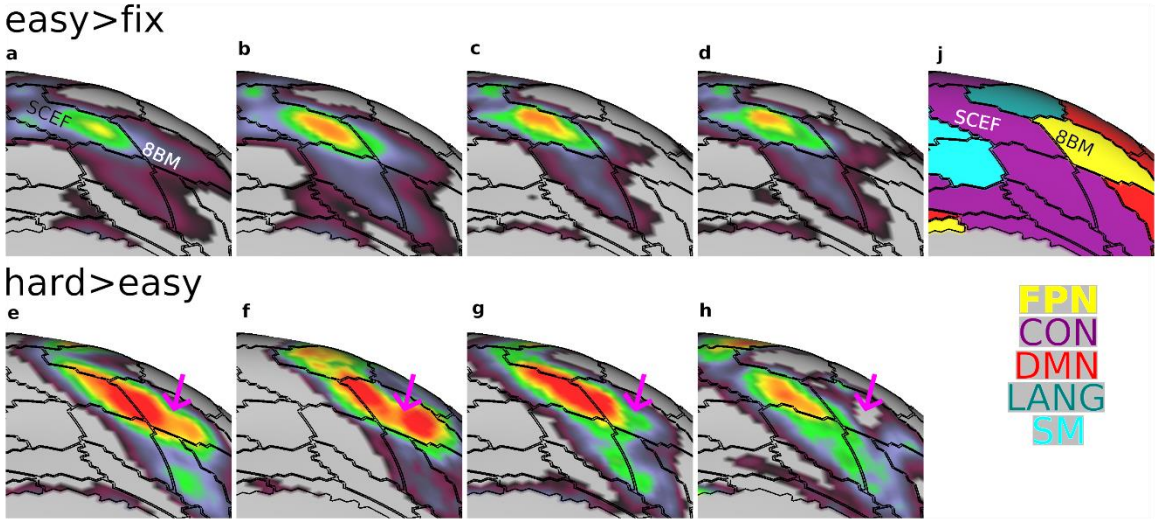

Figure 5.2 Univariate activations of the medial PFC. Only positive betas are shown, warmer colours mean stronger activations. Black lines represent borders of the HCP_MMP1.0. *(top row)* easy>fix contrasts, *(bottom row)* hard>easy contrasts. Tasks are (a) n-back 0>fix [HCP] (b) Relational easy>fix [HCP] (c) blocks of switching based on 1 rule>fix [unpublished data] (d) different blocks of switching based on 1 rule>fix [unpublished data] (e) n-back 2>0 [HCP] (f) Relational hard>easy [HCP] (g) switch hard (2-rules)>easy (1-rule) [unpublished data] (h) blocks with stop trials>blocks with no stop trials [unpublished data]. Note pink arrow highlighting a central region in 8BM which is selectively not activated by this contrast. This region is functionally connected with lateral temporal parcel TE1p (personal observations) (j) RSNs based on CAB-NP (Ji et al 2019).

5.3 MD beyond executive function tasks

A core proposal regarding the MD system is that its cognitive control operations are of central importance to all complex thought and behaviour. So far the MD system has almost exclusively been investigated using so-called executive tasks like working memory, inhibition, switching etc… However, a big knowledge gap exists regarding MD involvement during more diverse cognitive tasks such as emotional regulation, motor control, theory of mind (TOM), language comprehension and production to name a few. Most such tasks focus on investigating functionally related specialized modules like TOM or motor networks, with sporadic mentions of "frontal activations" usually attributed to increased cognitive demands (Koster-Hale and Saxe 2011; Kikkert et al. 2016). Though one recent line of work, using subject specific MD functional localizers,

argues strongly against the involvement of MD regions in passive language comprehension [(Diachek et al. 2020) but see (Hervais-Adelman et al. 2015)].

Hence an important new frontier for understanding the wider role of the MD system with other brain networks is to investigate its engagement during a wider range of tasks. Very likely, the blurred spatial resolution of traditional fMRI studies has missed out on characterizing MD involvement in these tasks. Through a set of exciting new HCP-style experiments, I plan on investigating the engagement of MD regions in a diverse set of non-traditional tasks e.g. theory of mind, language, with a focus on presenting stimuli through multiple sensory modalities and diversifying outputs (e.g. through verbal responses). These sets of experiments will also be important to investigate the proposed mechanism of differential spatial engagement of MD regions based on the engaged RSN.

The experiments in this thesis provide some of the strongest evidence in the literature for the existence of small but significant relative functional preferences. To "force out" more significant MD functional preferences aimed at generating new insights into the different roles of MD regions, I plan on examining MD behaviour during naturalistic problem solving tasks such as video games. Naturalistic tasks with their diverse cognitive demands might be better suited for teasing out novel dynamics and functional patterns in the brain.

5.4 A new frontier: subcortical and cerebellar MD regions

For long MD engagement beyond the cortex has been ignored. The studies in chapters 2 and 3 are among the few that systematically investigated subcortical and cerebellar MD regions across both task and rest fMRI, and many details remain unknown. For example in chapter 2, functional connectivity, but not task co-activation, highlighted the anterior thalamus as a putative MD region. During easy cognitive demands, task fMRI was shown to engage more middle/posterior thalamic regions. However, on increasing cognitive demands the anterior thalamus was engaged in 2 out of 3 tasks. This could reflect similar cortical observations mentioned above regarding spatially specific spread of activations

from penumbra to core. To investigate these finer-grained details, I plan on utilizing ultra-high magnetic fields such as of 7-Tesla.

The subcortex remains a largely uncharted territory in human neuroscience (Forstmann et al. 2016). Recent studies are starting to unravel the functional links between deep nuclei and cortical RSNs. For example, activity in the subthalamic nucleus was found to correlate with medial PFC activations during multiple alternative choice decision making (Keuken et al. 2015). The habenula was found to be functionally linked to the cortical CON (Ely et al. 2019). Multiple cortical RSNs were found to converge within overlapping thalamic regions (Greene et al. 2020). An anatomical tracing study intriguingly highlighted that the claustrum is the strongest subcortical structure projecting to the cortex (Markov et al. 2011). In the cerebellum, a recent study highlighted its rich task-related functional activations (King et al. 2019). These observations and many others are yet to be synthesised into preliminary view of how cortico-subcortico-cerebellar dynamics could support human intelligent behaviour. These non-cortical structures have been studied extensively in animal models. Thus, a better characterization of subcortical and cerebellar functional properties in humans, coupled with improved cross-species mapping (Balsters et al. 2020) is bound to provide a valuable link to mechanistic insights from the rich animal literature.

5.5 Relating electrophysiology to the MD pattern

As highlighted before, a critical limitation for human electrophysiology studies is the poor neuroanatomical localization of their findings. The finer-grained discoveries through fMRI demand new electrophysiological studies with wider coverage of cortical areas to investigate the neuronal dynamics behind the different activation topographies. For human ECoG studies, a step forward would be to utilize MSMSulc/Myelin (or MSMAll if functional data exist) to relate cortical electrodes with the HCP_MMP1.0. In chapter 4 this was not possible because the tumour prevented the correct extraction of the cortical surface. In more conventional ECoG studies, investigating epileptic patients, multiple structural and functional scans can be acquired from the same patient

and preprocessed using MSM approaches. This promises a better resolution for linking electrophysiological findings with fMRI findings.

5.6 Conclusion

For continued progress in understanding the brain basis of intelligence, the present work defines a precise set of MD regions, providing the groundwork for detailed functional analyses, cross-reference between studies, and identification of cross-species homologs. This holds promise for a new and more productive phase in study of this core brain network.

BIBLIOGRAPHY

Alexander GE, DeLong MR, Strick PL. 1986. Parallel Organization of Functionally Segregated Circuits Linking Basal Ganglia and Cortex. Annu Rev Neurosci. 9:357–381.

Amalric M, Dehaene S. 2016. Origins of the brain networks for advanced mathematics in expert mathematicians. Proc Natl Acad Sci. 113:4909–4917.

Amalric M, Dehaene S. 2017. Cortical circuits for mathematical knowledge: evidence for a major subdivision within the brain's semantic networks. Philos Trans R Soc B Biol Sci. 373:20160515.

Amiez C, Wutte MG, Faillenot I, Petrides M, Burle B, Procyk E. 2016. Single subject analyses reveal consistent recruitment of frontal operculum in performance monitoring. Neuroimage. 133:266–278.

Assem M, Glasser MF, Van Essen DC, Duncan J. 2020. A Domain-General Cognitive Core Defined in Multimodally Parcellated Human Cortex. Cereb Cortex. 30:4361–4380.

Averbeck BB, Lehman J, Jacobson M, Haber SN. 2014. Estimates of Projection Overlap and Zones of Convergence within Frontal-Striatal Circuits. J Neurosci. 34:9497–9505.

Azuma M, Suzuki H. 1984. Properties and distribution of auditory neurons in the dorsolateral prefrontal cortex of the alert monkey. Brain Res. 298:343–346.

Baddeley A. 2000. The episodic buffer: a new component of working memory? Trends Cogn Sci. 4:417–423.

Baddeley A. 2012. Working Memory: Theories, Models, and Controversies. Annu Rev Psychol. 63:1–29.

Baddeley AD, Hitch G. 1974. Working memory. Psychol Learn Motiv - Adv Res Theory. 8:47–89.

Badre D. 2008. Cognitive control, hierarchy, and the rostro–caudal organization of the frontal lobes. Trends Cogn Sci. 12:193–200.

Badre D, Nee DE. 2018. Frontal Cortex and the Hierarchical Control of Behavior. Trends Cogn Sci. 22:170–188.

Balsters JH, Whelan CD, Robertson IH, Ramnani N. 2013. Cerebellum and Cognition: Evidence for the Encoding of Higher Order Rules. Cereb Cortex. 23:1433–1443.

Balsters JH, Zerbi V, Sallet J, Wenderoth N, Mars RB. 2020. Primate homologs of mouse cortico-striatal circuits. Elife. 9.

Bamiou DE, Musiek FE, Luxon LM. 2003. The insula (Island of Reil) and its role in auditory processing: Literature review. Brain Res Rev.

Barch DM, Burgess GC, Harms MP, Petersen SE, Schlaggar BL, Corbetta M, Glasser MF, Curtiss S, Dixit S, Feldt C, Nolan D, Bryant E, Hartley T, Footer O, Bjork JM, Poldrack R, Smith S, Johansen-Berg H, Snyder AZ, Van Essen DC. 2013. Function in the human connectome: Task-fMRI and individual differences in behavior. Neuroimage. 80:169–189.

Basilakos A, Smith KG, Fillmore P, Fridriksson J, Fedorenko E. 2018. Functional Characterization of the Human Speech Articulation Network. Cereb Cortex. 28:1816–1830.

Bassett DS, Sporns O. 2017. Network neuroscience. Nat Neurosci. 20:353–364.

Bastos AM, Loonis R, Kornblith S, Lundqvist M, Miller EK. 2018. Laminar recordings in frontal cortex suggest distinct layers for maintenance and control of working memory. Proc Natl Acad Sci. 115:1117–1122.

Bertani G, Fava E, Casaceli G, Carrabba G, Casarotti A, Papagno C, Castellano A, Falini A, Gaini SM, Bello L. 2009. Intraoperative mapping and monitoring of brain functions for the resection of low-grade gliomas: technical considerations. Neurosurg Focus. 27:E4.

Bertolero MA, Yeo BTT, Bassett DS, D'Esposito M. 2018. A mechanistic model of connector hubs, modularity and cognition. Nat Hum Behav. 2:765–777.

Betzel RF, Medaglia JD, Kahn AE, Soffer J, Schonhaut DR, Bassett DS. 2019. Structural, geometric and genetic factors predict interregional brain connectivity patterns probed by electrocorticography. Nat Biomed Eng. 3:902–916.

Binder JR, Gross WL, Allendorfer JB, Bonilha L, Chapin J, Edwards JC, Grabowski TJ, Langfitt JT, Loring DW, Lowe MJ, Koenig K, Morgan PS, Ojemann JG, Rorden C, Szaflarski JP, Tivarus ME, Weaver KE. 2011. Mapping anterior temporal lobe language areas with fMRI: A multicenter normative study. Neuroimage.

Birba A, Hesse E, Sedeño L, Mikulan EP, García M del C, Ávalos J, Adolfi F, Legaz A, Bekinschtein TA, Zimerman M, Parra M, García AM, Ibáñez A. 2017. Enhanced Working Memory Binding by Direct Electrical Stimulation of the Parietal Cortex. Front Aging Neurosci. 9.

Blank IA, Kanwisher N, Fedorenko E. 2014. A functional dissociation between language and multiple-demand systems revealed in patterns of BOLD signal fluctuations. J Neurophysiol. 1105–1118.

Blume WT, Jones DC, Pathak P. 2004. Properties of after-discharges from cortical electrical stimulation in focal epilepsies. Clin Neurophysiol. 115:982–989.

Borchers S, Himmelbach M, Logothetis N, Karnath H-O. 2012. Direct electrical stimulation of human cortex — the gold standard for mapping brain functions? Nat Rev Neurosci. 13:63–70.

Bostan AC, Dum RP, Strick PL. 2013. Cerebellar networks with the cerebral cortex and basal ganglia. Trends Cogn Sci.

Botvinick M, Plaut DC. 2004. Doing Without Schema Hierarchies: A Recurrent Connectionist Approach to Normal and Impaired Routine Sequential Action. Psychol Rev. 111:395–429.

Bouyer J., Montaron M., Rougeul A. 1981. Fast fronto-parietal rhythms during combined focused attentive behaviour and immobility in cat: cortical and thalamic localizations. Electroencephalogr Clin Neurophysiol. 51:244–252.

Braga RM, Hellyer PJ, Wise RJS, Leech R. 2017. Auditory and visual connectivity gradients in frontoparietal cortex. Hum Brain Mapp. 38:255–270.

Braga RM, Wilson LR, Sharp DJ, Wise RJS, Leech R. 2013. Separable networks for top-down attention to auditory non-spatial and visuospatial modalities. Neuroimage. 74:77–86.

Buckner RL, Krienen FM, Castellanos A, Diaz JC, Yeo BTT. 2011. The organization of the human cerebellum estimated by intrinsic functional connectivity. J Neurophysiol. 106:2322–2345.

Bunge SA. 2004. Analogical Reasoning and Prefrontal Cortex: Evidence for Separable Retrieval and Integration Mechanisms. Cereb Cortex. 15:239–249.

Buschman TJ, Miller EK. 2007. Top-Down Versus Bottom-Up Control of

Attention in the Prefrontal and Posterior Parietal Cortices. Science (80-). 315:1860–1862.

Bushara KO, Weeks RA, Ishii K, Catalan M-J, Tian B, Rauschecker JP, Hallett M. 1999. Modality-specific frontal and parietal areas for auditory and visual spatial localization in humans. Nat Neurosci. 2:759–766.

Buxton RB, Wong EC, Frank LR. 1998. Dynamics of blood flow and oxygenation changes during brain activation: The balloon model. Magn Reson Med. 39:855–864.

Buzsáki G, Anastassiou CA, Koch C. 2012. The origin of extracellular fields and currents — EEG, ECoG, LFP and spikes. Nat Rev Neurosci. 13:407–420.

Buzsáki G, Wang X-J. 2012. Mechanisms of Gamma Oscillations. Annu Rev Neurosci. 35:203–225.

Cappe C, Barone P. 2005. Heteromodal connections supporting multisensory integration at low levels of cortical processing in the monkey. Eur J Neurosci. 22:2886–2902.

Cate AD, Herron TJ, Yund EW, Stecker GC, Rinne T, Kang X, Petkov CI, Disbrow EA, Woods DL. 2009. Auditory Attention Activates Peripheral Visual Cortex. PLoS One. 4:e4645.

Champod AS, Petrides M. 2010. Dissociation within the Frontoparietal Network in Verbal Working Memory: A Parametric Functional Magnetic Resonance Imaging Study. J Neurosci.

Chein JM, Moore AB, Conway ARA. 2011. Domain-general mechanisms of complex working memory span. Neuroimage. 54:550–559.

Choi EY, Tanimura Y, Vage PR, Yates EH, Haber SN. 2016. Convergence of prefrontal and parietal anatomical projections in a connectional hub in the striatum. Neuroimage. 146:821–832.

Christoff K, Keramatian K, Gordon AM, Smith R, Mädler B. 2009. Prefrontal organization of cognitive control according to levels of abstraction. Brain Res. 1286:94–105.

Coalson TS, Essen DC Van, Glasser MF. 2018. The impact of traditional neuroimaging methods on the spatial localization of cortical areas. Proc Natl Acad Sci. 115:E6356–E6365.

Cole MW, Reynolds JR, Power JD, Repovs G, Anticevic A, Braver TS. 2013. Multi-task connectivity reveals flexible hubs for adaptive task control. Nat

Neurosci. 16:1348–1355.

Cole MW, Schneider W. 2007. The cognitive control network: Integrated cortical regions with dissociable functions. Neuroimage. 37:343–360.

Cooper R, Shallice T. 2000. Contention Scheduling and the Control of Routine Activities. Cogn Neuropsychol. 17:297–338.

Cooper RP, Shallice T. 2006. Hierarchical schemas and goals in the control of sequential behavior. Psychol Rev. 113:887–916.

Corbetta M, Akbudak E, Conturo TE, Snyder AZ, Ollinger JM, Drury HA, Linenweber MR, Petersen SE, Raichle ME, Van Essen DC, Shulman GL. 1998. A common network of functional areas for attention and eye movements. Neuron.

Corbetta M, Shulman GL. 2002. Control of goal-directed and stimulus-driven attention in the brain. Nat Rev Neurosci. 3:201–215.

Courtney SM. 1998. An Area Specialized for Spatial Working Memory in Human Frontal Cortex. Science (80-). 279:1347–1351.

Courtney SM. 2004. Attention and cognitive control as emergent properties of information representation in working memory. Cogn Affect Behav Neurosci. 4:501–516.

Crittenden BM, Duncan J. 2014. Task difficulty manipulation reveals multiple demand activity but no frontal lobe hierarchy. Cereb Cortex. 24:532–540.

Crittenden BM, Mitchell DJ, Duncan J. 2016. Task Encoding across the Multiple Demand Cortex Is Consistent with a Frontoparietal and Cingulo-Opercular Dual Networks Distinction. J Neurosci. 36:6147–6155.

Crone NE, Sinai A, Korzeniewska A. 2006. High-frequency gamma oscillations and human brain mapping with electrocorticography. In: Progress in Brain Research. p. 275–295.

Dehaene S, Kerszberg M, Changeux J-P. 1998. A neuronal model of a global workspace in effortful cognitive tasks. Proc Natl Acad Sci. 95:14529–14534.

Di X, Biswal BB. 2014. Modulatory interactions between the default mode network and task positive networks in resting-state. PeerJ. 2014.

Diachek E, Blank I, Siegelman M, Affourtit J, Fedorenko E. 2020. The Domain-General Multiple Demand (MD) Network Does Not Support Core Aspects of Language Comprehension: A Large-Scale fMRI Investigation. J

Neurosci. 40:4536–4550.

Diamond A. 2013. Executive Functions. Annu Rev Psychol. 64:135–168.

Diedrichsen J, Zotow E. 2015. Surface-based display of volume-averaged cerebellar imaging data. PLoS One. 10:1–18.

Dodds CM, Morein-Zamir S, Robbins TW. 2011. Dissociating inhibition, attention, and response control in the frontoparietal network using functional magnetic resonance imaging. Cereb Cortex.

Donahue CJ, Sotiropoulos SN, Jbabdi S, Hernandez-Fernandez M, Behrens TE, Dyrby TB, Coalson T, Kennedy H, Knoblauch K, Van Essen DC, Glasser MF. 2016. Using diffusion tractography to predict cortical connection strength and distance: A quantitative comparison with tracers in the monkey. J Neurosci. 36:6758–6770.

Dosenbach NUF, Fair DA, Cohen AL, Schlaggar BL, Petersen SE. 2008. A dual-networks architecture of top-down control. Trends Cogn Sci. 12:99–105.

Dosenbach NUF, Fair DA, Miezin FM, Cohen AL, Wenger KK, Dosenbach RAT, Fox MD, Snyder AZ, Vincent JL, Raichle ME, Schlaggar BL, Petersen SE. 2007. Distinct brain networks for adaptive and stable task control in humans. Proc Natl Acad Sci U S A. 104:11073–11078.

Dosenbach NUF, Visscher KM, Palmer ED, Miezin FM, Wenger KK, Kang HC, Burgund ED, Grimes AL, Schlaggar BL, Petersen SE. 2006. A Core System for the Implementation of Task Sets. Neuron. 50:799–812.

Dotson NM, Hoffman SJ, Goodell B, Gray CM. 2018. Feature-Based Visual Short-Term Memory Is Widely Distributed and Hierarchically Organized. Neuron. 99:215–226.e4.

Downar J, Crawley AP, Mikulis DJ, Davis KD. 2000. A multimodal cortical network for the detection of changes in the sensory environment. Nat Neurosci. 3:277–283.

Drew PJ, Mateo C, Turner KL, Yu X, Kleinfeld D. 2020. Ultra-slow Oscillations in fMRI and Resting-State Connectivity: Neuronal and Vascular Contributions and Technical Confounds. Neuron. 107:782–804.

Dubois J, de Berker AO, Tsao DY. 2015. Single-Unit Recordings in the Macaque Face Patch System Reveal Limitations of fMRI MVPA. J Neurosci. 35:2791–2802.

Dumontheil I, Thompson R, Duncan J. 2011. Assembly and Use of New Task

Rules in Fronto-parietal Cortex. J Cogn Neurosci. 23:168–182.

Duncan J. 1980. The locus of interference in the perception of simultaneous stimuli. Psychol Rev. 87:272–300.

Duncan J. 1986. Disorganisation of behaviour after frontal lobe damage. Cogn Neuropsychol. 3:271–290.

Duncan J. 2000. A Neural Basis for General Intelligence. Science (80-). 289:457–460.

Duncan J. 2001. An adaptive coding model of neural function in prefrontal cortex. Nat Rev Neurosci. 2:820–829.

Duncan J. 2010. The multiple-demand (MD) system of the primate brain: mental programs for intelligent behaviour. Trends Cogn Sci. 14:172–179.

Duncan J. 2013. The Structure of Cognition: Attentional Episodes in Mind and Brain. Neuron. 80:35–50.

Duncan J, Assem M, Shashidhara S. 2020. Integrated Intelligence from Distributed Brain Activity. Trends Cogn Sci. 24:838–852.

Duncan J, Burgess P, Emslie H. 1995. Fluid intelligence after frontal lobe lesions. Neuropsychologia. 33:261–268.

Duncan J, Chylinski D, Mitchell DJ, Bhandari A. 2017. Complexity and compositionality in fluid intelligence. Proc Natl Acad Sci. 114:5295–5299.

Duncan J, Humphreys G, Ward R. 1997. Competitive brain activity in visual attention. Curr Opin Neurobiol. 7:255–261.

Duncan J, Owen AM. 2000. Common regions of the human frontal lobe recruited by diverse cognitive demands. Trends Neurosci. 23:475–483.

Dürschmid S, Edwards E, Reichert C, Dewar C, Hinrichs H, Heinze H-J, Kirsch HE, Dalal SS, Deouell LY, Knight RT. 2016. Hierarchy of prediction errors for auditory events in human temporal and frontal cortex. Proc Natl Acad Sci. 113:6755–6760.

Ely BA, Stern ER, Kim J won, Gabbay V, Xu J. 2019. Detailed mapping of human habenula resting-state functional connectivity. Neuroimage. 200:621–634.

Engel AK, Fries P, Singer W. 2001. Dynamic predictions: Oscillations and synchrony in top–down processing. Nat Rev Neurosci. 2:704–716.

Engelhardt LE, Harden KP, Tucker-Drob EM, Church JA. 2019. The neural architecture of executive functions is established by middle childhood.

Neuroimage.

Engell AD, Huettel S, McCarthy G. 2012. The fMRI BOLD signal tracks electrophysiological spectral perturbations, not event-related potentials. Neuroimage. 59:2600–2606.

Engle RW. 2002. Working memory capacity as executive attention. Curr Dir Psychol Sci. 11:19–23.

Erez Y, Duncan J. 2015. Discrimination of visual categories based on behavioral relevance in widespread regions of frontoparietal cortex. J Neurosci. 35:12383–12393.

Etzel JA, Courtney Y, Carey CE, Gehred MZ, Agrawal A, Braver TS. 2020. Pattern Similarity Analyses of FrontoParietal Task Coding: Individual Variation and Genetic Influences. Cereb Cortex. 30:3167–3183.

Falchier A, Clavagnier S, Barone P, Kennedy H. 2002. Anatomical Evidence of Multimodal Integration in Primate Striate Cortex. J Neurosci. 22:5749–5759.

Farooqui AA, Mitchell D, Thompson R, Duncan J. 2012. Hierarchical Organization of Cognition Reflected in Distributed Frontoparietal Activity. J Neurosci. 32:17373–17381.

Fedorenko E, Behr MK, Kanwisher N. 2011. Functional specificity for high-level linguistic processing in the human brain. Proc Natl Acad Sci U S A. 108:16428–16433.

Fedorenko E, Blank IA. 2020. Broca's Area Is Not a Natural Kind. Trends Cogn Sci. 24:270–284.

Fedorenko E, Duncan J, Kanwisher N. 2012. Language-selective and domain-general regions lie side by side within Broca's area. Curr Biol. 22:2059–2062.

Fedorenko E, Duncan J, Kanwisher N. 2013. Broad domain generality in focal regions of frontal and parietal cortex. Proc Natl Acad Sci. 110:16616–16621.

Fellner M-C, Gollwitzer S, Rampp S, Kreiselmeyr G, Bush D, Diehl B, Axmacher N, Hamer H, Hanslmayr S. 2019. Spectral fingerprints or spectral tilt? Evidence for distinct oscillatory signatures of memory formation. PLOS Biol. 17:e3000403.

Ford KA, Gati JS, Menon RS, Everling S. 2009. BOLD fMRI activation for anti-

saccades in nonhuman primates. Neuroimage. 45:470–476.

Forstmann BU, De Hollander G, Van Maanen L, Alkemade A, Keuken MC. 2016. Towards a mechanistic understanding of the human subcortex. Nat Rev Neurosci.

Friedman NP, Miyake A. 2017. Unity and diversity of executive functions: Individual differences as a window on cognitive structure. Cortex.

Fries P. 2001. Modulation of Oscillatory Neuronal Synchronization by Selective Visual Attention. Science (80-). 291:1560–1563.

Fries P. 2015. Rhythms for Cognition: Communication through Coherence. Neuron. 88:220–235.

Fusi S, Miller EK, Rigotti M. 2016. Why neurons mix: high dimensionality for higher cognition. Curr Opin Neurobiol. 37:66–74.

Fuster JM, Bodner M, Kroger JK. 2000. Cross-modal and cross-temporal association in neurons of frontal cortex. Nature. 405:347–351.

Gitelman DR, Nobre AC, Parrish TB, LaBar KS, Kim Y-H, Meyer JR, Mesulam M-M. 1999. A large-scale distributes network for covert spatial attention. Brain.

Glascher J, Adolphs R, Damasio H, Bechara A, Rudrauf D, Calamia M, Paul LK, Tranel D. 2012. Lesion mapping of cognitive control and value-based decision making in the prefrontal cortex. Proc Natl Acad Sci. 109:14681–14686.

Glascher J, Rudrauf D, Colom R, Paul LK, Tranel D, Damasio H, Adolphs R. 2010. Distributed neural system for general intelligence revealed by lesion mapping. Proc Natl Acad Sci. 107:4705–4709.

Glasser MF, Coalson TS, Bijsterbosch JD, Harrison SJ, Harms MP, Anticevic A, Van Essen DC, Smith SM. 2018. Using temporal ICA to selectively remove global noise while preserving global signal in functional MRI data. Neuroimage. 181:692–717.

Glasser MF, Coalson TS, Bijsterbosch JD, Harrison SJ, Harms MP, Anticevic A, Van Essen DC, Smith SM. 2019. Classification of temporal ICA components for separating global noise from fMRI data: Reply to Power. Neuroimage. 197:435–438.

Glasser MF, Coalson TS, Robinson EC, Hacker CD, Harwell J, Yacoub E, Ugurbil K, Andersson J, Beckmann CF, Jenkinson M, Smith SM, Van

Essen DC. 2016. A multi-modal parcellation of human cerebral cortex. Nature. 536:171–178.

Glasser MF, Goyal MS, Preuss TM, Raichle ME, Van Essen DC. 2014. Trends and properties of human cerebral cortex: Correlations with cortical myelin content. Neuroimage. 93:165–175.

Glasser MF, Smith SM, Marcus DS, Andersson JLR, Auerbach EJ, Behrens TEJ, Coalson TS, Harms MP, Jenkinson M, Moeller S, Robinson EC, Sotiropoulos SN, Xu J, Yacoub E, Ugurbil K, Van Essen DC. 2016. The Human Connectome Project's neuroimaging approach. Nat Neurosci. 19:1175–1187.

Glasser MF, Sotiropoulos SN, Wilson JA, Coalson TS, Fischl B, Andersson JL, Xu J, Jbabdi S, Webster M, Polimeni JR, Van Essen DC, Jenkinson M. 2013. The minimal preprocessing pipelines for the Human Connectome Project. Neuroimage. 80:105–124.

Glasser MF, Van Essen DC. 2011. Mapping Human Cortical Areas In Vivo Based on Myelin Content as Revealed by T1- and T2-Weighted MRI. J Neurosci. 31:11597–11616.

Gordon EM, Laumann TO, Marek S, Raut R V., Gratton C, Newbold DJ, Greene DJ, Coalson RS, Snyder AZ, Schlaggar BL, Petersen SE, Dosenbach NUF, Nelson SM. 2020. Default-mode network streams for coupling to language and control systems. Proc Natl Acad Sci U S A. 117:17308–17319.

Gordon EM, Lynch CJ, Gratton C, Laumann TO, Gilmore AW, Greene DJ, Ortega M, Nguyen AL, Schlaggar BL, Petersen SE, Dosenbach NUF, Nelson SM. 2018. Three Distinct Sets of Connector Hubs Integrate Human Brain Function. Cell Rep. 24:1687–1695.e4.

Gottwald B. 2004. Evidence for distinct cognitive deficits after focal cerebellar lesions. J Neurol Neurosurg Psychiatry. 75:1524–1531.

Gray JR, Chabris CF, Braver TS. 2003. Neural mechanisms of general fluid intelligence. Nat Neurosci. 6:316–322.

Greene DJ, Marek S, Gordon EM, Siegel JS, Gratton C, Laumann TO, Gilmore AW, Berg JJ, Nguyen AL, Dierker D, Van AN, Ortega M, Newbold DJ, Hampton JM, Nielsen AN, McDermott KB, Roland JL, Norris SA, Nelson SM, Snyder AZ, Schlaggar BL, Petersen SE, Dosenbach NUF. 2020. Integrative and Network-Specific Connectivity of the Basal Ganglia and

Thalamus Defined in Individuals. Neuron. 105:742–758.e6.

Gregoriou GG, Gotts SJ, Zhou H, Desimone R. 2009. High-Frequency, Long-Range Coupling Between Prefrontal and Visual Cortex During Attention. Science (80-). 324:1207–1210.

Gu Y, Cheng Z, Yang L, DeAngelis GC, Angelaki DE. 2016. Multisensory Convergence of Visual and Vestibular Heading Cues in the Pursuit Area of the Frontal Eye Field. Cereb Cortex. 26:3785–3801.

Haber SN. 2003. The primate basal ganglia: Parallel and integrative networks. J Chem Neuroanat. 26:317–330.

Halassa MM, Kastner S. 2017. Thalamic functions in distributed cognitive control. Nat Neurosci. 20:1669–1679.

Haller M, Case J, Crone NE, Chang EF, King-Stephens D, Laxer KD, Weber PB, Parvizi J, Knight RT, Shestyuk AY. 2018. Persistent neuronal activity in human prefrontal cortex links perception and action. Nat Hum Behav. 2:80–91.

Hampshire A, Chamberlain SR, Monti MM, Duncan J, Owen AM. 2010. The role of the right inferior frontal gyrus: inhibition and attentional control. Neuroimage. 50:1313–1319.

Hampshire A, Highfield RR, Parkin BL, Owen AM. 2012. Fractionating Human Intelligence. Neuron. 76:1225–1237.

Hampshire A, Thompson R, Duncan J, Owen AM. 2008. The Target Selective Neural Response — Similarity, Ambiguity, and Learning Effects. PLoS One. 3:e2520.

Hampson M, Driesen NR, Skudlarski P, Gore JC, Constable RT. 2006. Brain Connectivity Related to Working Memory Performance. J Neurosci. 26:13338–13343.

Han SW, Marois R. 2014. Functional Fractionation of the Stimulus-Driven Attention Network. J Neurosci. 34:6958–6969.

Hart MG, Romero-Garcia R, Price SJ, Santarius T, Suckling J. 2020. Connections, Tracts, Fractals, and the Rest: A Working Guide to Network and Connectivity Studies in Neurosurgery. World Neurosurg.

Havas V, Gabarrós A, Rifa-ros X, Plans G. 2015. Brain & Language Electrical stimulation mapping of nouns and verbs in Broca ' s area. 146:53–63.

Hayesroth B, Hayesroth F. 1979. A cognitive model of planning. Cogn Sci.

3:275–310.

Helfrich RF, Knight RT. 2016. Oscillatory Dynamics of Prefrontal Cognitive Control. Trends Cogn Sci. 20:916–930.

Hermes D, Miller KJ, Noordmans HJ, Vansteensel MJ, Ramsey NF. 2010. Automated electrocorticographic electrode localization on individually rendered brain surfaces. J Neurosci Methods. 185:293–298.

Hermes D, Miller KJ, Vansteensel MJ, Aarnoutse EJ, Leijten FSS, Ramsey NF. 2012. Neurophysiologic correlates of fMRI in human motor cortex. Hum Brain Mapp. 33:1689–1699.

Hervais-Adelman A, Moser-Mercer B, Michel CM, Golestani N. 2015. fMRI of Simultaneous Interpretation Reveals the Neural Basis of Extreme Language Control. Cereb Cortex. 25:4727–4739.

Howard MW. 2003. Gamma Oscillations Correlate with Working Memory Load in Humans. Cereb Cortex. 13:1369–1374.

Hugdahl K, Raichle ME, Mitra A, Specht K. 2015. On the existence of a generalized non-specific task-dependent network. Front Hum Neurosci. 9:430.

Hwang K, Bruss J, Tranel D, Boes AD. 2020. Network Localization of Executive Function Deficits in Patients with Focal Thalamic Lesions. J Cogn Neurosci. 1–16.

Ito T, Hearne L, Mill R, Cocuzza C, Cole MW. 2020. Discovering the Computational Relevance of Brain Network Organization. Trends Cogn Sci. 24:25–38.

Jackson RL. 2020. The Neural Correlates of Semantic Control Revisited. bioRxiv. 2020.07.15.204990.

Ji JL, Spronk M, Kulkarni K, Repovš G, Anticevic A, Cole MW. 2019. Mapping the human brain's cortical-subcortical functional network organization. Neuroimage. 185:35–57.

Jiang Y, Kanwisher N. 2003. Common Neural Mechanisms for Response Selection and Perceptual Processing. J Cogn Neurosci. 15:1095–1110.

Kadohisa M, Watanabe K, Kusunoki M, Buckley MJ, Duncan J. 2020. Focused Representation of Successive Task Episodes in Frontal and Parietal Cortex. Cereb Cortex. 30:1779–1796.

Kandel ER, Schwartz JH, Jessell TM, Siegelbaum SA, Hudspeth AJ. 2013.

Principles of neural science. 5th ed. McGraw-Hill Companies, Inc.

Kane MJ, Engle RW. 2002. The role of prefrontal cortex in working-memory capacity, executive attention, and general fluid intelligence: An individual-differences perspective. Psychon Bull Rev. 9:637–671.

Kemp JM, Powell TP. 1970. The cortico-striate projection in the monkey. Brain. 93:525–546.

Keuken MC, Van Maanen L, Bogacz R, Schäfer A, Neumann J, Turner R, Forstmann BU. 2015. The subthalamic nucleus during decision-making with multiple alternatives. Hum Brain Mapp. 36:4041–4052.

Kievit RA, van Rooijen H, Wicherts JM, Waldorp LJ, Kan KJ, Scholte HS, Borsboom D. 2012. Intelligence and the brain: A model-based approach. Cogn Neurosci. 3:89–97.

Kikkert S, Kolasinski J, Jbabdi S, Tracey I, Beckmann CF, Johansen-Berg H, Makin TR. 2016. Revealing the neural fingerprints of a missing hand. Elife. 5.

King M, Hernandez-Castillo CR, Poldrack RA, Ivry RB, Diedrichsen J. 2019. Functional boundaries in the human cerebellum revealed by a multi-domain task battery. Nat Neurosci. 22:1371–1378.

Kirschen MP, Chen SHA, Desmond JE. 2010. Modality specific cerebro-cerebellar activations in verbal working memory: An fMRI study. Behav Neurol. 23:51–63.

Klemen J, Chambers CD. 2012. Current perspectives and methods in studying neural mechanisms of multisensory interactions. Neurosci Biobehav Rev.

Koster-Hale J, Saxe RR. 2011. Theory of mind brain regions are sensitive to the content, not the structural complexity, of belief attributions. … 33rd Annu Cogn Sci …. 33:3356–3361.

LaBar KS, Gitelman DR, Parrish TB, Mesulam M-M. 1999. Neuroanatomic Overlap of Working Memory and Spatial Attention Networks: A Functional MRI Comparison within Subjects. Neuroimage. 10:695–704.

Lachaux J-P, Axmacher N, Mormann F, Halgren E, Crone NE. 2012. High-frequency neural activity and human cognition: Past, present and possible future of intracranial EEG research. Prog Neurobiol. 98:279–301.

Lashley K.S. 1951. The problem of serial order in behavior. Cereb Mech Behav. 112–136.

Laumann TO, Gordon EM, Adeyemo B, Snyder AZ, Joo SJ, Chen M, Gilmore AW, McDermott KB, Nelson SM, Dosenbach NUF, Schlaggar BL, Mumford JA, Poldrack RA, Petersen SE. 2015. Functional System and Areal Organization of a Highly Sampled Individual Human Brain. Neuron. 87:657–670.

Lefco RW, Brissenden JA, Noyce AL, Tobyne SM, Somers DC. 2020. Gradients of functional organization in posterior parietal cortex revealed by visual attention, visual short-term memory, and intrinsic functional connectivity. Neuroimage. 219:117029.

Lewis JW, Beauchamp MS, Deyoe EA. 2000. A comparison of visual and auditory motion processing in human cerebral cortex. Cereb Cortex. 10:873–888.

Logothetis NK. 2008. What we can do and what we cannot do with fMRI. Nature. 453:869–878.

Logothetis NK. 2012. Intracortical recordings and fMRI: An attempt to study operational modules and networks simultaneously. Neuroimage.

Logothetis NK, Pauls J, Augath M, Trinath T, Oeltermann a. 2001. Neurophysiological investigation of the basis of the fMRI signal. Nature. 412:150–157.

Lorenz K. 1970. Studies in Animal and Human Behaviour. Volume 1. ed. Methuen, London.

Lorenz R, Violante IR, Monti RP, Montana G, Hampshire A, Leech R. 2018. Dissociating frontoparietal brain networks with neuroadaptive Bayesian optimization. Nat Commun. 9:1227.

Lundqvist M, Herman P, Lansner A. 2011. Theta and Gamma Power Increases and Alpha/Beta Power Decreases with Memory Load in an Attractor Network Model. J Cogn Neurosci. 23:3008–3020.

Luria AR. 1966. Higher cortical functions in man., Higher cortical functions in man. Oxford, England: Basic Books.

Mainy N, Kahane P, Minotti L, Hoffmann D, Bertrand O, Lachaux J-P. 2007. Neural correlates of consolidation in working memory. Hum Brain Mapp. 28:183–193.

Mandal AS, Romero-Garcia R, Hart M, Suckling J. 2020. Genetic, Cellular, and Connectomic Characterization of the Adult Human Brain Regions

Commonly Plagued by Glioma. medRxiv.

Mante V, Sussillo D, Shenoy K V., Newsome WT. 2013. Context-dependent computation by recurrent dynamics in prefrontal cortex. Nature.

Marder E. 2015. Understanding Brains: Details, Intuition, and Big Data. PLOS Biol. 13:e1002147.

Marek S, Dosenbach NUF. 2018. The frontoparietal network: Function, electrophysiology, and importance of individual precision mapping. Dialogues Clin Neurosci.

Markov NT, Ercsey-Ravasz M, Van Essen DC, Knoblauch K, Toroczkai Z, Kennedy H. 2013. Cortical High-Density Counterstream Architectures. Science (80-). 342:1238406–1238406.

Markov NT, Ercsey-Ravasz MM, Ribeiro Gomes AR, Lamy C, Magrou L, Vezoli J, Misery P, Falchier A, Quilodran R, Gariel MA, Sallet J, Gamanut R, Huissoud C, Clavagnier S, Giroud P, Sappey-Marinier D, Barone P, Dehay C, Toroczkai Z, Knoblauch K, Van Essen DC, Kennedy H. 2014. A Weighted and Directed Interareal Connectivity Matrix for Macaque Cerebral Cortex. Cereb Cortex. 24:17–36.

Markov NT, Misery P, Falchier A, Lamy C, Vezoli J, Quilodran R, Gariel MA, Giroud P, Ercsey-Ravasz M, Pilaz LJ, Huissoud C, Barone P, Dehay C, Toroczkai Z, Van Essen DC, Kennedy H, Knoblauch K. 2011. Weight consistency specifies regularities of macaque cortical networks. Cereb Cortex. 21:1254–1272.

Marr DC, Poggio T. 1977. From understanding computation to understanding neural circuitry. Neurosci Res Program Bull. 15:470–488.

Mars RB, Sotiropoulos SN, Passingham RE, Sallet J, Verhagen L, Khrapitchev AA, Sibson N, Jbabdi S. 2018. Whole brain comparative anatomy using connectivity blueprints. Elife. 7.

Matsumoto R, Nair DR, LaPresto E, Najm I, Bingaman W, Shibasaki H, Lüders HO. 2004. Functional connectivity in the human language system: a cortico-cortical evoked potential study. Brain. 127:2316–2330.

Mayer AR, Ryman SG, Hanlon FM, Dodd AB, Ling JM. 2016. Look Hear! The Prefrontal Cortex is Stratified by Modality of Sensory Input During Multisensory Cognitive Control. Cereb Cortex. 27:bhw131.

McKenzie S, Frank AJ, Kinsky NR, Porter B, Rivière PD, Eichenbaum H. 2014.

Hippocampal representation of related and opposing memories develop within distinct, hierarchically organized neural schemas. Neuron. 83:202–215.

Meltzer JA, Zaveri HP, Goncharova II, Distasio MM, Papademetris X, Spencer SS, Spencer DD, Constable RT. 2008. Effects of Working Memory Load on Oscillatory Power in Human Intracranial EEG. Cereb Cortex. 18:1843–1855.

Mesulam M. 1998. From sensation to cognition. Brain. 121:1013–1052.

Meuwissen AS, Anderson JE, Zelazo PD. 2017. The creation and validation of the Developmental Emotional Faces Stimulus Set. Behav Res Methods. 49:960–966.

Michalka SW, Kong L, Rosen ML, Shinn-Cunningham BG, Somers DC. 2015. Short-Term Memory for Space and Time Flexibly Recruit Complementary Sensory-Biased Frontal Lobe Attention Networks. Neuron. 87:882–892.

Middleton FA, Strick PL. 2000. Basal ganglia and cerebellar loops: Motor and cognitive circuits. Brain Res Rev. 31:236–250.

Miller EK, Cohen JD. 2001. An integrative theory of prefrontal cortex function. Annu Rev Neurosci. 24:167–202.

Miller EK, Lundqvist M, Bastos AM. 2018. Working Memory 2.0. Neuron. 100:463–475.

Miller GA, Galanter E, Pribram KH. 1960. Plans and the structure of behavior. New York: Henry Holt and Co.

Miller KJ, Abel TJ, Hebb AO, Ojemann JG. 2011. Rapid online language mapping with electrocorticography. J Neurosurg Pediatr. 7:482–490.

Miller KJ, Leuthardt EC, Schalk G, Rao RPN, Anderson NR, Moran DW, Miller JW, Ojemann JG. 2007. Spectral Changes in Cortical Surface Potentials during Motor Movement. J Neurosci. 27:2424–2432.

Miller KJ, Schalk G, Fetz EE, Den Nijs M, Ojemann JG, Rao RPN. 2010. Cortical activity during motor execution, motor imagery, and imagery-based online feedback. Proc Natl Acad Sci U S A. 107:4430–4435.

Miller KJ, Sorensen LB, Ojemann JG, den Nijs M. 2009. Power-Law Scaling in the Brain Surface Electric Potential. PLoS Comput Biol. 5:e1000609.

Milner B. 1963. Effects of different brain lesions on card sorting: The role of the frontal lobes. Arch Neurol. 9:90–100.

Minxha J, Adolphs R, Fusi S, Mamelak AN, Rutishauser U. 2020. Flexible recruitment of memory-based choice representations by the human medial frontal cortex. Science (80-). 368:eaba3313.

Mitchell DJ, Bell AH, Buckley MJ, Mitchell AS, Sallet J, Duncan J. 2016. A Putative Multiple-Demand System in the Macaque Brain. J Neurosci. 36:8574–8585.

Miyake A, Friedman NP, Emerson MJ, Witzki AH, Howerter A, Wager TD. 2000. The Unity and Diversity of Executive Functions and Their Contributions to Complex "Frontal Lobe" Tasks: A Latent Variable Analysis. Cogn Psychol. 41:49–100.

Nagy A, Paróczy Z, Norita M, Benedek G. 2005. Multisensory responses and receptive field properties of neurons in the substantia nigra and in the caudate nucleus. Eur J Neurosci. 22:419–424.

Naya Y, Chen H, Yang C, Suzuki WA. 2017. Contributions of primate prefrontal cortex and medial temporal lobe to temporal-order memory. Proc Natl Acad Sci. 114:13555–13560.

Newell A. 1973. You can't play 20 questions with nature and win: Projective comments on the papers of this symposium BT - Visual Information Processing. In: Visual Information Processing. p. 283–308.

Newell A. 1990. Unified Theories of Cognition. Cambridge, MA, USA: Harvard University Press.

Nir Y, Fisch L, Mukamel R, Gelbard-Sagiv H, Arieli A, Fried I, Malach R. 2007. Coupling between Neuronal Firing Rate, Gamma LFP, and BOLD fMRI Is Related to Interneuronal Correlations. Curr Biol. 17:1275–1285.

Niv Y, Daniel R, Geana A, Gershman SJ, Leong YC, Radulescu A, Wilson RC. 2015. Reinforcement learning in multidimensional environments relies on attention mechanisms. J Neurosci. 35:8145–8157.

Norman DA, Shallice T. 1986. Attention to action: Willed and automatic control of behaviour (Revised reprint of Norman and Shallice (1980)). In: Consciousness and Self-Regulation: Advances in Research and Theory. p. 1–18.

Noyce AL, Cestero N, Michalka SW, Shinn-Cunningham BG, Somers DC. 2017. Sensory-Biased and Multiple-Demand Processing in Human Lateral Frontal Cortex. J Neurosci. 37:8755–8766.

Nyberg L, Marklund P, Persson J, Cabeza R, Forkstam C, Petersson KM, Ingvar M. 2003. Common prefrontal activations during working memory, episodic memory, and semantic memory. Neuropsychologia. 41:371–377.

Ojemann G, Ojemann J, Lettich E, Berger M. 1989. Cortical language localization in left, dominant hemisphere. J Neurosurg. 71:316–326.

Öngür D, Ferry AT, Price JL. 2003. Architectonic subdivision of the human orbital and medial prefrontal cortex. J Comp Neurol. 460:425–449.

Owen AM, McMillan KM, Laird AR, Bullmore E. 2005. N-back working memory paradigm: A meta-analysis of normative functional neuroimaging studies. In: Human Brain Mapping.

Pandya DN, Yeterian EH. 1985. Architecture and Connections of Cortical Association Areas. In: Association and Auditory Cortices. p. 3–61.

Parvizi J, Jacques C, Foster BL, Withoft N, Rangarajan V, Weiner KS, Grill-Spector K. 2012. Electrical Stimulation of Human Fusiform Face-Selective Regions Distorts Face Perception. J Neurosci. 32:14915–14920.

Pei X, Leuthardt EC, Gaona CM, Brunner P, Wolpaw JR, Schalk G. 2011. Spatiotemporal dynamics of electrocorticographic high gamma activity during overt and covert word repetition. Neuroimage. 54:2960–2972.

Petacchi A, Laird AR, Fox PT, Bower JM. 2005. Cerebellum and auditory function: An ALE meta-analysis of functional neuroimaging studies. Hum Brain Mapp. 25:118–128.

Petersen SE, Posner MI. 2012. The attention system of the human brain: 20 years after. Annu Rev Neurosci. 35:73–89.

Petersen SE, Sporns O. 2015. Brain Networks and Cognitive Architectures. Neuron. 88:207–219.

Petrides M, Pandya DN. 1999. Dorsolateral prefrontal cortex: comparative cytoarchitectonic analysis in the human and the macaque brain and corticocortical connection patterns. Eur J Neurosci. 11:1011–1036.

Phillips JM, Vinck M, Everling S, Womelsdorf T. 2014. A Long-Range Fronto-Parietal 5- to 10-Hz Network Predicts “Top-Down” Controlled Guidance in a Task-Switch Paradigm. Cereb Cortex. 24:1996–2008.

Piazza M, Mechelli A, Price CJ, Butterworth B. 2006. Exact and approximate judgements of visual and auditory numerosity: An fMRI study. Brain Res. 1106:177–188.

Pobric G, Jefferies E, Ralph MAL. 2007. Anterior temporal lobes mediate semantic representation: Mimicking semantic dementia by using rTMS in normal participants. Proc Natl Acad Sci. 104:20137–20141.

Podvalny E, Noy N, Harel M, Bickel S, Chechik G, Schroeder CE, Mehta AD, Tsodyks M, Malach R. 2015. A unifying principle underlying the extracellular field potential spectral responses in the human cortex. J Neurophysiol. 114:505–519.

Postle BR. 2006. Working memory as an emergent property of the mind and brain. Neuroscience. 139:23–38.

Power JD, Cohen AL, Nelson SM, Wig GS, Barnes KA, Church JA, Vogel AC, Laumann TO, Miezin FM, Schlaggar BL, Petersen SE. 2011. Functional Network Organization of the Human Brain. Neuron. 72:665–678.

Power JD, Schlaggar BL, Lessov-Schlaggar CN, Petersen SE. 2013. Evidence for hubs in human functional brain networks. Neuron. 79:798–813.

Prabhakaran V, Narayanan K, Zhao Z, Gabrieli JDE. 2000. Integration of diverse information in working memory within the frontal lobe. Nat Neurosci. 3:85–90.

Prabhakaran V, Smith JAL, Desmond JE, Glover GH, Gabrieli JDE. 1997. Neural Substrates of Fluid Reasoning: An fMRI Study of Neocortical Activation during Performance of the Raven's Progressive Matrices Test. Cogn Psychol. 33:43–63.

Premereur E, Janssen P, Vanduffel W. 2018. Functional MRI in Macaque Monkeys during Task Switching. J Neurosci. 38:10619–10630.

Qiao L, Zhang L, Chen A, Egner T. 2017. Dynamic trial-by-trial recoding of task-set representations in the frontoparietal cortex mediates behavioral flexibility. J Neurosci. 37:11037–11050.

Rabbitt P. 2004. Methodology Of Frontal And Executive Function. Routledge.

Raghavachari S, Kahana MJ, Rizzuto DS, Caplan JB, Kirschen MP, Bourgeois B, Madsen JR, Lisman JE. 2001. Gating of Human Theta Oscillations by a Working Memory Task. J Neurosci. 21:3175–3183.

Ramnani N, Owen AM. 2004. Anterior prefrontal cortex: insights into function from anatomy and neuroimaging. Nat Rev Neurosci. 5:184–194.

Raven JC. 1982. Revised manual for Raven's Progressive Matrices and Vocabulary Scale. Revis Man Raven's Progress Matrices Vocab Scale.

Ray S, Crone NE, Niebur E, Franaszczuk PJ, Hsiao SS. 2008. Neural Correlates of High-Gamma Oscillations (60-200 Hz) in Macaque Local Field Potentials and Their Potential Implications in Electrocorticography. J Neurosci. 28:11526–11536.

Ray S, Maunsell JHR. 2011. Different Origins of Gamma Rhythm and High-Gamma Activity in Macaque Visual Cortex. PLoS Biol. 9:e1000610.

Ray S, Niebur E, Hsiao SS, Sinai A, Crone NE. 2008. High-frequency gamma activity (80–150Hz) is increased in human cortex during selective attention. Clin Neurophysiol. 119:116–133.

Remedios R, Logothetis NK, Kayser C. 2009. An Auditory Region in the Primate Insular Cortex Responding Preferentially to Vocal Communication Sounds. J Neurosci. 29:1034–1045.

Rigotti M. 2010. Internal representation of task rules by recurrent dynamics: the importance of the diversity of neural responses. Front Comput Neurosci. 4.

Rigotti M, Barak O, Warden MR, Wang XJ, Daw ND, Miller EK, Fusi S. 2013. The importance of mixed selectivity in complex cognitive tasks. Nature. 497:585–590.

Robbins TW, Anderson EJ, Barker DR, Bradley AC, Fearnyhough C, Henson R, Hudson SR, Baddeley AD. 1996. Working memory in chess. Mem Cogn. 24:83–93.

Robinson EC, Garcia K, Glasser MF, Chen Z, Coalson TS, Makropoulos A, Bozek J, Wright R, Schuh A, Webster M, Hutter J, Price A, Cordero Grande L, Hughes E, Tusor N, Bayly P V., Van Essen DC, Smith SM, Edwards AD, Hajnal J, Jenkinson M, Glocker B, Rueckert D. 2018. Multimodal surface matching with higher-order smoothness constraints. Neuroimage. 167:453–465.

Robinson EC, Jbabdi S, Glasser MF, Andersson J, Burgess GC, Harms MP, Smith SM, Van Essen DC, Jenkinson M. 2014. MSM: A new flexible framework for multimodal surface matching. Neuroimage. 100:414–426.

Roca M, Parr A, Thompson R, Woolgar A, Torralva T, Antoun N, Manes F, Duncan J. 2010. Executive function and fluid intelligence after frontal lobe lesions. Brain. 133:234–247.

Romanski LM. 2007. Representation and Integration of Auditory and Visual Stimuli in the Primate Ventral Lateral Prefrontal Cortex. Cereb Cortex.

17:i61–i69.

Romero-Garcia R, Suckling J, Owen M, Assem M, Sinha R, Coelho P, Woodberry E, Price SJ, Burke AGA, Santarius T, Erez Y, Hart MG. 2019. Disruptive and protective outcomes to memory and attention when treating diffuse glioma. medRxiv. 19008581.

Russin J, O'Reilly RC, Bengio Y. 2020. Deep Learning Needs a Prefrontal Cortex. Work "Bridging AI Cogn Sci (ICLR 2020). 1–11.

Saalmann YB, Pigarev IN, Vidyasagar TR. 2007. Neural Mechanisms of Visual Attention: How Top-Down Feedback Highlights Relevant Locations. Science (80-). 316:1612–1615.

Sacerdoti ED. 1974. Planning in a hierarchy of abstraction spaces. Artif Intell. 5:115–135.

Sadaghiani S, Kleinschmidt A. 2016. Brain Networks and α-Oscillations: Structural and Functional Foundations of Cognitive Control. Trends Cogn Sci. 20:805–817.

Saez A, Rigotti M, Ostojic S, Fusi S, Salzman CD. 2015. Abstract Context Representations in Primate Amygdala and Prefrontal Cortex. Neuron. 87:869–881.

Sagar S, Rick J, Chandra A, Yagnik G, Aghi MK. 2019. Functional brain mapping: overview of techniques and their application to neurosurgery. Neurosurg Rev. 42:639–647.

Salimi-Khorshidi G, Douaud G, Beckmann CF, Glasser MF, Griffanti L, Smith SM. 2014. Automatic denoising of functional MRI data: Combining independent component analysis and hierarchical fusion of classifiers. Neuroimage. 90:449–468.

Sanai N, Polley M-Y, Berger MS. 2010. Insular glioma resection: assessment of patient morbidity, survival, and tumor progression. J Neurosurg. 112:1–9.

Schafer RJ, Moore T. 2007. Attention Governs Action in the Primate Frontal Eye Field. Neuron. 56:541–551.

Schwartz MF, Reed ES, Montgomery M, Palmer C, Mayer NH. 1991. The Quantitative Description of Action Disorganisation after Brain Damage: A Case Study. Cogn Neuropsychol. 8:381–414.

Schweizer TA, Levine B, Rewilak D, O'Connor C, Turner G, Alexander MP, Cusimano M, Manly T, Robertson IH, Stuss DT. 2008. Rehabilitation of

executive functioning after focal damage to the cerebellum. Neurorehabil Neural Repair. 22:72–77.

Shallice T, Burgess PW. 1991. Deficits in strategy application following frontal lobe damage in man. Brain. 114 (Pt 2:727–741.

Shashidhara S, Mitchell DJ, Erez Y, Duncan J. 2019. Progressive Recruitment of the Frontoparietal Multiple-demand System with Increased Task Complexity, Time Pressure, and Reward. J Cogn Neurosci. 31:1617–1630.

Shashidhara S, Spronkers FS, Erez Y. 2020. Individual-subject Functional Localization Increases Univariate Activation but Not Multivariate Pattern Discriminability in the "Multiple-demand" Frontoparietal Network. J Cogn Neurosci. 32:1348–1368.

Shine JM, Bissett PG, Bell PT, Koyejo O, Balsters JH, Gorgolewski KJ, Moodie CA, Poldrack RA. 2016. The Dynamics of Functional Brain Networks: Integrated Network States during Cognitive Task Performance. Neuron. 92:544–554.

Siegel M, Donner TH, Engel AK. 2012. Spectral fingerprints of large-scale neuronal interactions. Nat Rev Neurosci. 13:121–134.

Sigala N, Kusunoki M, Nimmo-Smith I, Gaffan D, Duncan J. 2008. Hierarchical coding for sequential task events in the monkey prefrontal cortex. Proc Natl Acad Sci U S A. 105:11969–11974.

Smith SM, Vidaurre D, Beckmann CF, Glasser MF, Jenkinson M, Miller KL, Nichols TE, Robinson EC, Salimi-Khorshidi G, Woolrich MW, Barch DM, Uğurbil K, Van Essen DC. 2013. Functional connectomics from resting-state fMRI. Trends Cogn Sci. 17:666–682.

Soreq E, Leech R, Hampshire A. 2019. Dynamic network coding of working-memory domains and working-memory processes. Nat Commun. 10:936.

Spearman C. 1904. "General Intelligence," Objectively Determined and Measured. Am J Psychol. 15:201.

Spearman C. 1927. The Abilities of Man. Macmillan.

Sporns O. 2014. Contributions and challenges for network models in cognitive neuroscience. Nat Neurosci. 17:652–660.

Stein BE, Stanford TR. 2008. Multisensory integration: current issues from the perspective of the single neuron. Nat Rev Neurosci. 9:255–266.

Stokes MG, Kusunoki M, Sigala N, Nili H, Gaffan D, Duncan J. 2013. Dynamic

Coding for Cognitive Control in Prefrontal Cortex. Neuron. 78:364–375.

Stolk A, Griffin S, van der Meij R, Dewar C, Saez I, Lin JJ, Piantoni G, Schoffelen J-M, Knight RT, Oostenveld R. 2018. Integrated analysis of anatomical and electrophysiological human intracranial data. Nat Protoc. 13:1699–1723.

Suess O, Suess S, Brock M, Kombos T. 2006. Intraoperative electrocortical stimulation of Brodman area 4: a 10-year analysis of 255 cases. Head Face Med. 2:20.

Swann N, Tandon N, Canolty R, Ellmore TM, McEvoy LK, Dreyer S, DiSano M, Aron AR. 2009. Intracranial EEG Reveals a Time- and Frequency-Specific Role for the Right Inferior Frontal Gyrus and Primary Motor Cortex in Stopping Initiated Responses. J Neurosci. 29:12675–12685.

Szameitat AJ, Schubert T, Müller K, Von Yves Cramon D. 2002. Localization of executive functions in dual-task performance with fMRI. J Cogn Neurosci. 14:1184–1199.

Szczepanski SM, Crone NE, Kuperman RA, Auguste KI, Parvizi J, Knight RT. 2014. Dynamic Changes in Phase-Amplitude Coupling Facilitate Spatial Attention Control in Fronto-Parietal Cortex. PLoS Biol. 12:e1001936.

Szelényi A, Bello L, Duffau H, Fava E, Feigl GC, Galanda M, Neuloh G, Signorelli F, Sala F. 2010. Intraoperative electrical stimulation in awake craniotomy: Methodological aspects of current practice. Neurosurg Focus. 28:1–8.

Tavor I, Jones OP, Mars RB, Smith SM, Behrens TE, Jbabdi S. 2016. Task-free MRI predicts individual differences in brain activity during task performance. Science (80-). 352:216–220.

Thompson KG, Biscoe KL, Sato TR. 2005. Neuronal basis of covert spatial attention in the frontal eye field. J Neurosci. 25:9479–9487.

Thomson GH. 1939. The factorial analysis of human ability., The factorial analysis of human ability. Oxford, England: Houghton Mifflin.

Tinbergen N. 1951. The Study of Instinct. Clarendon Press, Oxford.

Tobyne SM, Osher DE, Michalka SW, Somers DC. 2017. Sensory-biased attention networks in human lateral frontal cortex revealed by intrinsic functional connectivity. Neuroimage. 162:362–372.

Tombu MN, Asplund CL, Dux PE, Godwin D, Martin JW, Marois R. 2011. A

Unified attentional bottleneck in the human brain. Proc Natl Acad Sci. 108:13426–13431.

Tremblay P, Gracco VL. 2006. Contribution of the frontal lobe to externally and internally specified verbal responses: fMRI evidence. Neuroimage. 33:947–957.

Tschentscher N, Mitchell D, Duncan J. 2017. Fluid Intelligence Predicts Novel Rule Implementation in a Distributed Frontoparietal Control Network. J Neurosci. 37:4841–4847.

Turner R. 2002. How much codex can a vein drain? Downstream dilution of activation-related cerebral blood oxygenation changes. Neuroimage. 16:1062–1067.

Uğurbil K, Xu J, Auerbach EJ, Moeller S, Vu AT, Duarte-Carvajalino JM, Lenglet C, Wu X, Schmitter S, Van de Moortele PF, Strupp J, Sapiro G, De Martino F, Wang D, Harel N, Garwood M, Chen L, Feinberg DA, Smith SM, Miller KL, Sotiropoulos SN, Jbabdi S, Andersson JLR, Behrens TEJ, Glasser MF, Van Essen DC, Yacoub E. 2013. Pushing spatial and temporal resolution for functional and diffusion MRI in the Human Connectome Project. Neuroimage. 80:80–104.

Vallesi A, Arbula S, Capizzi M, Causin F, D'Avella D. 2015. Domain-independent neural underpinning of task-switching: An fMRI investigation. Cortex. 65:173–183.

van Es DM, van der Zwaag W, Knapen T. 2019. Topographic Maps of Visual Space in the Human Cerebellum. Curr Biol. 29:1689–1694.e3.

Van Essen DC, Glasser MF. 2018. Parcellating Cerebral Cortex: How Invasive Animal Studies Inform Noninvasive Mapmaking in Humans. Neuron. 99:640–663.

Van Essen DC, Jbabdi S, Sotiropoulos SN, Chen C, Dikranian K, Coalson T, Harwell J, Behrens TEJ, Glasser MF. 2014. Mapping Connections in Humans and Non-Human Primates. In: Diffusion MRI. Elsevier. p. 337–358.

Vansteensel MJ, Bleichner MG, Dintzner LT, Aarnoutse EJ, Leijten FSS, Hermes D, Ramsey NF. 2013. Task-free electrocorticography frequency mapping of the motor cortex. Clin Neurophysiol. 124:1169–1174.

Visser M, Jefferies E, Lambon Ralph MA. 2010. Semantic Processing in the

Anterior Temporal Lobes: A Meta-analysis of the Functional Neuroimaging Literature. J Cogn Neurosci. 22:1083–1094.

Vohn R, Fimm B, Weber J, Schnitker R, Thron A, Spijkers W, Willmes K, Sturm W. 2007. Management of attentional resources in within-modal and cross-modal divided attention tasks: An fMRI study. Hum Brain Mapp. 28:1267–1275.

Voytek B, Kayser AS, Badre D, Fegen D, Chang EF, Crone NE, Parvizi J, Knight RT, D'Esposito M. 2015. Oscillatory dynamics coordinating human frontal networks in support of goal maintenance. Nat Neurosci. 18:1318–1324.

Vyas S, Golub MD, Sussillo D, Shenoy K. 2020. Computation Through Neural Population Dynamics. Annu Rev Neurosci. 249–275.

Wager TD, Sylvester CYC, Lacey SC, Nee DE, Franklin M, Jonides J. 2005. Common and unique components of response inhibition revealed by fMRI. Neuroimage. 27:323–340.

Wagner AD, Shannon BJ, Kahn I, Buckner RL. 2005. Parietal lobe contributions to episodic memory retrieval. Trends Cogn Sci.

Wang X-J. 2010. Neurophysiological and Computational Principles of Cortical Rhythms in Cognition. Physiol Rev. 90:1195–1268.

Warren DE, Power JD, Bruss J, Denburg NL, Waldron EJ, Sun H, Petersen SE, Tranel D. 2014. Network measures predict neuropsychological outcome after brain injury. Proc Natl Acad Sci. 111:14247–14252.

Watanabe M. 1992. Frontal units of the monkey coding the associative significance of visual and auditory stimuli. Exp Brain Res. 89:233–247.

Watson CE, Chatterjee A. 2012. A bilateral frontoparietal network underlies visuospatial analogical reasoning. Neuroimage. 59:2831–2838.

Wen T, Duncan J, Mitchell DJ. 2020. Hierarchical representation of multi-step tasks in multiple-demand and default mode networks. J Neurosci. JN-RM-0594-20.

Wen T, Mitchell DJ, Duncan J. 2018. Response of the multiple-demand network during simple stimulus discriminations. Neuroimage. 177:79–87.

Woolgar A, Duncan J, Manes F, Fedorenko E. 2018. Fluid intelligence is supported by the multiple-demand system not the language system. Nat Hum Behav. 2:200–204.

Woolgar A, Hampshire A, Thompson R, Duncan J. 2011. Adaptive Coding of Task-Relevant Information in Human Frontoparietal Cortex. J Neurosci. 31:14592–14599.

Woolgar A, Jackson J, Duncan J. 2016. Coding of Visual, Auditory, Rule, and Response Information in the Brain: 10 Years of Multivoxel Pattern Analysis. J Cogn Neurosci. 28:1433–1454.

Woolgar A, Parr A, Cusack R, Thompson R, Nimmo-Smith I, Torralva T, Roca M, Antoun N, Manes F, Duncan J. 2010. Fluid intelligence loss linked to restricted regions of damage within frontal and parietal cortex. Proc Natl Acad Sci U S A. 107:14899–14902.

Woolgar A, Williams MA, Rich AN. 2015. Attention enhances multi-voxel representation of novel objects in frontal, parietal and visual cortices. Neuroimage. 109:429–437.

Woolnough O, Forseth KJ, Rollo PS, Tandon N. 2019. Uncovering the functional anatomy of the human insula during speech. Elife. 8.

Woolrich MW, Ripley BD, Brady M, Smith SM. 2001. Temporal Autocorrelation in Univariate Linear Modeling of FMRI Data. Neuroimage. 14:1370–1386.

Yeo BTT, Krienen FM, Eickhoff SB, Yaakub SN, Fox PT, Buckner RL, Asplund CL, Chee MWL. 2015. Functional Specialization and Flexibility in Human Association Cortex. Cereb Cortex. 25:3654–3672.

Yeo BTT, Krienen FM, Sepulcre J, Sabuncu MR, Lashkari D, Hollinshead M, Roffman JL, Smoller JW, Zöllei L, Polimeni JR, Fischl B, Liu H, Buckner RL. 2011a. The organization of the human cerebral cortex estimated by intrinsic functional connectivity. J Neurophysiol. 106:1125–1165.

Yeo BTT, Krienen FM, Sepulcre J, Sabuncu MR, Lashkari D, Hollinshead M, Roffman JL, Smoller JW, Zöllei L, Polimeni JR, Fischl B, Liu H, Buckner RL. 2011b. The organization of the human cerebral cortex estimated by intrinsic functional connectivity. J Neurophysiol. 106:1125–1165.

Yeterian EH, Pandya DN. 1991. Prefrontostriatal connections in relation to cortical architectonic organization in rhesus monkeys. J Comp Neurol. 312:43–67.

Yeung N. 2006. Between-Task Competition and Cognitive Control in Task Switching. J Neurosci. 26:1429–1438.